

©[2013]

Shanshan Li

ALL RIGHTS RESERVED

REGULATION OF ORGANIC ANION TRANSPORTERS

– Molecular and Cellular Mechanisms

By

Shanshan Li

A dissertation submitted to the Graduate School-New Brunswick

Rutgers, The State University of New Jersey

In partial fulfillment of the requirements

For the degree of

Doctor of Philosophy

Graduate Program in Pharmaceutical Sciences

Written under the direction of

Professor Guofeng You, Ph.D.

And approved by

New Brunswick, New Jersey

Oct, 2013

ABSTRACT OF THE DISSERTATION

Regulation of Organic Anion Transporters

– Molecular and Cellular Mechanisms

By Shanshan Li

Dissertation Director:

Guofeng You

Human organic anion transporters (hOATs) play critical roles in the body disposition of clinically important drugs. Understanding the regulation of hOATs has profound clinical significance. My thesis work focuses on delineating molecular and cellular mechanisms underlying hOAT regulation, and consists of three parts.

In the first part, we examined the regulation of hOAT trafficking and function by ubiquitination through cell signaling pathways (protein kinase C, protein kinase A, and their upstream hormones AngII and bradykinin) by combined approaches of cellular biology, site-directed mutagenesis and mass spectroscopy. We identified PKC isoforms involved in OAT regulation. We also identified lysine residues serving as ubiquitin-conjugating sites.

In the second part, we examined transporter-mediated drug-drug interactions by screening two prescription drug libraries against hOAT1 and hOAT3. High potent inhibitors were identified. Computational analyses reveal several important properties which differentiate between inhibitors and non-inhibitors. Such model provides mechanistic insights for predicting new OAT inhibitors.

In the third part, we studied structure and function relationship of hOATs. Critical transmembrane domain and amino acid residues were identified, which play important role in OAT stability, maturation efficiency as well as oligomerization.

DEDICATION AND ACKNOWLEDGEMENTS

To my great supervisor, Professor Guofeng You, who recruited me at first and guided me so well and taught me not only the science but the ability to learn, think, and interact with others. She is such a great mentor for me and led me from a fresh student to a professional scientist step by step. I could not accomplish this thesis without her dedicated education, patient guidance, and valuable suggestions on me.

To my beloved parents, who supported me whenever I need them. I could not survive without their love and moral support when I just came to the US. They will always be my best beloved dad and mom. They have sacrificed so much for me all these years and I want to show them my dedicated thesis work to demonstrate all my hard work and effort.

To my great husband, Fan, who has supported and encouraged me so much all these years, and build up such a warm and comfort home with me. I am always grateful for his unconditional love on me.

To my loving son, Justin, who was just born on Dec 30, 2012. His arrival brought me so much joy, love, and courage. That has been the best gift for me. I have got so much encouragement from him and he will always be my best treasure.

I would also like to thank all my committee members: Dr. Tamara Minko, Dr. Bozena Michniack-Kohn, Dr. Longqing Hu, and Dr. Zui Pan for supporting me for my entire PhD study and helpful suggestions. I am also thankful to many of my colleagues for their generous help on my research in Dr. You's group. They are Dr. Fanfan Zhou, Dr. Qiang

Zhang, Dr. Xinxiang Peng, Dr. Peng Duan, Ms. Jinwei Wu, Mr. Da Xu, Mr. Wonmo Suh, and Mr. Haoxun Wang.

Finally, I also need to thank the entire department of pharmaceuticals at Rutgers. Thank Marianne Shen, Hui Pung, Sharana Taylor, and many other colleagues for their kind help and support. This whole department is like a big family, which offered me lots of advantages. And I do love this environment very much and thank everyone here in our big family.

TABLE OF CONTENTS

ABSTRACT OF THE DISSERTATION	ii
DEDICATION AND ACKNOWLEDGEMENT.....	iv
TABLE OF CONTENTS	vi
Chapter 1. Overview.....	1
1.1 General properties of OATs.....	1
1.1.1 Structure features of OATs.....	1
1.1.2 Transport mechanism of OATs.....	2
1.1.3 Substrate specificity of OATs.....	3
1.2 Involvement of OATs in Drug-Drug interaction.....	4
1.3 Clinical implications of OATs.....	5
1.4 Regulation of OAT.....	6
1.5 Significance of my thesis work.....	7
1.6 References.....	8
Chapter 2. Regulation of OATs by Angiotensin II and Bradykinin.....	10
2.1 Introduction	10
2.2 Materials and methods	10
2.3 Results	12
2.4 References.....	26
Chapter 3. Regulation of OATs by Ubiquitination.....	27
3.1 Introduction	27
3.2 Materials and methods	29
3.3 Results	33

3.4 Discussion.....	48
3.5 References	50
Chapter 4. High throughput screen of OAT inhibitors.....	51
4.1 Introduction	51
4.2 Materials and methods	51
4.3 Results	54
4.4 Discussion	62
4.5 References.....	66
Chapter 5. Role of transmembrane domain 12 (TM12) of hOAT1 on its function.....	67
5.1 Introduction	67
5.2 Materials and methods.....	68
5.3 Results.....	71
5.4 Discussion.....	81
5.5 References.....	85
Chapter 6. Regulation of OATs by Oligomerization.....	87
6.1 Introduction	87
6.2 Materials and methods	87
6.3 Results	91
6.4 Discussion.....	97
6.5 References	101
7 Curriculum Vitae.....	102

Chapter 1. Overview

1.1 General Properties of OATs

Belong to the amphiphilic solute carrier transporters family 22a (SLC22a), the organic anion transporter (OAT) family has a broad diversity of substrates including endogenous metabolites, toxins and clinical drugs such as β -lactam antibiotics, antivirals, ACE inhibitors, diuretics and NASIDs (1-3). Since the cloning and identification of the first organic anion transporter OAT1, ten members of organic anion transporters have been identified, which are named after from OAT1 to OAT10 (4-13). They are different from each other by expression level, tissue distribution and substrate specificity.

1.1.1 Structure Features of OATs

All of these transporters have important features in common. As membrane proteins, all OATs have twelve trans-membrane spanning domains (TMD) with both amino and carboxy termini localized intracellularly. Between the TMDs 1 and 2, there is a big extracellular loop with a cluster of glycosylation sites. There are several phosphorylation sites in the intracellular loop between the TMDs 6 and 7, and in the carboxyl terminus (Fig 1).

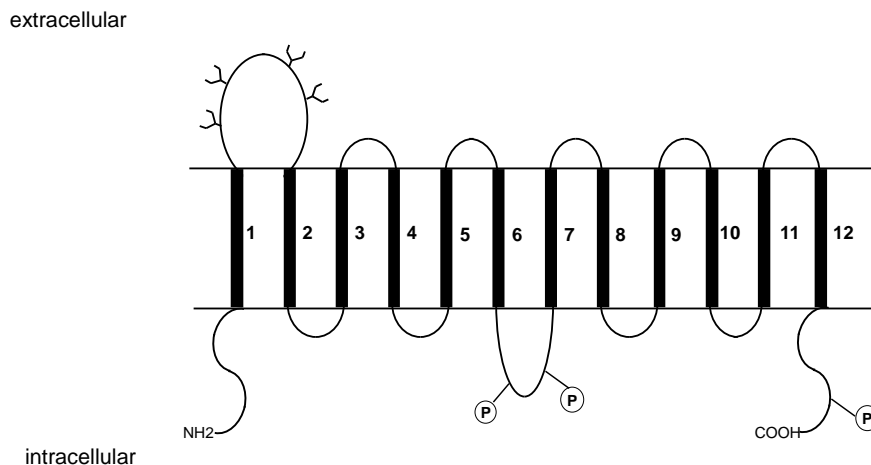


Fig. 1. Predicted transmembrane topology of hOAT1. Twelve transmembrane domains are numbered from 1 to 12. Potential glycosylation sites are denoted by tree-like structures. P: phosphorylation sites.

1.1.2 Transport Mechanism of OATs

In the kidney, OAT1 and OAT3 are localized at the basolateral membrane of the kidney proximal tubule, where they are responsible for the rate-limiting step of drug elimination. OATs utilize a tertiary system to move organic anions across the basolateral membrane from the blood into the proximal tubular cells for subsequent exit across the apical membrane into the urine for elimination (Fig 2). $\text{Na}^+\text{K}^+\text{-ATPase}$ pumps Na^+ out of the cells, establishes an inwardly directed Na^+ gradient. This Na^+ gradient then moves dicarboxylates such as α -ketoglutarate (α -KG) into the cells through a $\text{Na}/\text{dicarboxylate}$ cotransporter (SDCT2). This process, in conjunction with an ongoing cellular metabolic activity, sustains an outwardly directed dicarboxylate gradient, which is utilized by OAT1 or OAT3 to transfer organic anions such as PAH, and/or drugs into the cells. Exit into the urine across the apical membrane occurs via an OA exchanger (Ex) and/or a membrane potential-sensitive facilitative diffusion carrier (FD), depending upon the species studied.

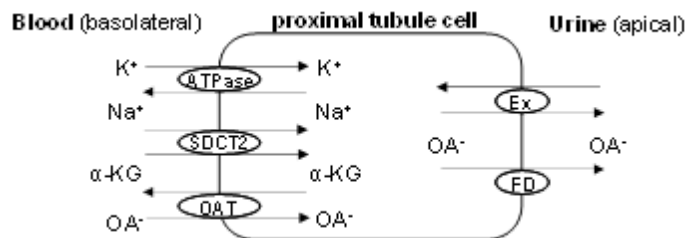


Fig. 2. Transport Mechanism of OATs

1.1.3 Substrate specificity of OATs

One prominent feature of the OAT system is its interaction with and transport of a wide variety of clinically important anionic drugs. The primary requirements for the substrates to be recognized by OATs are a negative charge and a hydrophobic region, where multiple points of interaction exists between the carrier and substrate functional groups (carbonyl and carboxyl). OAT substrates include a wide variety of clinically important anionic drugs, such as b-lactam antibiotics, diuretics, non-steroidal anti-inflammatory drugs; NSAIDs, anti-HIV therapeutics, anti-tumor drugs, and inhibitors for angiotensin-converting enzyme (1-3). OAT substrates also include numerous endogenous organic anions, such as cyclic nucleotides, dicarboxylates, and neurotransmitter metabolites, as well as exogenous organic anionic environmental chemicals, organic anion, such as mycotoxins, sulfate conjugates, cysteine conjugates, glucuronide conjugates, and glycine conjugates.

1.2 Involvement of OATs in Drug–Drug Interaction

Since the diverse substrate spectrum of OATs, multiple substrates especially drugs can compete the same transporter sites while they are co-administrated, thus resulting drug-drug interaction and mutually influencing each other's pharmacokinetics. Drug transporter mediated drug-drug interaction is increasingly aware to be one of the most common reasons causing drug adverse side effects. Administration of one drug sometimes can cause a change in the activity of certain other drug transporters, and subsequently affect elimination and absorption of drugs whose elimination process is mediated by this drug transporter. Methotrexate (MTX), which is a substrate of OATs, was used widely in various disease treatments. It was found that concomitant use of MTX with organic anion drugs such as non-steroidal anti-inflammatory drugs and β -lactam antibiotics would inhibit the activity of the renal OAT system and subsequently reduced the renal elimination of MTX and resulted in severe suppression of bone marrow. Recently, Duan et al (14) found that novobiocin, one of the specific inhibitor for the Breast Cancer Resistance Protein (BCRP), could potentially inhibit the activity of hOAT1, hOAT3 and hOAT4, which elucidates the possibility of potential drug-drug interaction between OATs substrates and novobiocin or other BCRP inhibitors. Drug-drug interaction would also affect the efficacy of the drugs. For example, diuretics are mostly secreted by the renal OATs for subsequent elimination by transporters such as NaK_2Cl or NaCl transporters in the luminal membrane of thin ascending limb or the distal tubule. Administration of diuretics with inhibitors of OATs inhibited the tubular secretion and thus diminishing the diuretic effects of the drug.

1.3 Clinical Implications of OATs

OAT1 and OAT3 have been reported to be responsible for the impaired drug elimination in many clinical conditions. For example, bilateral ureteral obstruction (BUO) is a common clinical disease characterized by the development of hemodynamic and tubular lesions. Obstruction of the urinary tract results in adverse effect on the renal blood flow, glomerular filtration rate (GFR), tubular function and parenchymal (15). A lower renal excretion of PAH was found in BUO rats. Further studies demonstrated that BUO was associated with down-regulation of OAT1 and OAT3.

Acute renal failure (ARF) is a common clinical condition and associated with a higher than 50% mortality rate (16). In ischemic acute renal failure (iARF), the excretion of PAH was significantly reduced. Further studies showed that in iARF rats, down-expression in both mRNA and protein level of OAT1 and OAT3 was correlated with impaired secretion of PAH (17). Kwon et al also found the maldistribution and altered expression of OAT1 in iARF (18). Due to the importance of OAT1 and OAT3 to renal elimination and clearance, the down-regulation of OAT1 and OAT3 probably would have a substantial impact on renal retention and elimination of organic anions in iARF.

Indoxyl sulfate, one of the uremic toxins accumulated in chronic renal failure was recently found to be novel substrates of OAT1, OAT3 and OAT4 (19, 20). The level of Indoxyl sulfate, a metabolite of indole derived from dietary protein, was elevated in patients with chronic renal failure. Indoxyl sulfate was transported by OATs to various organs and tissue and thereby causing various pathological conditions not only in kidney but also in central nervous system, placenta and muscles (21,22). Recently, besides URAT1, OAT1, 2, 3 and OAT4 are also found to transport urate, which demonstrated the importance of OATs in hyperuricemia involved diseases such as gout.

1.4 Regulations of OAT

OATs are subjected to loops and layers of regulation. Dr. You's lab has uncovered several factors/mechanisms, which affect OAT transport activities. These factors/mechanisms include physiological hormones, membrane trafficking, glycosylation, phosphorylation, and environmental pH. Among these factors/mechanisms, membrane trafficking is particular interesting. We have recently shown that members of OAT family constitutively internalize from and recycle back to cell surface (Fig. 3), and that inhibition of OAT activity by activation of PKC results from an accelerated internalization of these transporters from cell surface to intracellular compartments. However, the mechanisms of PKC effect on OAT internalization and function are largely unknown. PKC-induced direct phosphorylation has been reported for other membrane proteins. However, our results showed that a range of PKC activators failed to elevate the phosphorylation level of OATs under various experimental conditions (23). This suggests that direct phosphorylation of OATs is unlikely to be the cause for PKC-induced inhibition of OAT activity. One part of my thesis work was to further explore the mechanisms underlying PKC-regulated OAT trafficking.

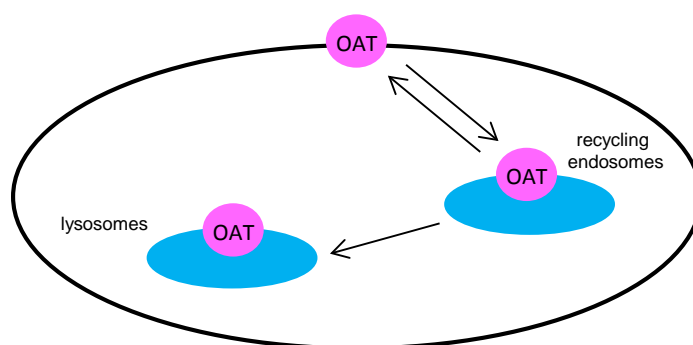


Fig. 3. Membrane Trafficking of OATs

1.5 Significance of My Thesis Work

The OAT family mediates the absorption, distribution, and excretion of a diverse array of environmental toxins, and clinically important drugs, including anti-HIV therapeutics, anti-cancer drugs, antibiotics, anti-hypertensives, and anti-inflammatories, and therefore is critical for the survival of mammalian species. OATs are expressed in kidney, liver, brain and placenta. OAT dysfunction in these organs significantly contributes to the renal, hepatic, neurological and fetal toxicity and disease. Despite such a vital role, many questions related to the structure/function relationship of OATs and the mechanisms of their regulation remain to be answered. Answering these questions is the goal of my thesis work, which will provide the insights into the molecular, cellular, and clinical bases of renal, hepatic, neurological and fetal toxicity and disease.

1.6 References:

1. Anzai N, Kanai Y and Endou H (2006) Organic anion transporter family: current knowledge. *J Pharmacol Sci* 100:411-426.
2. You G (2004) The role of organic anion transporters in drug disposition: an update. *Curr Drug Metab* 5:55-62.
3. Srimaroeng C, Perry JL and Pritchard JB (2008) Physiology, structure, and regulation of the cloned organic anion transporters. *Xenobiotica* 38:889-935.
4. Cha SH, Sekine T, Kusuhashi H, Yu E, Kim JY, Kim DK, Sugiyama Y, Kanai Y and Endou H (2000) Molecular cloning and characterization of multispecific organic anion transporter 4 expressed in the placenta. *J Biol Chem* 275:4507-4512.
5. Bahn A, Hagos Y, Reuter S, Balen D, Brzica H, Krick W, Burckhardt BC, Sabolic I and Burckhardt G (2008) Identification of a new urate and high affinity nicotinate transporter, hOAT10 (SLC22A13). *J Biol Chem* 283:16332-16341.
6. Kusuhashi H, Sekine T, Utsunomiya-Tate N, Tsuda M, Kojima R, Cha SH, Sugiyama Y, Kanai Y and Endou H (1999) Molecular cloning and characterization of a new multispecific organic anion transporter from rat brain. *J Biol Chem* 274:13675-13680.
7. Sekine T, Cha SH, Tsuda M, Apiwattanakul N, Nakajima N, Kanai Y and Endou H (1998) Identification of multispecific organic anion transporter 2 expressed predominantly in the liver. *FEBS Lett* 429:179-182.
8. Sekine T, Watanabe N, Hosoyamada M, Kanai Y and Endou H (1997) Expression cloning and characterization of a novel multispecific organic anion transporter. *J Biol Chem* 272:18526-18529.
9. Sweet DH, Wolff NA and Pritchard JB (1997) Expression cloning and characterization of ROAT1. The basolateral organic anion transporter in rat kidney. *J Biol Chem* 272:30088-30095.
10. Shin HJ, Anzai N, Enomoto A, He X, Kim do K, Endou H and Kanai Y (2007) Novel liver-specific organic anion transporter OAT7 that operates the exchange of sulfate conjugates for short chain fatty acid butyrate. *Hepatology* 45:1046-1055.
11. Schnabolk GW, Youngblood GL and Sweet DH (2006) Transport of estrone sulfate by the novel organic anion transporter Oat6 (Slc22a20). *Am J Physiol Renal Physiol* 291:F314-321.
12. Yokoyama H, Anzai N, Ljubojevic M, Ohtsu N, Sakata T, Miyazaki H, Nonoguchi H, Islam R, Onozato M, Tojo A, Tomita K, Kanai Y, Igarashi T, Sabolic I and Endou H (2008) Functional and immunochemical characterization of a novel organic anion transporter Oat8 (Slc22a9) in rat renal collecting duct. *Cell Physiol Biochem* 21:269-278.

13. Youngblood GL and Sweet DH (2004) Identification and functional assessment of the novel murine organic anion transporter Oat5 (Slc22a19) expressed in kidney. *Am J Physiol Renal Physiol* 287:F236-244.
14. Duan P and You G (2009) Novobiocin is a potent inhibitor for human organic anion transporters. *Drug Metab Dispos* 37:1203-1210.
15. Dal Canton A, Corradi A, Stanziale R, Maruccio G and Migone L (1980) Glomerular hemodynamics before and after release of 24-hour bilateral ureteral obstruction. *Kidney Int* 17:491-496.
16. Uchino S, Kellum JA, Bellomo R, Doig GS, Morimatsu H, Morgera S, Schetz M, Tan I, Bouman C, Macedo E, Gibney N, Tolwani A and Ronco C (2005) Acute renal failure in critically ill patients: a multinational, multicenter study. *JAMA* 294:813-818.
17. Schneider R, Sauvant C, Betz B, Otremba M, Fischer D, Holzinger H, Wanner C, Galle J and Gekle M (2007) Downregulation of organic anion transporters OAT1 and OAT3 correlates with impaired secretion of para-aminohippurate after ischemic acute renal failure in rats. *Am J Physiol Renal Physiol* 292:F1599-1605.
18. Kwon O, Wang WW and Miller S (2008) Renal organic anion transporter 1 is maldistributed and diminishes in proximal tubule cells but increases in vasculature after ischemia and reperfusion. *Am J Physiol Renal Physiol* 295:F1807-1816.
19. Enomoto A and Endou H (2005) Roles of organic anion transporters (OATs) and a urate transporter (URAT1) in the pathophysiology of human disease. *Clin Exp Nephrol* 9:195-205.
20. Enomoto A and Niwa T (2007) Roles of organic anion transporters in the progression of chronic renal failure. *Ther Apher Dial* 11 Suppl 1:S27-31.
21. Deguchi T, Kusuhashi H, Takadate A, Endou H, Otagiri M and Sugiyama Y (2004) Characterization of uremic toxin transport by organic anion transporters in the kidney. *Kidney Int* 65:162-174.
22. Motojima M, Hosokawa A, Yamato H, Muraki T and Yoshioka T (2002) Uraemic toxins induce proximal tubular injury via organic anion transporter 1-mediated uptake. *Br J Pharmacol* 135:555-563.
23. You GF, Kuze K, Kohanski RA, Amsler K, and Henderson S. Regulation of mOAT-mediated organic anion transport by okadaic acid and protein kinase C in LLC-PK1 cells. *J Biol Chem* 275: 10278-10284

Chapter 2. Regulation of OATs by Angiotensin II and Bradykinin

2.1 INTRODUCTION

Angiotensin II (Ang II) and Bradykinin (BK) are two physiological hormones that have been shown to regulate the function of numerous kidney membrane transport processes such as chloride conductance, Na⁺ transport, Na⁺/H⁺ exchange, organic anion and organic cation transport. Multiple signaling pathways including protein kinase A (PKA) pathway and protein kinase C (PKC) pathway are involved in Ang II and bradykinin-induced regulation (1, 2). More importantly, these hormones regulate kidney transport through different protein kinase isoforms. In this part of my thesis work, I investigated the effects of Ang II and BK on OAT-mediated drug transport and the cellular signaling pathways involved in these processes.

2.2 MATERIALS AND METHODS

Materials – [³H] para-aminohipurate (PAH) was purchased from Perkin-Elmer Life and Analytical Sciences (Boston, MA). NHS-SS-biotin and streptavidin-agarose beads were purchased from Pierce Chemical (Rockford, IL). PKC isoform-specific antibodies were from BD biosciences (San Jose, CA). Gö6976 was from LC laboratories (Woburn, MA). All other reagents were from Sigma-Aldrich (St. Louis, MO).

Cell culture – Parental COS-7 cells were grown in DMEM supplemented with 5% fetal bovine serum, penicillin/ streptomycin (100 U/ml), and glucose (100 mg/ml) in a 5% CO₂ atmosphere at 37°C. COS-7 cells stably expressing hOAT1 were maintained in the same medium containing 0.5 mg/ml geneticin (G418; Invitrogen, Carlsbad, CA).

Transport measurement – Cells plated in 48-well plates were treated with each reagent at 37°C for certain time periods as indicated. For each well, uptake solution was added. The uptake solution consisted of phosphate-buffered saline/ $\text{Ca}^{2+}/\text{Mg}^{2+}$ (137 mM NaCl, 2.7 mM KCl, 4.3 mM Na_2HPO_4 , 1.4 mM KH_2PO_4 , 1 mM CaCl_2 , and 1 mM MgCl_2 , pH 7.4) and [^3H]PAH. At the times indicated, the uptake was stopped by aspirating off the uptake solution and rapidly washing the well with ice-cold PBS. The cells were then solubilized in 0.2 N NaOH, neutralized in 0.2 N HCl, and aliquotted for liquid scintillation counting. The uptake count was standardized by the amount of protein in each well. Values are means \pm SE ($n = 3$).

Cell surface biotinylation – Cell surface expression levels of hOAT1 were examined using the membrane-impermeant biotinylation reagent NHS-SS-biotin (Pierce Chemical). The cells were seeded onto six-well plates at 8×10^5 cells per well. After 24 h, the medium was removed and the cells were washed twice with 3 ml of ice-cold PBS, pH 8.0. The plates were kept on ice, and all solutions were kept ice-cold for the rest of the procedure. Each well of cells was incubated with 1 ml of NHS-SS-biotin (0.5 mg/ml in PBS) in two successive 20-min incubations on ice with very gentle shaking. The reagent was freshly prepared for incubation. After biotinylation, each well was briefly rinsed with 3 ml of PBS containing 100 mM glycine and then incubated with the same solution for 20 min on ice to ensure complete quenching of the unreacted NHS-SS-biotin. The cells were then dissolved on ice for 1 h in 400 μl of lysis buffer [10 mM Tris, 150 mM NaCl, 1 mM EDTA, 0.1% SDS, 1% Triton X-100, and protease inhibitors (200 $\mu\text{g}/\text{ml}$ phenylmethylsulfonyl fluoride and 3 $\mu\text{g}/\text{ml}$ leupeptin), pH 7.4]. The unlysed cells were removed by centrifugation at 13,000 rpm at 4°C. Streptavidin-agarose beads (50 μl ; Pierce Chemical) were then added to the supernatant to isolate cell membrane protein. hOAT1 was detected in the pool of surface proteins by polyacrylamide gel electrophoresis and

immunoblotting using an anti-myc antibody (1:500). Myc was tagged at the carboxyl terminus of hOAT1 for its immunodetection.

Subcellular Fractionation – The cells grown on a 100-mm dish were homogenized in isolation buffer (25 mM hepes, pH 7.2, 10% glycerol, 1mM EDTA, 1mM EGTA, 1mM dithiothreitol) containing complete protease inhibitor mixture. The harvested cells were sonicated twice for 10 s each and the cell lysate were then centrifuged at 1000 x g for 10 min at 4 °C to remove unbroken cells. Ultracentrifugation was followed to separate the supernatant into cytosolic and crude membrane fractions at 120,000 x g for 45 min at 4 °C. The particular fraction was resuspended in the same buffer.

Electrophoresis and Western blotting – Protein samples (100 µg) were resolved on 7.5% SDS-PAGE minigels and electroblotted onto polyvinylidene difluoride membranes. The blots were blocked for 1 h with 5% nonfat dry milk in PBS-0.05% Tween, washed, and incubated overnight at 4°C with polyclonal anti-myc antibody (1:500). The membranes were washed and then incubated with goat anti-rabbit IgG conjugated to horseradish peroxidase (1:5,000), and signals were detected using a SuperSignal West Dura extended duration substrate kit (Pierce Chemical).

Data analysis – Each experiment was repeated a minimum of three times. The statistical analysis given was from multiple experiments. Statistical analysis was performed using Student's paired *t*-tests. A *P* value <0.05 was considered significant.

2.3 RESULTS

Effects of Ang II on hOAT1 activity – First, we examined whether treatment with Ang II could affect hOAT1 transport activity in COS-7 cells. Since the hOAT1 expression vector for the current study does not contain the promoter region of hOAT1, the long-term

regulation at the transcriptional level cannot be investigated. We only focused on the short-term regulation of the transporter (within a time frame of 1 h). Ang II induced a time- and concentration-dependent inhibition of PAH uptake (Fig. 1a, 1b). To further examine the mechanism of Ang II-induced inhibition of hOAT1 activity, we determined [^3H]PAH uptake at different substrate concentrations. An Eadie-Hofstee analysis of the derived data (Fig 1c) shows that pretreatment with Ang II resulted in a decreased V_{max} ($0.569 \pm 0.042 \text{ pmol} \cdot \mu\text{g}^{-1} \cdot 3 \text{ min}^{-1}$ with untreated cells and $0.293 \pm 0.011 \text{ pmol} \cdot \mu\text{g}^{-1} \cdot 3 \text{ min}^{-1}$ in the presence of Ang II) with no significant change in the affinity for PAH ($20.2 \pm 1.5 \text{ } \mu\text{M}$ with untreated cells and $18.3 \pm 0.08 \mu\text{M}$ in the presence of Ang II). Determination of the protein concentrations in control cells confirmed that Ang II treatment did not change the total protein content of the cultures (data not shown).

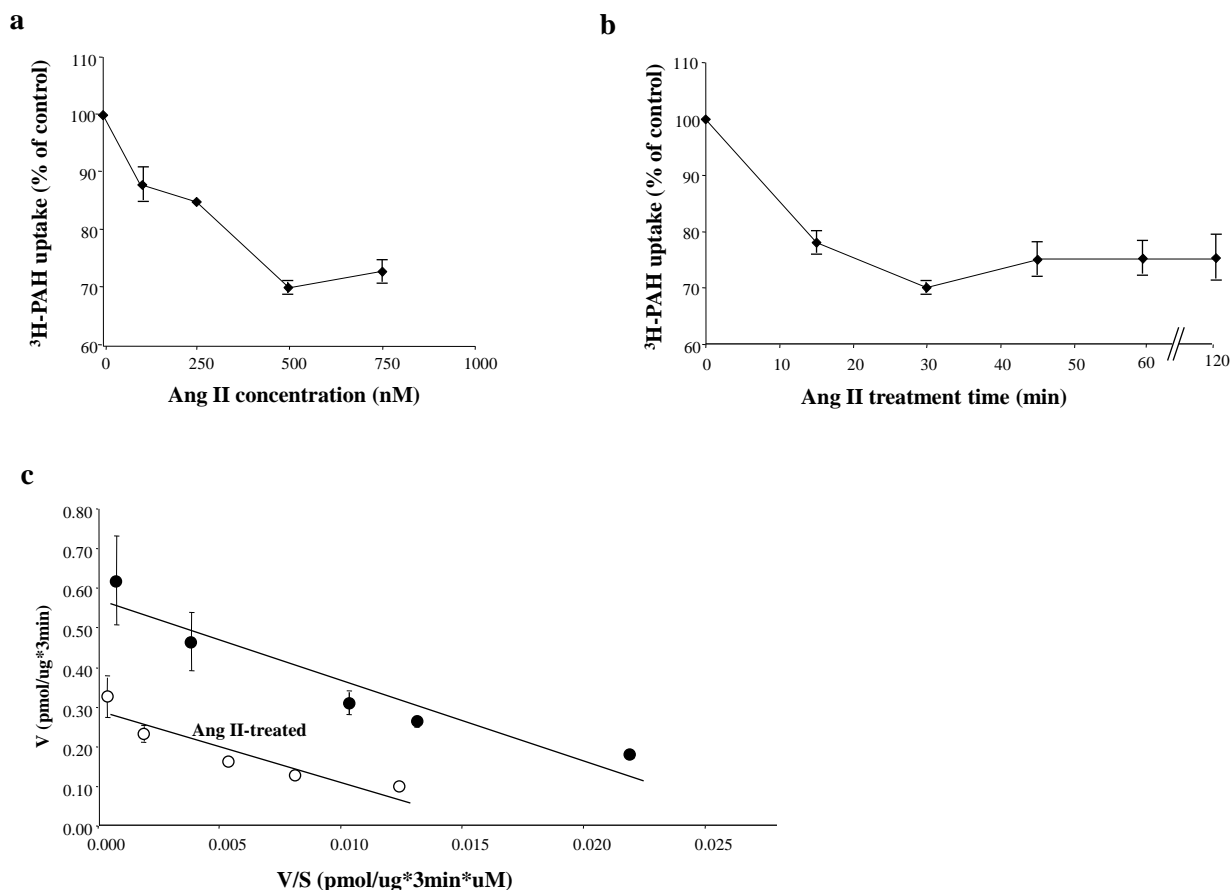


Fig. 1. Effect of Ang II on hOAT1. hOAT1-expressing cells were treated with Ang II at various concentrations (a), or at various periods of time (b), followed by [³H]PAH uptake (3 min, 20 μ M). Uptake activity was expressed as a percentage of the uptake measured in untreated cells. The results represent data from 3 experiments. The uptake values in mock cells (parental COS-7 cells) were subtracted. Values are means \pm SE ($n = 3$). c. Effect of Ang II on the kinetics of PAH transport. COS-7 cells expressing hOAT1 were pretreated with or without Ang II (500 nM) for 30 min, and initial uptake (3 min) of [³H]PAH was measured at 8–800 μ M PAH. The data represent uptake into hOAT1-transfected cells minus uptake into mock cells (parental COS-7 cells). Values are means \pm SE ($n = 3$). V, velocity; S, substrate concentration.

Effects of Ang II on hOAT1 expression – A decreased V_{\max} could be affected by either a reduced number of the transporter at the cell surface or a reduced transporter turnover number (3-6). To differentiate between these possibilities, we determined transporter expression both at the cell surface and in the total cell lysates. We showed that Ang II treatment resulted in a reduced cell surface expression of hOAT1 without affecting the total cell expression of the transporter (Fig. 2).

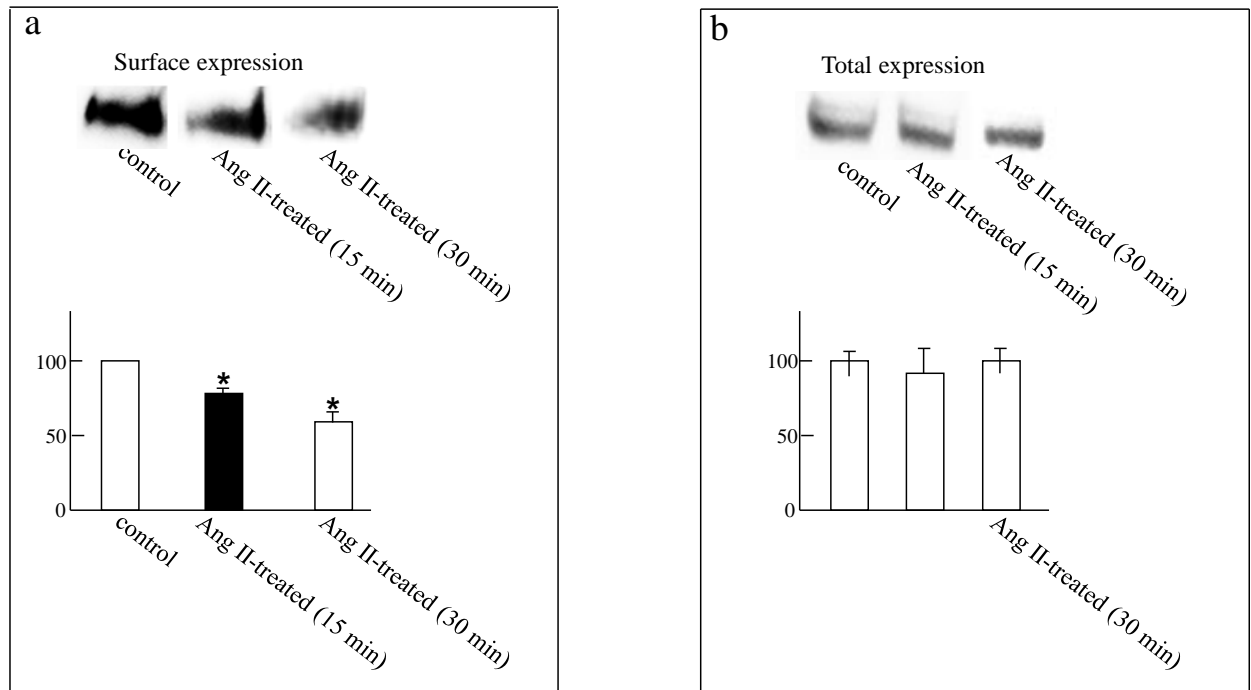


Fig. 2 Effect of Ang II on cell surface and total cell expression of hOAT1. *A:* Western blot analysis of cell surface expression of hOAT1 in cells treated with or without Ang II (500 nM, 30 min). *Top:* Cos 7 Cells stably expressing hOAT1 were biotinylated, and the labeled cell surface proteins were precipitated with streptavidin beads and separated by SDS-PAGE, followed by Western blotting with anti-myc antibody (1:500). *Bottom:* the intensity of the transporter expression from the experiment shown at *top* and other experiments was quantified. * $P < 0.05$, significantly different from untreated cells. *B:* Western blot analysis of total cell expression of hOAT1 in cells treated with or without Ang II (500 nM, 30 min). *Top:* total cell expression of hOAT1 in cells treated with or without Ang II (500 nM, 30 min). Cells were lysed, and their proteins were separated by SDS-PAGE, followed by Western blotting with anti-myc antibody. *Bottom:* the intensity of the transporter expression from the experiment shown at *top* and other experiments was quantified.

Ang II regulation of hOAT1 activity through PKC – Ang II was shown to exert its effects through PKC. To determine whether Ang II regulates hOAT1 function through PKC, we treated hOAT1-expressing COS-7 cells with Ang II in the presence of staurosporine, a general PKC inhibitor. As shown in Fig. 3, staurosporine efficiently reversed the inhibitory effect of Ang II on hOAT1 activity.

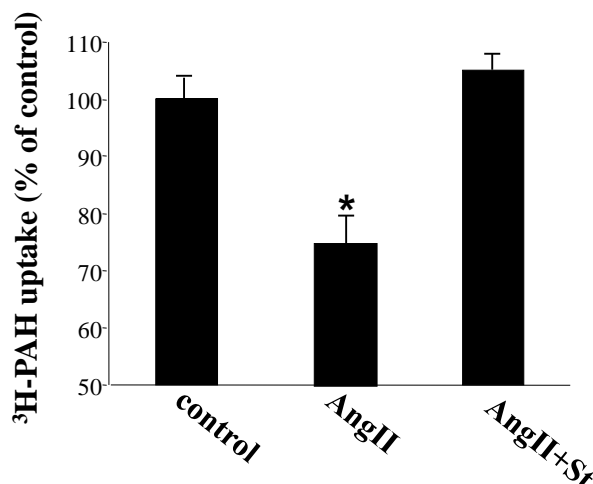


Fig. 3. Effect of PKC inhibitor staurosporine on Ang II-induced inhibition of hOAT1 activity. hOAT1-expressing cells were pretreated with staurosporine (2 μ M, 5 min) followed by incubation with Ang II (500 nM, 30 min) in the presence or absence of staurosporine (2 μ M). The uptake of [³H]PAH (3 min, 20 μ M) was then performed. The results represent data from three experiments. The uptake values in mock cells (parental COS-7 cells) were subtracted. Values are mean \pm SE ($n = 3$).

Identification of PKC isoforms involved in Ang II effect on hOAT1 – The PKC isoforms are divided into three categories based upon the cofactors that are required for optimal catalytic activity. Conventional PKCs (α , β , and γ) are calcium-dependent and are stimulated by a second messenger, diacylglycerol. Novel PKCs (δ , ϵ , ζ , and θ) are also activated by diacylglycerol but are calcium-independent. Typical PKCs (ζ and λ) require neither calcium nor diacylglycerol for optimal activity. Although most cells express more than one type of PKC, differences among the isoforms with respect to activation conditions and subcellular locations suggest that individual PKC isoforms mediate distinct cellular processes in a cell type-dependent manner. In COS-7 cells, it was shown that PKC α , PKC δ , PKC ζ and PKC ϵ were abundantly expressed (7). Our Western blotting (Fig. 4) showed that in contrast to other PKC isoforms, treatment of cells with Ang II resulted in a significant translocation of PKC α from cytosol to membrane fraction.

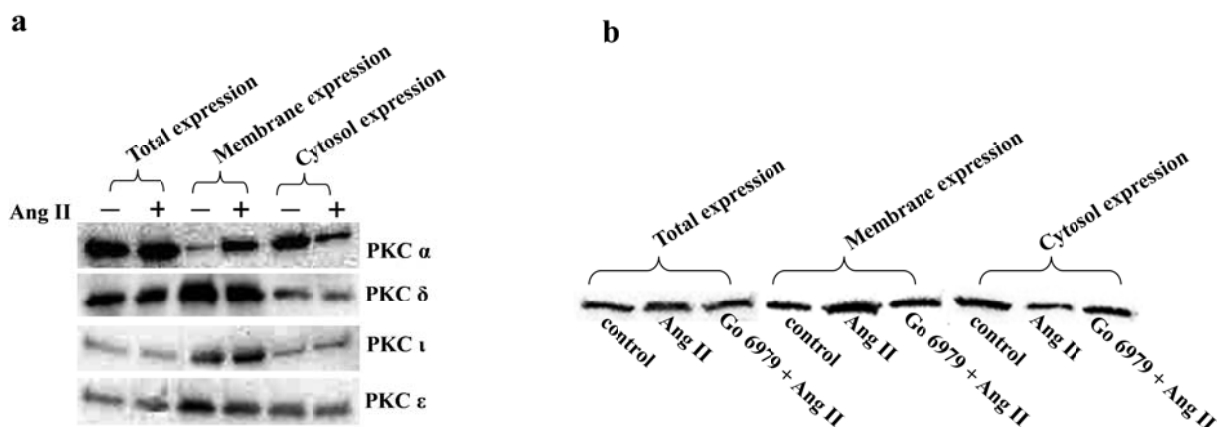


Fig. 4. Identification of PKC isoforms involved in Ang II effect on hOAT1. A: Western blot analysis of subcellular fraction expression of hOAT1 in cells treated with or without Ang II (500 nM, 30 min). COS-7 Cells stably expressing hOAT1 treated with or without Ang II were lysed and fractionated into crude membrane and cytosol, and the proteins were separated by SDS-PAGE, followed by Western blotting with PKC isoforms specific antibodies. Total cell lysate was also prepared. B: the intensity of the transporter expression from the experiment shown at top and other experiments was quantified. * $P < 0.05$, significantly different from untreated cells.

Ang II regulation of hOAT1 activity through PKC α – The involvement of PKC α in Ang II regulation of hOAT1 was investigated through functional assay. We treated hOAT1-expressing COS-7 cells with Ang II in the presence of Gö6976, a PKC α -specific inhibitor (8). As shown in Fig. 5, Gö6976 efficiently reversed the inhibitory effect of Ang II on hOAT1 activity.

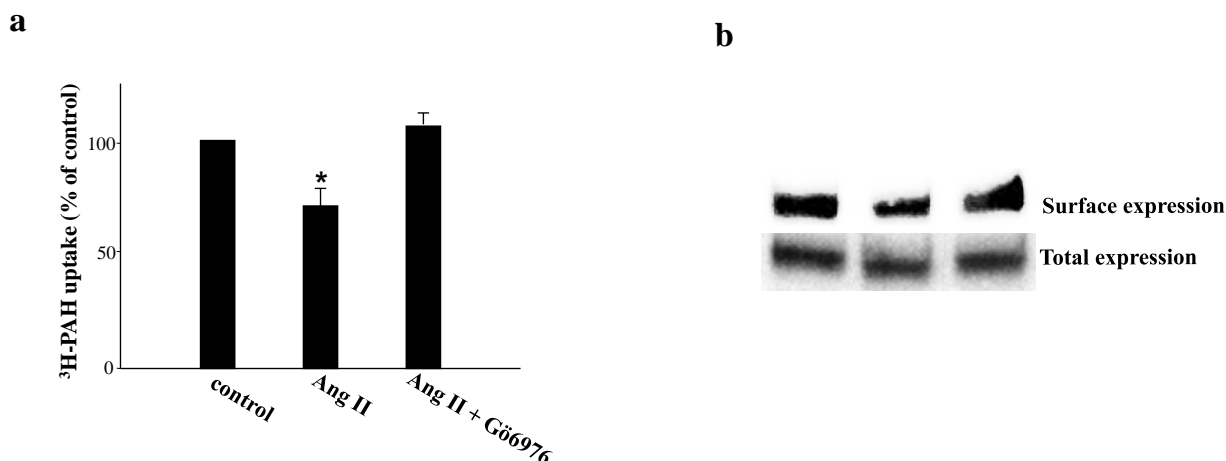


Fig. 5. Effect of PKC α specific inhibitor Gö6976 on Ang II-induced inhibition of hOAT1 activity. hOAT1-expressing cells were pretreated with Gö6976 (1 μ M, 20 min) followed by incubation with Ang II (500 nM, 30 min). The uptake of [3 H]PAH (3 min, 20 μ M) was then performed. The results represent data from three experiments. The uptake values in mock cells (parental COS-7 cells) were subtracted. Values are mean \pm SE (n = 3).

Conclusion on regulation of OATs by Ang II – In the current study, we examined the regulation of hOAT1 by angiotensin II (Ang II) in kidney COS-7 cells. Ang II induced a concentration- and time-dependent inhibition of hOAT1 transport activity. Such inhibition mainly resulted from a decreased cell surface expression without a change in total cell expression of the transporter, kinetically revealed as a decreased V_{\max} without significant change in K_m . Ang II-induced inhibition of hOAT1 activity could be prevented by treating hOAT1-expressing cells with staurosporine, a general PKC inhibitor. To obtain further information on which PKC isoform mediates Ang II regulation of hOAT1 activity, cellular distribution of various PKC isoforms were examined in cells treated with or without Ang II. We showed that Ang II treatment resulted in a significant translocation of PKC α from cytosol to membrane, and such translocation was blocked by treating hOAT1-expressing cells with Gö6976, a PKC α -specific inhibitor. We further showed that Ang II-induced inhibition of hOAT1 activity and retrieval of hOAT1 from cell surface could also be

prevented by treating hOAT1-expressing cells with Gö6976. We concluded that Ang II inhibited hOAT1 activity through activation of PKC α , which led to the redistribution of the transporter from cell surface to the intracellular compartments.

It is shown (9) that in rats with bilateral ureteral obstruction (BUO), elimination of drugs was impaired partly due to a redistribution of OAT1 from cell surface to intracellular compartment. BUO is a serious and common clinical condition, and an important cause of acute renal failure (9, 10). In BUO, angiotensin II has elevated level of expression (10-12). Therefore, angiotensin II may affect OAT1 cellular distribution through such signaling pathway. Our current studies may provide important insight into the molecular, cellular, and clinical bases underlying BUO.

Effects of BK on hOAT3 Activity – We examined whether treatment with BK could affect hOAT3 transport activity in COS-7 cells. Since the hOAT3 expression vector used in the current study does not contain the promoter region of hOAT3, the long-term regulation at the transcriptional level cannot be investigated. We only focused on the short-term regulation of the transporter (within a time frame of 2 hr). BK induced a concentration-dependent regulation of [3 H] estrone sulfate uptake with the concentration of maximum stimulation at 500 nM (Fig. 6a). At this concentration, we observed a time-dependent stimulation of estrone sulfate uptake (Fig. 6b), with maximum stimulation after 30 min treatment. To examine the mechanism of BK-induced stimulation of hOAT3 activity, we determined [3 H] estrone sulfate uptake at different substrate concentrations. An Eadie-Hofstee analysis of the derived data (Fig. 7) showed that pretreatment with BK resulted in an increased V_{\max} (0.015 ± 0.001 pmol $\cdot\mu\text{g}^{-1}\cdot\text{min}^{-1}$ with untreated cells and 0.020 ± 0.001 pmol $\cdot\mu\text{g}^{-1}\cdot\text{min}^{-1}$ in the presence of BK) with no significant change in the affinity (K_m) for estrone sulfate (5.09 ± 0.27 μM with untreated cells and 4.81 ± 0.31 μM in the presence of BK). The K_m of hOAT3 for estrone sulfate determined in our system is

comparable to that obtained from other systems (13). Determination of the protein concentrations in control cells confirmed that BK treatment did not change the total protein content of the cultures (data not shown).

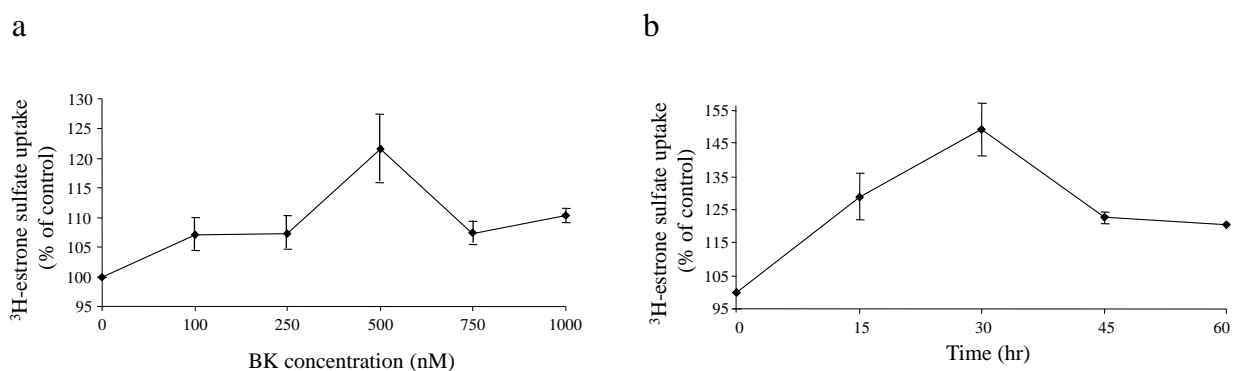


Fig. 6. Effect of BK on hOAT3. hOAT3-expressing cells were treated with BK at various concentrations (a), or at various periods of time (b), followed by [³H] estrone sulfate uptake (4 min, 100 nM). Uptake activity was expressed as a percentage of the uptake measured in untreated cells. The results represent data from 3 experiments. The uptake values in mock cells (parental COS-7 cells) were subtracted. Values are means \pm SE ($n = 3$).

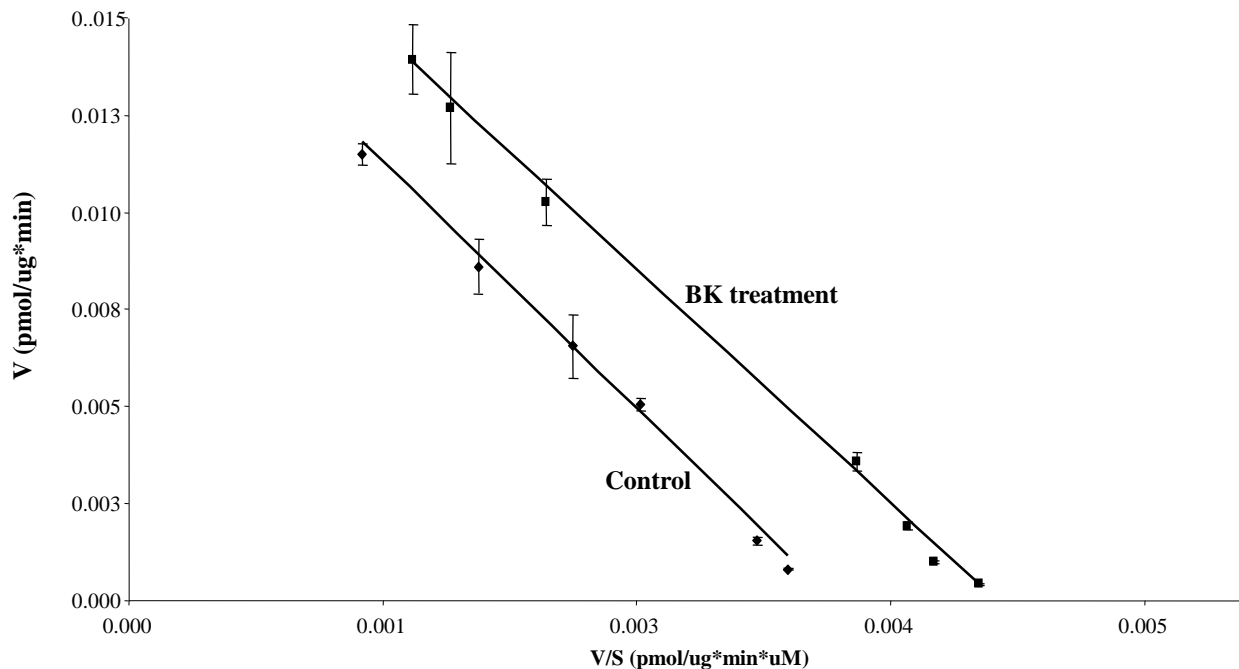


Fig. 7. Effect of BK on the kinetics of estrone sulfate transport. COS-7 cells expressing hOAT3 were pretreated with or without BK (500 nM) for 30 min, and initial uptake (4 min) of [³H] estrone sulfate was measured at 0.1–10 μ M estrone sulfate. The data represent uptake into hOAT3-transfected cells minus

uptake into mock cells (parental COS-7 cells). Values are means \pm SE ($n = 3$). V, velocity; S, substrate concentration.

Effect of BK on hOAT3 Expression – An increased V_{\max} could be affected by either an increased number of the transporter at the cell surface or an increased transporter turnover number. Experiments that differentiate between these possibilities were conducted by measuring transporter expression both at the cell surface and in the total cell lysates. We showed that BK treatment resulted in an increased cell surface expression of hOAT3 without affecting the total cell expression of the transporter (Fig. 8).

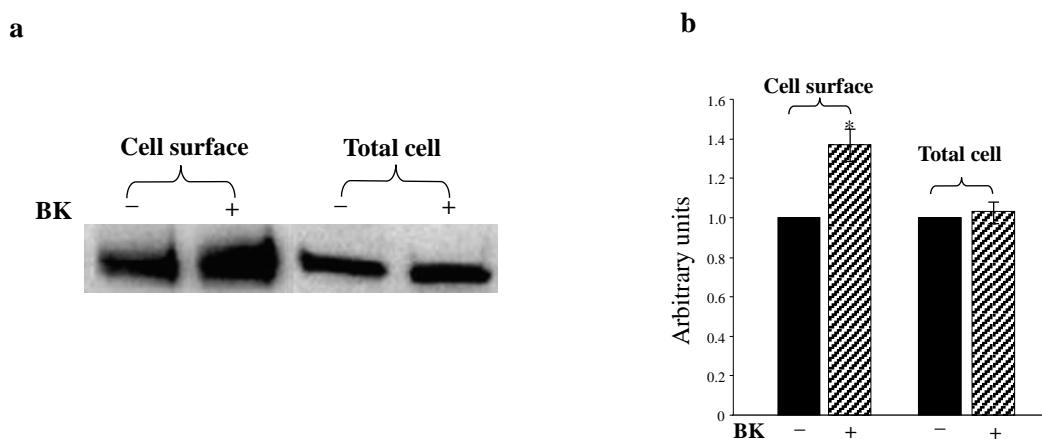


Fig. 8. Effect of BK on cell surface and total cell expression of hOAT3. a. Western blot analysis of total cell expression and cell surface expression of hOAT3. COS-7 cells stably expressing hOAT3 were treated with or without BK (500 nM for 30 min). The lysed cell proteins, or the biotinylated, and the labeled cell surface proteins were precipitated with streptavidin beads and separated by SDS-PAGE, followed by Western blotting with anti-myc antibody (1:500). b. Densitometry analyses of the transporter expression from the experiment shown in Fig. 3a and other experiments. * $P < 0.05$.

BK Regulation of hOAT3 Activity through Protein Kinase C (PKC) – hOAT3-expressing COS-7 cells were treated with BK in the presence of staurosporine, a general inhibitor for PKC. As shown in Fig. 9, staurosporine efficiently reversed the stimulating effect of BK on hOAT3 activity.

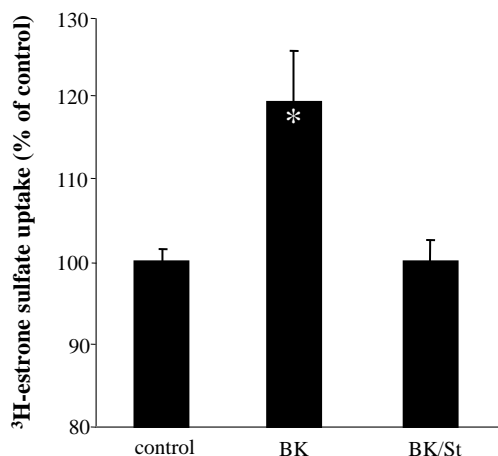


Fig. 9. Effect of inhibitor for PKC on BK-induced stimulation of hOAT3 activity. hOAT3-expressing cells were pretreated with staurosporine (St, 2 μ M, 5 min, a PKC inhibitor) followed by incubation with BK (500 nM, 30 min) in the presence or absence of staurosporine (St, 2 μ M). The uptake of [³H] estrone sulfate (4 min, 100 nM) was then performed. The results represent data from three experiments. The uptake values in mock cells (parental COS-7 cells) were subtracted. Values are mean \pm SE ($n = 3$).

Identification of PKC Isoforms Involved in BK Effect – COS-7 cells have been shown to express several PKC isoforms including PKC α , PKC ϵ , PKC δ , PKC ζ , and PKC ι (Chen and Exton, 2004). Our results showed that, among all these PKC isoforms, treatment of cells with BK resulted in a significant translocation of PKC δ , PKC ζ and PKC ϵ from cytosol to membrane fraction (Fig. 10). We further showed, through co-immunoprecipitation experiments, that BK enhanced the association of hOAT3 with PKC δ , PKC ζ and PKC ϵ (Fig. 11). Finally, BK-induced stimulation of hOAT3 activity was prevented by pretreating the cells with each of the PKC isoform-specific inhibitors (Fig. 12). These results confirm the involvement of PKC δ , PKC ζ and PKC ϵ in the action of BK on hOAT3.

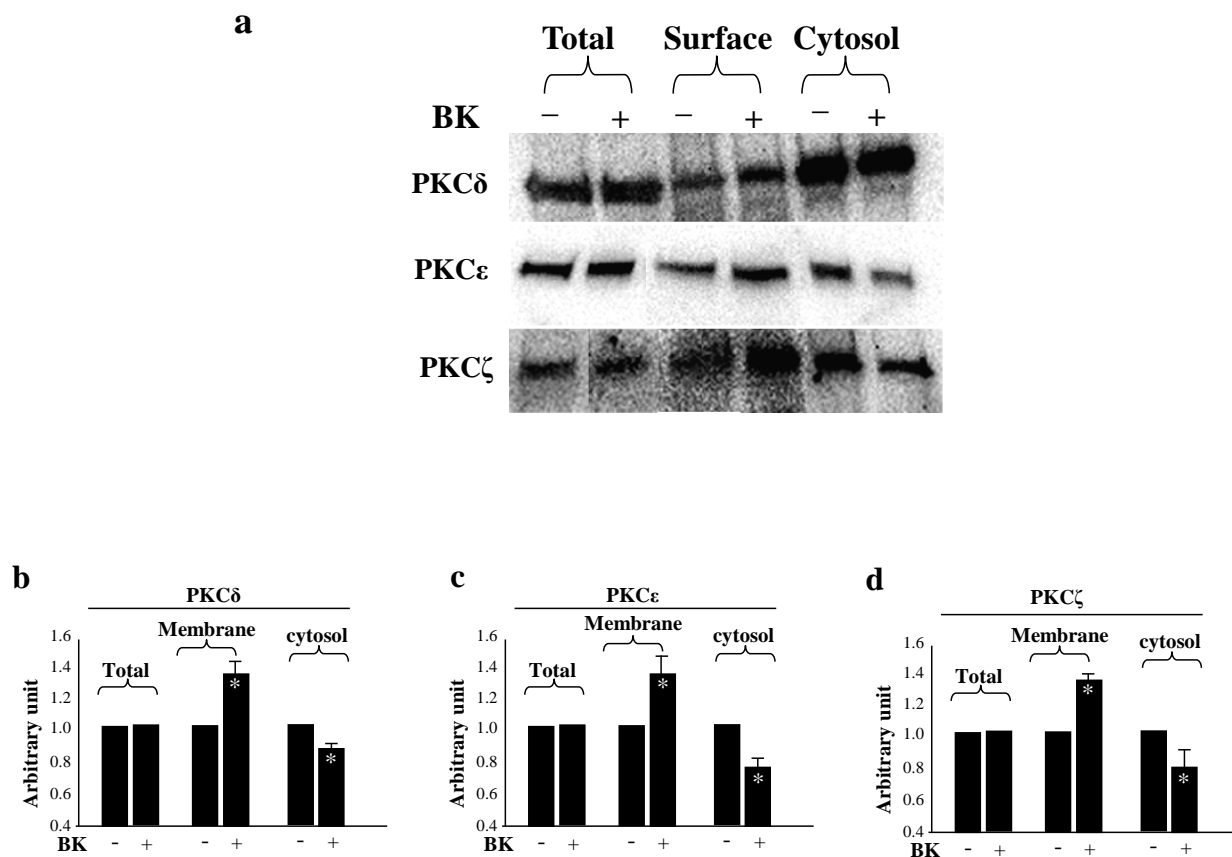


Fig. 10. Western blot analyses of subcellular fraction expression of PKC isoforms in cells treated with or without BK. COS-7 cells stably expressing hOAT3 treated with or without BK (500 nM, 30 min) were lysed and fractionated into crude membrane and cytosol, and the proteins were separated by SDS-PAGE, followed by Western blotting with PKC isoform-specific antibodies. Total cell lysate was also prepared. Only the PKC isoforms that showed translocations are shown here.

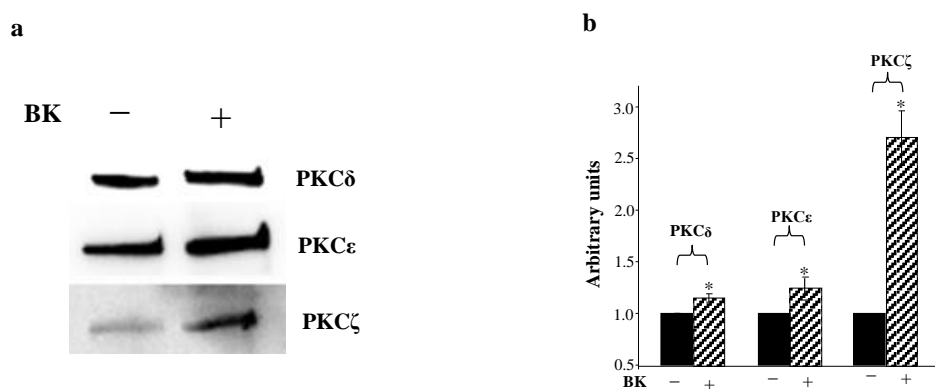


Fig. 11. Effect of BK on the association of hOAT3 with PKCδ, PKCζ and PKCε. a, Co-immunoprecipitation of hOAT3 with PKC isoforms. COS-7 cells expressing hOAT3 were lysed in 0.5–1% Triton X-100 and subjected to immunoprecipitation with anti-myc antibody, followed by immunoblotting with

PKC isoform-specific antibodies. *b*, Densitometry analyses of results in Fig. 6a as well as other experiments. * $P < 0.05$.

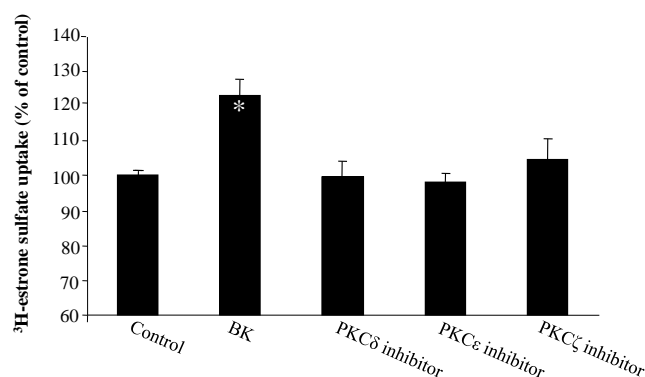


Fig. 12. Effect of PKC α specific inhibitor Gö6976 on Ang II-induced inhibition of hOAT1 activity. hOAT1-expressing cells were pretreated with Gö6976 (1 μ M, 20 min) followed by incubation with Ang II (500 nM, 30 min). The uptake of [³H]PAH (3 min, 20 μ M) was then performed. The results represent data from three experiments. The uptake values in mock cells (parental COS-7 cells) were subtracted. Values are mean \pm SE ($n = 3$).

Conclusion of regulation of OAT by BK – In the current study, we examined the regulation of hOAT3 by peptide hormone bradykinin (BK) in COS-7 cells. BK (≤ 500 nM) induced a concentration- and time-dependent stimulation of hOAT3 activity, kinetically revealed as an increased V_{\max} . Such an increase in V_{\max} resulted from an increased cell surface expression without a change in total cell expression of the transporter. BK-induced stimulation of hOAT3 activity could be prevented by treating hOAT3-expressing cells with staurosporine, a general inhibitor for protein kinase C (PKC). To obtain further information on which PKC isoform mediates BK regulation of hOAT3 activity, cellular distribution of various PKC isoforms was examined in cells treated with BK. We showed that BK treatment resulted in a significant translocation of PKC δ , PKC ϵ and PKC ζ from cytosol to membrane. We further showed that BK treatment enhanced association of hOAT3 with PKC δ , PKC ϵ and PKC ζ and that isoform-specific inhibitor for PKC δ , PKC ϵ and PKC ζ reversed BK effect on hOAT3 activity. We therefore concluded that BK

stimulated hOAT3 activity through activation of PKC δ , PKC ϵ and PKC ζ , which then led to the redistribution of hOAT3 from the intracellular compartments to the cell surface and to the up-regulation of hOAT3 activity.

2.4 REFERENCES

1. Shuprisha A, Lynch RM, Wright SH, and Dantzler WH. PKC regulation of organic anion secretion in perfused S2 segments of rabbit proximal tubules. *American journal of physiology* 278: F104-109, 2000.
2. Gekle M, Mildenberger S, Sauvant C, Bednarczyk D, Wright SH, and Dantzler WH. Inhibition of initial transport rate of basolateral organic anion carrier in renal PT by BK and phenylephrine. *The American journal of physiology* 277: F251-256, 1999.
3. Anderson GM and Horne WC. Activators of protein kinase C decrease serotonin transport in human platelets. *Biochimica et biophysica acta* 1137: 331-337, 1992.
4. Hong M, Zhou F, and You G. Critical amino acid residues in transmembrane domain 1 of the human organic anion transporter hOAT1. *The Journal of biological chemistry* 279: 31478-31482, 2004.
5. Kilic F, Murphy DL, and Rudnick G. A human serotonin transporter mutation causes constitutive activation of transport activity. *Molecular pharmacology* 64: 440-446, 2003.
6. Vayro S and Silverman M. PKC regulates turnover rate of rabbit intestinal Na⁺-glucose transporter expressed in COS-7 cells. *The American journal of physiology* 276: C1053-1060, 1999.
7. Chen JS and Exton JH. Regulation of phospholipase D2 activity by protein kinase C alpha. *The Journal of biological chemistry* 279: 22076-22083, 2004.
8. Sampson SR, Lupowitz Z, Braiman L, and Zisapel N. Role of protein kinase Calpha in melatonin signal transduction. *Molecular and cellular endocrinology* 252: 82-87, 2006.
9. Villar SR, Brandoni A, Anzai N, Endou H, Torres AM. Altered expression of rat renal cortical OAT1 and OAT3 in response to bilateral ureteral obstruction. *Kidney Int* 68: 2704-2713, 2005.
10. Klahr S. *The kidney physiology and pathophysiology* (3rd ed). Edited by Seldin DW and Giebisch G. Philadelphia, PA: Lippincott Williams and Wilkins, 2000, p. 2473-2512.
11. Klahr S. Obstructive nephropathy. *Kidney international* 54: 286-300, 1998.
12. Klahr S and Morrissey J. Obstructive nephropathy and renal fibrosis. *American journal of physiology* 283: F861-875, 2002.
13. Cha SH, Sekine T, Kusuvara H, Yu E, Kim JY, Kim DK, Sugiyama Y, Kanai Y, and Endou H. Molecular cloning and characterization of multispecific organic anion transporter 4 expressed in the placenta. *The Journal of biological chemistry* 275: 4507-4512, 2000.

Chapter 3. Regulation of OATs by ubiquitination

3.1 Introduction

The amount of OATs at the cell surface is critical for their drug transport activity. Although once considered static resident plasma membrane proteins, a growing body of evidence demonstrated that many transporters undergo internalization from and recycling back to cell surface constitutively or in response to stimuli. Abnormal membrane trafficking of the transporters is the key cause for many clinical syndromes. We have recently shown that members of OAT family constitutively internalize from and recycle back to cell surface, and that inhibition of OAT activity by activation of PKC results from an accelerated internalization of these transporters from cell surface to intracellular compartments (1). However, the mechanisms of PKC effect on OAT internalization and function are largely unknown. PKC-induced direct phosphorylation has been reported for other membrane proteins. However, our results showed that a range of PKC activators failed to elevate the phosphorylation level of OATs under various experimental conditions (2). This suggests that direct phosphorylation of OATs is unlikely to be the cause for PKC-induced inhibition of OAT activity.

Recently, modification of receptors and channels by ubiquitin conjugation has emerged as the major regulatory mechanism of internalization, intracellular sorting, and turnover of these membrane proteins. Ubiquitin moieties can be recognized by the components of plasma membrane internalization and endosomal sorting machinery.

Ubiquitin is a highly conserved polypeptide of 76 amino acids. Ubiquitination occurs in a sequence of three enzymatic steps. The initial step is the formation of a thioester bond between the COOH terminus of ubiquitin and the active cysteine residue of an

ubiquitin-activating enzyme (E1). Next, the activated ubiquitin is transferred to an ubiquitin-conjugating enzyme (E2). The E2 enzymes are catalytically similar to E1 in that a thioester bond is formed with ubiquitin. The third and last step in ubiquitination is a reaction catalyzed by an ubiquitin-protein ligase (E3) in which an isopeptide bond between the COOH-terminal glycine of ubiquitin and the amino group of a lysine (K) residue on the target protein is formed. It is the E3 that is responsible for substrate recognition. An ubiquitin molecule itself has seven lysine residues (K6, K11, K27, K29, K33, K48, and K63) that can serve as a base for chain elongation. Therefore, a substrate can be modified by different types of ubiquitin conjugation: monoubiquitination (conjugation of one single ubiquitin to one single lysine on the substrate), multiubiquitination (conjugation of several monoubiquitin molecules to multiple lysine residues on the substrate), and polyubiquitination (extended polyubiquitin chain). In addition, a polyubiquitin chain can bear different linkages such as K48 linkage (K48 in the ubiquitin serves as a base for chain elongation) and K63 linkage (K63 in the ubiquitin serves as a base for chain elongation). It has been shown that different type and linkage of ubiquitination have different physiologic outcome for the ubiquitinated substrate.

Recent evidences have shown that proteins that are ubiquitinated in the plasma membrane are internalized into early endosomes, where these proteins are then either deubiquitinated by deubiquitinating enzymes and recycle back to the plasma membrane or, via interactions with the endosomal sorting complexes required for transport machinery, are sorted to late endosomes, and ultimately, to the lysosomes for degradation. Thus, the balance between ubiquitination, mediated by E3 ligases and deubiquitination, mediated by deubiquitinating enzymes (DUB), regulates the plasma membrane abundance of membrane proteins. Fig. 2 depicts a simplified model for

ubiquitination-regulated endocytic trafficking of cell surface proteins. In this part of the thesis, we examined whether PKC regulates OATs activity through ubiquitinating these transporters.

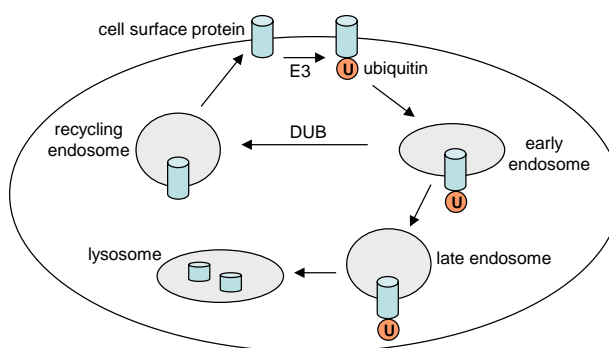


Fig. 1. Simplified model for ubiquitination-regulated endocytic trafficking of cell surface proteins.

3.2 Materials and methods

Materials – Membrane impermeable biotinylation reagent NHS-SS-biotin and streptavidin agarose beads were purchased from Pierce (Rockford, IL). COS-7 cells and Dynamin-2/K44A mutant were purchased from American Type Culture Collection (Manassas, VA). cDNA for HA-tagged mutant ubiquitin HA-Ub Δ G was generously provided by Dr. N. Tony Eissa, Department of Medicine, Baylor College of Medicine, Houston, TX, USA. cDNAs for HA-tagged wild type ubiquitin and HA-tagged ubiquitin mutants HA-K48R and HA-K63R were generously provided by Dr. Cam Patterson, Carolina Cardiovascular Biology Center, University of North Carolina, Chapel Hill, North Carolina, USA. Mouse anti-myc antibody (9E10) and mouse anti-HA antibody 12CA5 were purchased from Roche Diagnostics Corporation (Indianapolis, IN). Mouse anti-ubiquitin antibody P4D1 was purchased from Santa Cruz Biotechnology (Santa Cruz, CA). Mouse anti-ubiquitin antibody FK2 was purchased from Enzo Life Sciences (Farmingdale, NY). PKC activator Phorbol 12-myristate

13-acetate (PMA) and all other reagents were purchased from Sigma (St. Louis, MO).

Cell cultures – COS-7 cells stably expressing human OAT1 (tagged with epitope myc at its carboxyl terminus for immuno-detection) (Zhang et al., 2008) were maintained in DMEM medium supplemented with 0.2 mg/ml G418, 10 % fetal bovine serum, penicillin/streptomycin (100 U/ml), and glucose (100 mg/ml).

Ubiquitination Assay – Cells expressing OAT1-myc were treated with DMSO or 1 μ M PMA at 37 °C for indicated time periods. Treated cells were lysed with lysis buffer I (50 mM Tris-HCl, pH 8.0, 150 mM NaCl, 1% Triton X-100, 10% glycerol, 5 mM EDTA, and 1 mM NaF) freshly added with 1% of proteinase inhibitor cocktail and 20 mM *N*-ethylmaleimide (NEM, deubiquitination inhibitor). OAT1 was then immunoprecipitated with anti-myc antibody, followed by immunoblotting with anti-ubiquitin antibody P4D1 or anti-myc antibody 9E10.

Preparation of rat kidney slices – Male Sprague Dawley rats were euthanized by CO₂ inhalation, and the kidneys were immediately placed into freshly oxygenated ice-cold saline. Tissue slices (<0.5 mm; 5-10 mg wet weight) were cut with a Stadie-Riggs microtome and maintained in ice-cold modified Cross and Taggart saline (95 mM NaCl, 80 mM mannitol, 5 mM KCl, 0.74 mM CaCl₂, and 9.5 mM Na₂PO₄, pH 7.4) for ubiquitination studies.

Cell Surface Biotinylation – Cell surface expression level of OAT1 was examined using the membrane-impermeable biotinylation reagent, NHS-SS-biotin. Cells were plated in six-well plates. Each well of cells was incubated with 1 ml of NHS-SS-biotin (0.5 mg/ml in PBS) in two successive 20 min incubations on ice with very gentle shaking. The reagent was freshly prepared each time. After biotinylation, each well was briefly rinsed with 3 ml of PBS/CM containing 100 mM glycine then incubated with the same solution for 30 min on ice, to ensure complete quenching of the unreacted NHS-SS-biotin. The cells were then lysed on ice for 1 h in 400 μ l of lysis buffer (10 mM Tris, 150 mM NaCl, 1 mM EDTA, 0.1 % SDS, 1%

Triton-X 100 with 1/100 protease inhibitor cocktail). The cell lysates were cleared by centrifugation at 16,000 x g at 4°C. 50 µl of streptavidin-agarose beads were then added to the supernatant to isolate cell membrane proteins. OAT1 was detected in the pool of surface proteins by immunoblotting using an anti-myc antibody 9E10.

To determine ubiquitinated OAT1 in the biotinylated protein fraction, cell surface proteins were biotinylated. OAT1 was immunoprecipitated with anti-myc antibody. Immunoprecipitated proteins were eluted from the beads with 1% SDS (37 °C, 15 min). Next, SDS was diluted to 0.1%, and the eluted OAT1 proteins were incubated with streptavidin-agarose beads, followed by immunoblotting using anti-ubiquitin antibody P4D1 or anti-myc antibody.

Internalization Assay – We followed the procedure previously established in our lab (Zhang et al., 2008). OAT1-expressing cells underwent biotinylation with 0.5 mg/ml sulfo-NHS-SS-biotin at 4 °C. Following biotinylation, OAT1 internalization was initiated by incubating the cells (37 °C) in PBS containing either 1 µM PMA or vehicle for designated periods of time. Residual cell surface biotin was stripped by incubating cells three times for 20 min with freshly prepared 50 mM MesNa in NT buffer (150 mM NaCl, 1 mM EDTA, 0.2% bovine serum albumin, 20 mM Tris, pH 8.6). Cells were lysed in lysis buffer with protease inhibitor cocktail. Biotinylated (internalized) proteins were separated from nonbiotinylated proteins by streptavidin pull-down from equivalent amounts of cellular proteins, followed by immunoblotting with anti-myc antibody.

Purification of ubiquitinated OAT1 by sequential immunoprecipitation – Six 10-cm-diameter dishes of COS-7 cells expressing OAT1 were treated with 1µM PMA for 30 min at 37 °C. Treated cells were solubilized with lysis buffer I with 3% proteinase inhibitor cocktail and 40 mM NEM. Total cell lysate was pre-cleared with protein G-agarose for 2 h at 4°C, followed

by immunoprecipitation with anti-myc antibody that was cross-linked to protein G beads with dimethyl pimelimidate (Pierce). After extensive wash with lysis buffer I containing 500 mM NaCl, the immunoprecipitated proteins were eluted with 1% SDS and immunoprecipitated again with anti-ubiquitin antibody FK2 that was cross-linked to protein G beads with dimethyl pimelimidate. After the second immunoprecipitation, 10% of precipitated proteins were analyzed by immunoblotting with anti-ubiquitin antibody P4D1 or anti-myc antibody and 90% by Coomassie blue staining.

Protein identification by LC-MS/MS – The gel bands of interest were reduced, carboxymethylated with iodoacetamide, digested with trypsin. Peptides were extracted, solubilized in 0.1% trifluoroacetic acid, and analyzed by nanoLC-MS/MS using a RSLC system (Dionex, Sunnyvale CA) interfaced with a Velos-LTQ-Orbitrap (ThermoFisher, San Jose, CA). Samples were loaded onto a self-packed 100 μ m x 2 cm trap packed with Magic C18AQ, 5 μ m 200 A (Michrom Bioresources Inc, Auburn, CA) and washed with Buffer A (0.2% formic acid) for 5 min with flow rate of 10 μ L/min. The trap was brought in-line with the homemade analytical column (Magic C18AQ, 3 μ m 200 A, 75 μ m x 50cm) and peptides were fractionated at 300 nL/min with a 90 min linear gradient of 2 to 45% Buffer B (0.2% formic acid, acetonitrile). Mass spectrometry data were acquired using a data-dependent acquisition procedure with a cyclic series of a full scan acquired in Orbitrap with resolution of 60,000 followed by MSMS scans (acquired in linear ion trap) of 20 most intense ions with a repeat count of two and the dynamic exclusion duration of 60 sec.

The LC-MS/MS data were searched against the ENSEMBL human database using a local version of the Global Proteome Machine (GPM USB, Beavis Informatics Ltd, Winnipeg, Canada) with carbamidoethyl on cysteine as fixed modification and ubiquitination on lysine (+114 Da) as well as oxidation of methionine and tryptophan as variable modifications using a 10 ppm precursor ion tolerance and a 0.4 Da fragment ion tolerance. Polyubiquitin sites

were identified on ubiquitin lysine residues.

Site-directed Mutagenesis – Mutant transporters were generated by site-directed mutagenesis using human OAT1-*myc* as a template. hOAT1-*myc* contains a 10-amino acid c-*myc* tag at the C terminus of hOAT1. Previous studies from our laboratory (1) showed that the *myc*-tagged protein retained the functional properties of the native (unmodified) structure. The mutant sequence was confirmed by the dideoxy chain termination method.

Electrophoresis and Immunoblotting – Protein samples were resolved on 7.5% SDS-PAGE minigels and electroblotted on to PVDF membranes. The blots were blocked for 1 hour with 5% nonfat dry milk in PBS-0.05% Tween-20, washed, and incubated for 1 hour at room temperature with appropriate primary antibodies followed by horseradish peroxidase-conjugated secondary antibodies. The signals were detected by SuperSignal West Dura Extended Duration Substrate kit (Pierce, Inc., Rockford, IL). Nonsaturating, immunoreactive protein bands were quantified by scanning densitometry with FluorChem 8000 imaging system (Alpha Innotech Corporation, San Leandro, CA).

Data Analysis – Each experiment was repeated a minimum of three times. The statistical analysis was from multiple experiments. Statistical analysis was performed using Student's paired *t* tests. A *p* value of <0.05 was considered significant.

3.3 Results

PKC-induced ubiquitination of OAT1 by endogenous ubiquitin – To examine whether OAT1 undergoes ubiquitination, COS-7 cells stably expressing OAT1 were treated with or without PMA, a PKC activator, for different periods of time. OAT1 was then immunoprecipitated by anti-*myc* antibody (*myc* was tagged to OAT1), followed by immunoblotting with anti-ubiquitin antibody. As shown in Fig. 2, OAT1 ubiquitination was

barely detectable under the basal condition. Interestingly, PMA treatment induced a time-dependent ubiquitination of the transporter with maximum ubiquitination around 15-30 min. Moreover, when the immunoblot was reprobed with anti-myc antibody, it was shown that these short-term treatments did not produce any major change in the amount of OAT1 (not shown).

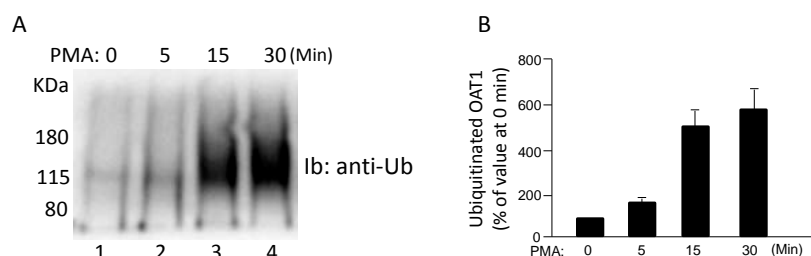


Fig. 2. Time dependence of PMA-induced OAT1 ubiquitination in COS-7 cells. (A) OAT1-expressing COS-7 cells were treated with PKC-activator PMA (1 mM) for the time periods as indicated. Treated cells were then lysed, and OAT1 was immunoprecipitated with anti-myc antibody, followed by immunoblotting (lb) with anti-ubiquitin antibody. (B) densitometry plot of results from (A) as well as from other experiments. The values are mean \pm S.E. (n = 3).

The PMA-induced OAT1 ubiquitination was blocked by staurosporin, a general PKC inhibitor (Fig. 3) without affecting the total amount of OAT1 (not shown), demonstrating the specific involvement of PKC in OAT1 ubiquitination. The ubiquitin-immunoreactive signal displayed a smeary band centered \sim 140 kDa, \sim 60 kDa larger than the size of OAT1 (\sim 80 kDa). Given that each ubiquitin molecule is \sim 8 kDa, OAT1 most likely is either multiubiquitinated or polyubiquitinated.



Fig. 3. PKC specificity of OAT1 ubiquitination in COS-7 cells. (A) OAT1-expressing COS-7 cells were treated with PKC-activator PMA (1 μ M) in the presence or absence of the PKC-inhibitor staurosporine (St, 2 μ M) for 30 minutes. The treated cells were then lysed, and OAT1 was immunoprecipitated with anti-myc antibody, followed by immunoblotting (Ib) with anti-ubiquitin antibody. (B) densitometry plot of results from (A) as well as from other experiments. The values are mean \pm 6 S.E. (n = 3).

A similar experiment was then performed with rat kidney slices (Fig. 4). Upon PMA treatment, dramatic increase of OAT1 ubiquitination was detected. Again, such ubiquitination was blocked by PKC inhibitor staurosporin. These results suggest that OAT1, regardless of species origin, undergoes PKC-regulated ubiquitination both in cultured cells and in rat kidney tissue.

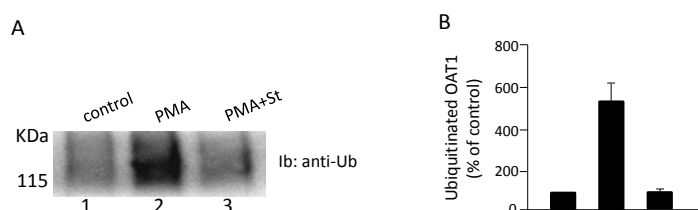


Fig. 4. PKC specificity of OAT1 ubiquitination in the rat kidney. (A) rat kidney slices were treated with PKC-activator PMA (1 μ M) in the presence or absence of the PKC-inhibitor staurosporine (St, 2 μ M) for 30 minutes. The treated slices were then lysed, and OAT1 was immunoprecipitated with anti-OAT1 antibody, followed by immunoblotting (Ib) with antiubiquitin antibody P4D1. (B) densitometry plot of results from (A) as well as from other experiments. Values are mean \pm 6 S.E. (n = 3).

PKC-induced ubiquitination of OAT1 by ectopically expressed ubiquitin – OAT1-expressing cells were transiently transfected with HA-tagged ubiquitin. Transfected cells were treated with PMA in the presence and the absence of PKC inhibitor staurosporin. OAT1 was then immunoprecipitated, followed by immunoblotting with anti-HA antibody (to detect HA-tagged ubiquitin). HA immunoreactivity was dramatically increased in the samples treated with PMA, and was significantly decreased in the presence of staurosporin (Fig. 5), indicating that the conjugation of HA-ubiquitin to OAT1 is PKC-dependent.

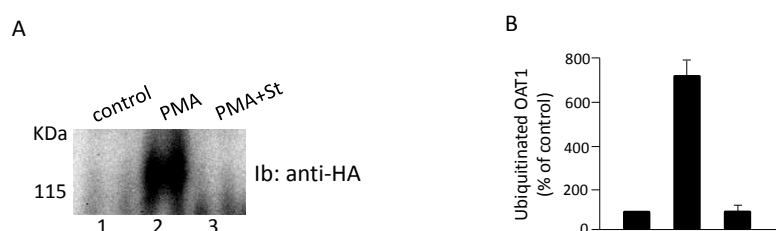


Fig. 5. PMA-induced OAT1 ubiquitination by ectopically expressed ubiquitin. (A) OAT1-expressing COS-7 cells were transiently transfected with HA-tagged ubiquitin. The transfected cells were treated with PMA (1mM) in the presence or absence of the PKC-inhibitor staurosporine (St, 2mM) for 30 minutes. OAT1 was then immunoprecipitated by anti-myc antibody, followed by immunoblotting (Ib) with anti-HA antibody. (B) Densitometry plot of results from (A) as well as from other experiments. The values are mean \pm 6 S.E. (n = 3).

OAT1 ubiquitination at the cell surface – To determine whether OAT1 ubiquitination occurs at the cell surface, we developed a two-step procedure to ensure that only cell surface OAT1 ubiquitination was detected (Fig. 6A). Briefly, cell surface proteins were labeled with or without membrane impermeable reagent NHS-SS-biotin. Labeled cells were lysed. OAT1 was then immunoprecipitated, with subsequent streptavidin pull-down to isolate cell surface OAT1. Immunoblotting of this streptavidin pull-down with anti-ubiquitin

antibody showed no signal for ubiquitin in cells not labeled with biotin. However in cells labeled with biotin, ubiquitin signal dramatically increased in the presence of PMA. This result demonstrated that the two-step procedure detected only cell surface OAT1 ubiquitination. Using this procedure, we next examined the effect of a dominant negative mutant of dynamin-2 (Dyn-2m) on OAT1 ubiquitination. We previously demonstrated that OAT1 internalization occurred partly through a dynamin- and clathrin-dependent pathway and that such internalization was blocked in cells transfected with a Dyn-2m. As a result, OAT1 accumulated at the cell surface (1). In the current experiment, we transfected OAT1-expressing cells with Dyn-2m (or empty vector as control). Transfected cells were treated with PMA for 30 min and cell surface proteins were biotinylated, followed by the same procedure shown in Fig. 6A for the detection of cell surface OAT1 ubiquitination. Our results showed that ubiquitinated OAT1 was significantly elevated in cells transfected with Dyn-2m (Figs. 6B & 6C), a maneuver that blocked OAT1 internalization. These data indicate that OAT1 is preferentially ubiquitinated when present at the cell surface and that ubiquitination of OAT1 precedes its internalization.

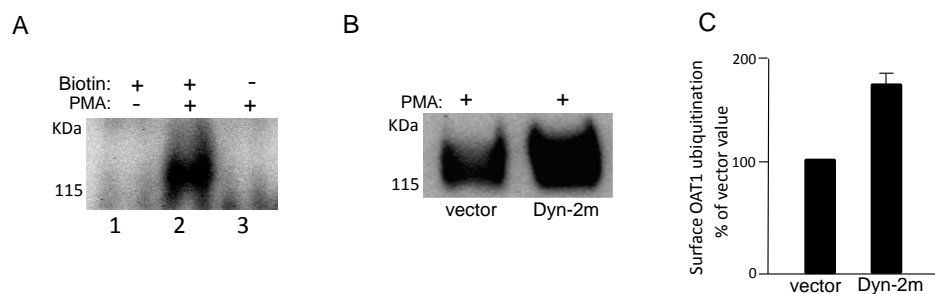


Fig. 6. Cell-surface OAT1 ubiquitination. (A) cell-surface proteins of OAT1-expressing cells were labeled with or without the membrane-impermeable reagent biotin. The cells were treated with or without PMA for 30 minutes. The labeled cells were lysed. OAT1 was then immunoprecipitated with subsequent streptavidin pull-down to isolate cell-surface OAT1, followed by immunoblotting with anti-ubiquitin antibody. (B) OAT1-expressing cells were transfected with the cDNA encoding dominant negative mutant of dynamin-2 (Dyn-2m, empty vector as control). The transfected cells were treated with PMA (1 mM) for 30 minutes. Cell-surface OAT1 was isolated by cell-surface biotinylation, as described in (A), followed by immunoblotting with antiubiquitin antibody. (C) Densitometry plot of results from (B) as well as from other experiments. Surface OAT1 in PMA-treated cells was expressed as the percentage of surface OAT1 in control cells. The values are mean \pm 6 S.E. ($n = 3$).

Identification of ubiquitination linkage of OAT1 – As mentioned above, different types of ubiquitination (mono- versus polyubiquitination via different types of linkages) have different physiologic outcomes for the ubiquitinated substrate. To identify the ubiquitination type of OAT1, we employed a sequential immunoprecipitation procedure to purify ubiquitinated OAT1. Briefly, we treated OAT1-expressing cells with PKC activator PMA for 30 min. Treated cells were then lysed. OAT1 was immunoprecipitated, followed by a second immunoprecipitation using ubiquitin-specific antibody to purify ubiquitinated OAT1 (normal IgG as negative control). The ubiquitinated OAT1 was then separated on SDS-PAGE, followed by Coomassie blue-staining. A Coomassie blue-stained broad band centered ~140 kDa was dissected for mass spectrometric analysis, and a sufficient amount of information regarding the peptides which originated from ubiquitin sequences was obtained. Among various peptides identified from ubiquitin, which cover all its seven lysine residues, only K48-linked ubiquitin was detected (Table 1). These results indicate that OAT1 is ubiquitinated mainly through K48-linked polyubiquitin chains.

Identification	Peptides ^a	Charge
Ubiquitin	R.LIFAG K ^{48*} QLEDGR.T	+2
	R.LIFAG K ^{48*} QLEDGR.T	+3
^a An asterisk Denotes Gly-Gly modification of the –amino group of the lysine side chain.		

Table 1. Ubiquitinated peptides of ubiquitin. Modified amino acid is shown in boldface periods represent the beginning and the end of the tryptic peptide.

The role of K48-linked polyubiquitin chains in PKC-regulated OAT1 ubiquitination – To explore the role of K48-linked polyubiquitin chains in PKC-regulated OAT1 ubiquitination, we employed four HA-tagged-ubiquitin constructs: wild type ubiquitin Ub, mutant ubiquitin Ub Δ G (3), which has the C-terminal Gly residue deleted and therefore prevents the conjugation of ubiquitin to OAT1, mutant ubiquitin Ub-K48R (4), which has the invariant Lys in position 48 mutated to Arg and prevents the formation of K48-linked polyubiquitin chains, and mutant ubiquitin Ub-K63R (4), which has the invariant Lys in position 63 mutated to Arg and prevents the formation of K63-linked polyubiquitin chains. cDNAs encoding these ubiquitin constructs were transfected into OAT1-expressing cells. Transfected cells were treated with or without PMA. OAT1 was then immunoprecipitated, followed by immunoblotting with anti-HA antibody. Our results (Fig. 7) showed that PMA treatment resulted in a strong HA-immuno-reactive signal in both Ub- and Ub-K63R-transfected cells, suggesting that significant amount of Ub and Ub-K63R were incorporated into OAT1. In contrast, the same treatment resulted in almost no detection of HA-immuno-reactive signal in both Ub Δ G- and Ub-K48R-transfected cells. There was no major change in the total amount of OAT1 immunoprecipitated under these conditions (not shown). These results strongly support our mass spectrometric data that majority of OAT1 ubiquitination consists of K48-linked polyubiquitin chains.

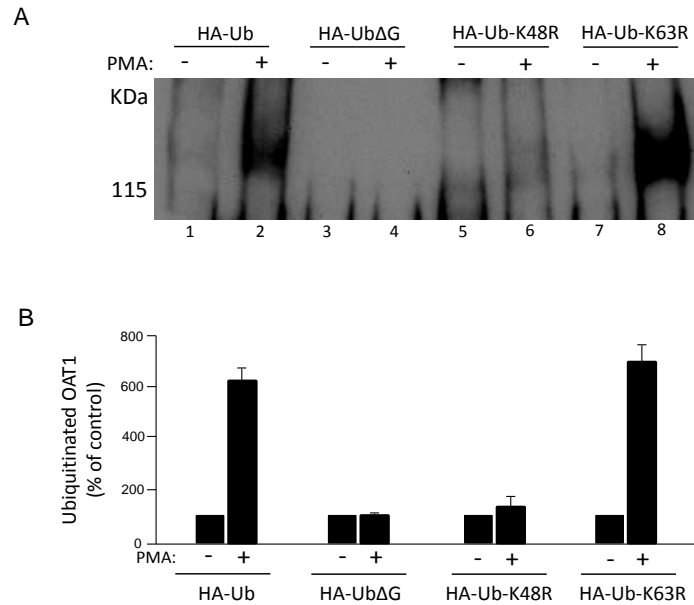


Fig. 7. Effects of wild-type ubiquitin and ubiquitin mutants on OAT1 ubiquitination. (A) cDNA for HA-tagged wild-type ubiquitin (Ub), ubiquitin mutants UbΔG, Ub-K48R, and Ub-K63R were transfected into COS-7 cells, respectively, followed by treatment with or without PMA for 30 minutes. The treated cells were lysed. OAT1 was immunoprecipitated by anti-myc antibody, followed by immunoblotting with anti-HA antibody. (B) Densitometry plot of results from (A) as well as from other experiments. Ubiquitinated OAT1 in PMA-treated cells was expressed as the percentage of that found in control cells. The values are mean ± S.E. (n = 3).

The role of K48-linked polyubiquitin chains in PKC - regulated OAT1 surface expression and internalization – We previously demonstrated that acute activation of PKC inhibits OAT1 activity by reducing OAT1 surface expression through accelerating internalization of this transporter from cell surface to intracellular compartments (1). To explore the role of K48-linked polyubiquitin chains of OAT1 in this process, we examined PKC-regulated OAT1 surface expression and internalization in cells transfected with Ub-K48R. As shown in Fig. 8, PMA treatment resulted in a significant decrease in OAT1 surface expression in control cells, whereas such PMA effect was substantially reversed in Ub-K48R-transfected cells.

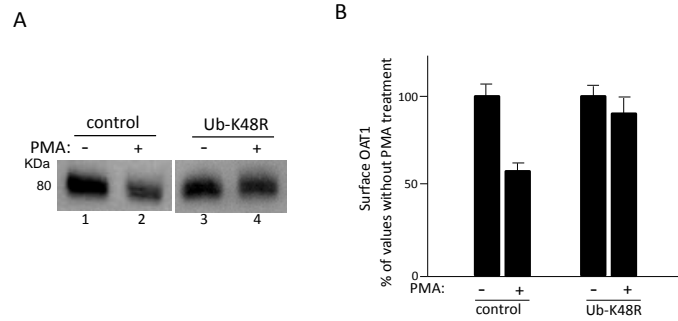


Fig. 8. Effect of ubiquitin mutant Ub-K48R on PMA-regulated OAT1 surface expression. (A) OAT1-expressing cells were transfected with Ub-K48R (or vector as control), followed by treatment with or without PMA (1 μ M) for 30 minutes. The treated cells underwent cell-surface biotinylation. Biotinylated proteins were isolated with streptavidin beads and analyzed by immunoblotting with an anti-myc antibody. (B) Densitometry plot of results from (A) as well as from other experiments. Surface OAT1 in PMA-treated cells was expressed as the percentage of surface OAT1 in control cells. The values are mean \pm 6 S.E. ($n = 3$).

Similarly, PMA treatment resulted in a significant increase in OAT1 internalization in control cells, whereas such PMA effect was substantially reversed in Ub-K48R-transfected cells (Fig. 9). These data indicate that K48-linked polyubiquitin chains of OAT1 are essential for PKC-regulated OAT1 surface expression and internalization.

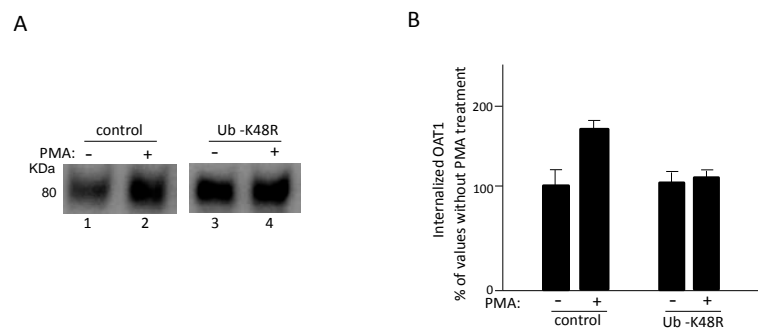


Fig. 9. Effect of ubiquitin mutant Ub-K48R on PMA-regulated OAT1 internalization. (A) COS-7 cells were transfected with OAT1 (1 mg) and Ub-K48R (4 mg) (or vector as control). OAT1 internalization (15 minutes) was then determined as described under Materials and Methods, followed by immunoblotting using anti-myc antibody. (B) Densitometry plot of results from (A) as well as from other experiments. The internalized surface OAT1 in PMA-treated cells was expressed as the percentage of internalized surface OAT1 in control cells. The values are mean \pm 6 S.E. ($n = 3$).

Site-directed mutagenesis of intracellular lysine residues of hOAT1 – Our data above showed that activation of PKC induced ubiquitination of hOAT1 (5). Ubiquitination occurs through the formation of an isopeptide bond between the C-terminal glycine of ubiquitin and a lysine residue on the target protein. hOAT1 has 10 intracellular lysine residues (Fig. 3.1). To identify which lysine(s) serves as acceptor(s) for hOAT1 ubiquitination, we initially generated two lysine mutants by simultaneously replacing multiple lysine residues (K) with arginine (R) using site-directed mutagenesis approach. The mutant K523/525/535/547R had all the lysine residues at the carboxyl terminus mutated, whereas the mutant K163/297/303/315/321R had the rest of the lysine residues mutated. Lys382, a residue conserved across species, was not included in the mutants because it was previously shown that mutation of this residue to arginine resulted in complete loss of transport function of rat OAT3 and flounder OAT1 (6, 7).

extracellular

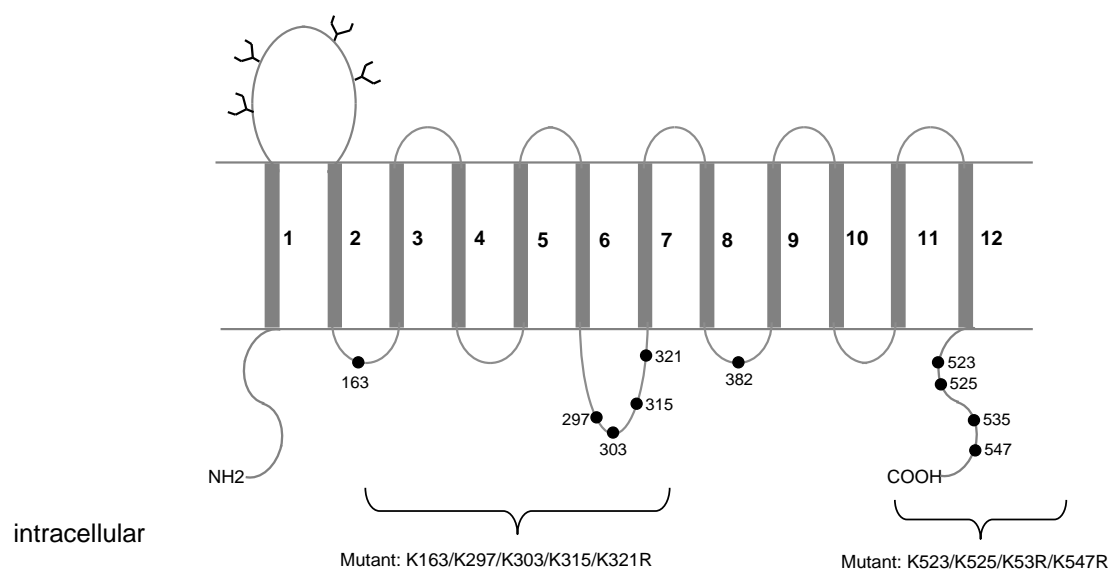


Fig. 10. Predicted transmembrane topology of hOAT1. Twelve transmembrane domains are numbered from 1 to 12. Potential glycosylation sites are denoted by tree-like structures. Intracellular lysine residues are indicated by • and numbered.

Mutant transporters were analyzed for their ability to transport PAH, a prototypical substrate of hOAT1. As shown in Fig. 11, both mutants retained transport activities and the levels of expression comparable to that of wild type transporter.

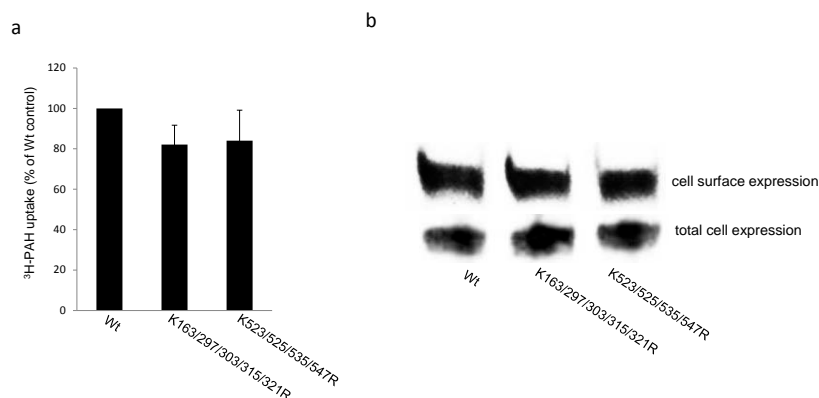


Fig. 11. Characterization of hOAT1 wild type (Wt) and its lysine mutants. a. Transport activity. cDNAs for hOAT1 Wt and its lysine mutants were transfected into COS-7 cells. Transport of ^3H -PAH (20 μM , 3 min) in transfected cells was then measured. Uptake activity was expressed as a percentage of the uptake measured in Wt. The results represent data from three experiments, with triplicate measurements. b. Cell surface and total expression. *Top panel: Cell surface expression.* Cells were biotinylated, and the labeled cell surface proteins were precipitated with streptavidin beads, separated by SDS-PAGE, followed by immunoblotting with anti-myc antibody (1:100). *Bottom panel: Total cell expression.* Cells were lysed, and their proteins were separated by SDS-PAGE, followed by immunoblotting with anti-myc antibody (1:100).

Sensitivity of mutant transporters to PKC - induced inhibition of transport activity – We recently showed that activation of PKC inhibited hOAT1 activity by enhancing hOAT1 ubiquitination, which led to an acceleration of hOAT1 internalization from cell surface to intracellular compartments (1, 5). To examine the sensitivity of mutant transporters to PKC-induced inhibition of transport activity, cDNAs for wild type hOAT1 and its mutants were individually transfected into the cells. Transfected cells were treated with or without PKC activator PMA (30 min), followed by measurement of PAH transport. As shown in Fig. 12, mutant K523/525/535/547R was equally sensitive to PKC-induced inhibition of transport activity as compared to that of the wild type transporter, whereas mutant K163/297/303/315/321R was insensitive to PKC-induced inhibition.

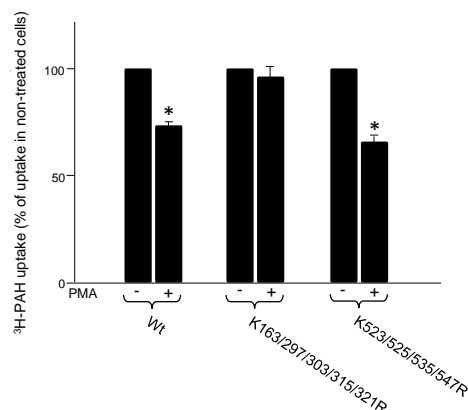


Fig. 12. Effect of PMA on transport activities of hOAT1 wild type (Wt) and its lysine mutants. cDNAs for hOAT1 Wt and its lysine mutants were transfected into COS-7 cells. Transfected cells were treated with PKC activator PMA (1 μ M, 30 min), followed by measurement of 3 H-PAH transport (20 μ M, 3 min). Uptake activity was expressed as a percentage of the uptake measured in non-treated cells.

Sensitivity of mutant transporters to PKC-induced ubiquitination – We next examined whether mutants K523/525/535/547R and K163/297/303/315/321R were subjected to ubiquitination in response to PKC activation as that of wild type transporter. cDNAs for wild type hOAT1 and the mutants were transfected into the cells individually. Transfected cells were treated with or without PKC activator PMA. Treated cells were lysed and hOAT1 was immunoprecipitated, followed by immunoblotting with anti-ubiquitin antibody. As shown in Fig. 13, PMA treatment resulted in significant increase in the ubiquitination of wild type hOAT1 and mutant K523/525/535/547R, whereas mutant K163/297/303/315/321R was insensitive to PMA-induced ubiquitination, suggesting that mutant K163/297/303/315/321R serves as an acceptor for PKC-induced ubiquitination of the transporter.

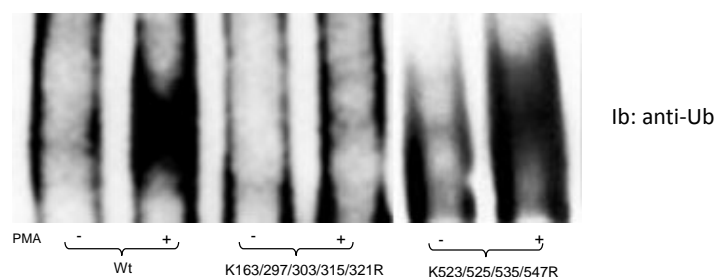


Fig. 13. Effect of PMA on ubiquitination of hOAT1 wild type (Wt) and its lysine mutant. cDNAs for hOAT1 Wt and its lysine mutant were transfected into COS-7 cells. Transfected cells were treated with PKC activator PMA (1 μ M, 30 min). OAT1 was then immunoprecipitated by anti-myc antibody, followed by immunoblotting with anti-ubiquitin antibody.

Sensitivity of mutant *K163/297/303/315/321R* to PKC - induced decrease in surface expression – cDNAs for wild type hOAT1 and mutant *K163/297/303/315/321R* were transfected into the cells individually. Transfected cells were treated with or without PMA (30 min), followed by cell surface biotinylation to isolate cell surface hOAT1. As shown in Fig. 14, Activation of PKC by PMA resulted in a reduction in cell surface expression of the wild type hOAT1 without affecting its total expression. In contrast, PMA had no effect on the surface expression of the mutant transporter.

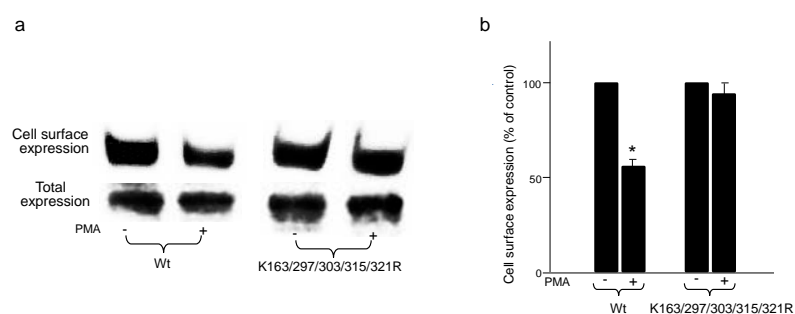


Fig. 14. Effect of PMA on cell surface and total expression of hOAT1 wild type (Wt) and its). Treated cells were biotinylated, and the labeled cell surface proteins were precipitated with streptavidin beads, separated by SDS-PAGE, followed by immunoblotting with anti-myc antibody (1:100). *Bottom panel: Total cell expression.* Cells were lysed, and their proteins were separated by SDS-PAGE, followed by immunoblotting with anti-myc antibody (1:100). *b.* Densitometry plot of results from Fig. 5a as well as from other experiments. Surface OAT1 in PMA-treated lysine mutant. *a. Top panel: Cell surface expression.* cDNAs for hOAT1 Wt and its lysine mutant were transfected into COS-7 cells. Transfected cells were treated with PKC activator PMA (1 μ M, 30 min cells was expressed as % of surface OAT1 in control cells. Values are mean \pm S.E. ($n = 3$).

Sensitivity of mutant K163/297/303/315/321R to PKC - induced acceleration of transporter internalization – PKC-induced acceleration of transporter internalization was subsequently examined in both wild type transporter- and mutant-transfected cells. As shown in Fig. 15, PMA treatment (30 min) of cells resulted in an acceleration of wild type hOAT1 internalization, whereas no significance difference in the rate of mutant internalization was observed between PMA-treated and control cells.

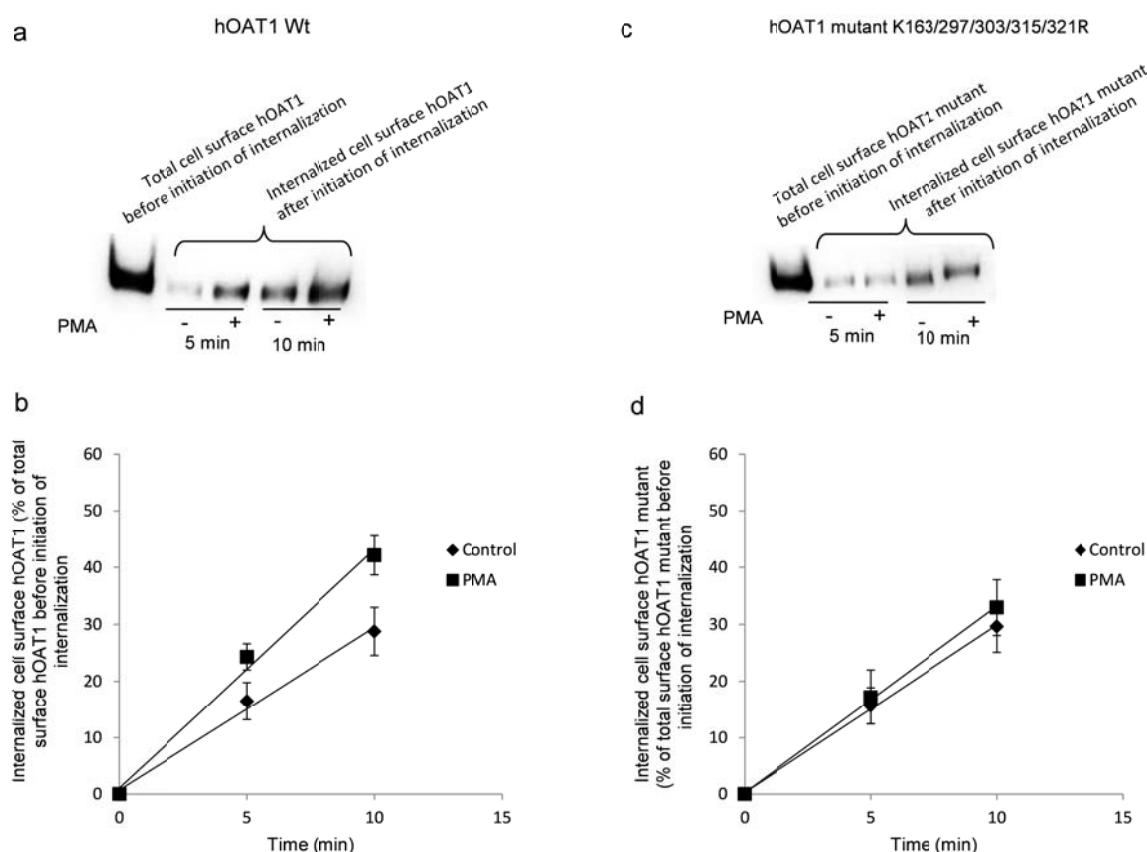


Fig. 15. Effect of PMA on the internalization of hOAT1 wild type (Wt) and its lysine mutant. a. Internalization of hOAT1 Wt. *Top panel:* cDNA for hOAT1 Wt was transfected into COS-7 cells. Internalization (5 min and 10 min) was analyzed as described in “Materials and Methods” section in the presence and the absence of PMA followed by immunoblotting using anti-myc antibody. *Bottom panel:* As a loading control for *Top panel*, total expression of OAT1 Wt in cell lysate was measured in parallel by immunoblotting using anti-myc antibody. b. Densitometry plot of results from Fig. 6a, *Top panel* as well as from other experiments. Internalized OAT1 was expressed as % of total initial cell surface OAT1 pool. Values are mean \pm S.E. ($n = 3$). c. Internalization of hOAT1 lysine mutant. *Top panel:* cDNA for hOAT1 lysine mutant was transfected into COS-7 cells. Internalization (5 min and 10 min) was analyzed in the presence and the absence of PMA followed by immunoblotting using anti-myc antibody. *Bottom panel:* As a loading control for *Top panel*, total expression of OAT1 lysine mutant in cell lysate was measured in parallel by immunoblotting using anti-myc antibody. d. Densitometry plot of results from Fig. 6c, *Top panel* as well as from other experiments. Internalized

OAT1 mutant was expressed as % of total initial cell surface OAT1 mutant pool. Values are mean \pm S.E. ($n = 3$).

Identification of single lysine residue(s) responsible for PKC - induced ubiquitination –

The results above indicate that one or more lysine residue(s) within K163/297/303/315/321R is responsible for PKC-induced ubiquitination. To identify such residues, the five lysine residues were individually mutated into arginine: K163R, K297R, K303R, K315R, and K321R. PKC-induced ubiquitination of wild type hOAT1 and its mutants was subsequently examined. As shown in Fig. 16, PMA treatment resulted in significant increase in the ubiquitination of wild type hOAT1, and mutants K163R and K321R, whereas mutants K297R, K303R and K315R were insensitive to PMA-induced ubiquitination.

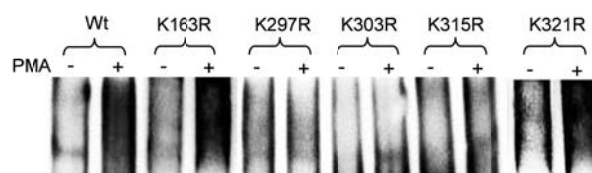


Fig. 16. Effect of PMA on the incorporation of endogenous ubiquitin into hOAT1 wild type (Wt) and its lysine mutants. cDNAs for hOAT1 Wt and its lysine mutants were transfected into COS-7 cells respectively, followed by treatment with or without PMA (1 μ M, 30 min). Treated cells were lysed. OAT1 was immunoprecipitated by anti-myc antibody, followed by immunoblotting with anti-ubiquitin antibody.

To further confirm our observation, we next examined the incorporation of ectopically expressed ubiquitin into wild type hOAT1 and its mutants. Cells were transfected with wild type hOAT1, K163R, K297R, K303R, K315R, and K321R individually together with HA-tagged ubiquitin. Transfected cells were treated with PMA. As shown in Fig. 17, HA-tagged ubiquitin significantly incorporated into wild type hOAT1, K163R, and K321R in response to PMA treatment, whereas no such incorporation was observed into mutants K297R, K303R and K315R.

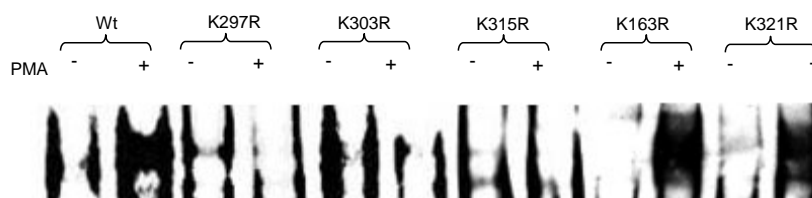


Fig. 17. Effect of PMA on the incorporation of ectopically expressed ubiquitin into hOAT1 wild type (Wt) and its lysine mutants. cDNAs for hOAT1 Wt and its lysine mutants were co-transfected with HA-ubiquitin into COS-7 cells respectively, followed by treatment with or without PMA (1 μ M, 30 min). Treated cells were lysed. OAT1 was immunoprecipitated by anti-myc antibody, followed by immunoblotting with anti-HA antibody.

3.4 Discussion

We previously established (1) that OAT1 undergoes constitutive internalization from and recycling back to cell surface and that acute activation of protein kinase C (PKC) inhibits OAT1 activity by reducing OAT1 cell surface expression through accelerating its internalization from cell surface to intracellular compartments. However, the underlying mechanisms are poorly understood. In the current study, we provided novel evidence that acute activation of PKC significantly enhanced OAT1 ubiquitination both *in vitro* and *ex vivo*. We further showed that ubiquitination of cell surface OAT1 increased in cells transfected with dominant negative mutant of dynamin-2, a maneuver blocking OAT1 internalization, suggesting that OAT1 ubiquitination proceeds before OAT1 internalization. Mass spectroscopy revealed that ubiquitination of OAT1 consisted of polyubiquitin chains primarily through lysine 48 (K48) linkage. Transfection of cells with dominant negative mutant of ubiquitin Ub-K48R, which prevents the formation of K48-linked polyubiquitin chains, abolished PKC-stimulated OAT1 ubiquitination and internalization. Together, our findings demonstrated for the first time that K48-linked polyubiquitination is essential for PKC-regulated OAT1 trafficking (Fig. 18).

To directly address the role of OAT1 ubiquitination, we generated two OAT1 mutants,

each having multiple lysines (K) simultaneously mutated to arginine (R). One mutant K163/297/303/315/321R lost sensitivities to PKC-induced inhibition of transport activity, to PKC-induced ubiquitination, and to PKC-induced acceleration of transporter internalization. Further dissecting each lysine within this mutant, we identified Lys297, Lys303 and Lys315 being the ubiquitin-conjugation sites. Interestingly, mutating any one of the three lysines prevented the ubiquitin-conjugation to the other two lysines, suggesting that Lys297, Lys303 and Lys315 may form an optimal structure to interact with ubiquitination machineries. This is the first demonstration that Lys297, Lys303 and Lys315 play synergistic role in PKC-regulated OAT1 ubiquitination, trafficking and transport activity.

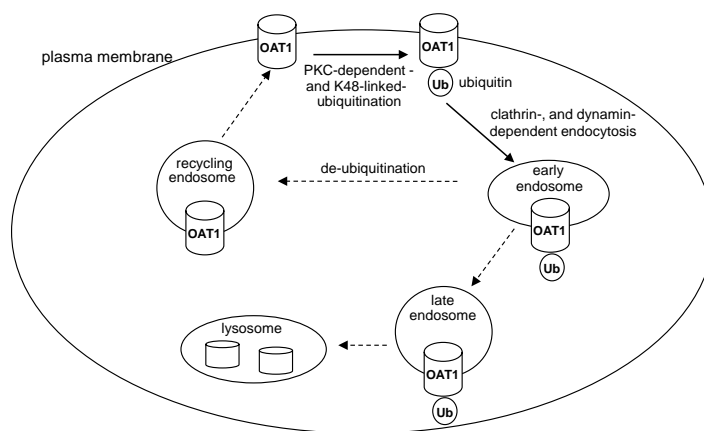


Fig. 18. The role of ubiquitination in OAT1 internalization. Dashed arrows: steps that were not explored in the current study.

3.5 References

1. Zhang Q, Hong M, Duan P, Pan Z, Ma J, and You G (2008) Organic anion transporter OAT1 undergoes constitutive and protein kinase C-regulated trafficking through a dynamin- and clathrin-dependent pathway. *J Biol Chem* 283:32570-32579.
2. You GF, Kuze K, Kohanski RA, Amsler K, and Henderson S. Regulation of mOAT-mediated organic anion transport by okadaic acid and protein kinase C in LLC-PK1 cells. *J Biol Chem* 275: 10278-10284
3. Kolodzieiski PJ, Musial A, Koo JS, and Eissa NT. Ubiquitination of inducible nitric oxide synthase is required for its degradation. *Proc Natl Acad Sci* 99: 12315-12320
4. Li HH, Wilis MS, Lockyer P, Miller N, McDonough H, Glass DJ, and Patterson C. Atrogin-1 inhibits alct-dependent cardiac hyperthrophy in mice via ubiquitin dependent coactivation of forkhead protein. *J Clin Invest* 117: 3211-3223
5. Zhang Q, Li S, Patterson C, and You G(2013) Lysine 48-linked polyubiquitination of organic anion transporter-1 is essential for its protein kinase C-regulated endocytosis. *Mol Pharmacol* 83(1):217-24.
6. Burckhardt G, Wolff NA and Bahn A (2002) Molecular characterization of the renal organic anion transporter 1. *Cell Biochem Biophys* 36 (2-3):169-74.
7. Feng B, Dresser MJ, Shu Y, Johns SJ, and Giacomini KM (2001) Arginine 454 and lysine 370 are essential for the anion specificity of the organic anion transporter, rOAT3. *Biochemistry* 40(18):5511-20.

Chapter 4. High throughput screen of OAT inhibitors

4.1 Introduction

Drug–drug interactions (DDIs) are one of the leading causes of drug withdraw from the market. Although drug interactions with drug metabolizing enzymes have been extensively studied, transporter-mediated DDIs have only recently been brought into significant attention. OAT1, OAT3 are among several important transporters specified in the newly published FDA guidance for which DDIs should be evaluated during drug development (1). In the current study, we analyzed the inhibition of hOAT1 and hOAT3 with a collection of clinical prescription drugs by high-throughput screening. Drugs with high hits were then subjected to computational analysis and mechanistic insight into the structural requirements for the inhibition of these transporters is provided.

4.2 Materials and methods

The NIH Clinical Collection (NCC) and NIH Clinical Collection 2 (NCC2) were acquired from Evotec CA, USA. 6-carboxyfluorescein (6-CF) was acquired from Sigma-aldrich. All compounds unless defined are all acquired from Sigma-aldrich with an analytical grade of at least 95% purity.

Cell culture — Monkey kidney COS-7 cells stably expressing human OAT1 and 3 (hOAT1 and hOAT3) were previously established in our lab (2, 3). Cells were cultured in Dulbecco's modified Eagle's medium (Invitrogen, USA) supplemented with 10% fetal bovine serum and 100 unit /ml penicillin, 100 µg/ml streptomycin and 0.5 mg/ml

geneticin (G418; Invitrogen, Carlsbad, CA) at 37 °C in a humidified incubator with 5% CO₂.

Fluorescence uptake assay — Cells (~5 X 10⁴/well) were seeded in black wall poly-D-lysine-coated 96 well plates (COSTAR®, Corning Inc, USA) 24 hr prior to experiments. Uptake was initiated by adding uptake solution (PBS supplemented with 1 μM of MgCl₂ and 1 μM of CaCl₂) containing 20 μM fluorescent substrate 6-CF in the presence of other drugs from the drug libraries, and incubating at room temperature for 12 min. The uptake was stopped by application of 200 μl of ice cold PBS followed by washing cells one more time with cold PBS. Cells were then lysed with 0.2 N NaOH for 1 hr. All compounds were measured duplicate or triplicate. The intensity of accumulated 6-CF inside the cells was measured using an FLx800 microplate fluorescence reader, (Bio-Tek instrument Inc., USA) with excitation and emission wavelength at 485 and 560 nm respectively.

Transport kinetics were characterized by measuring the uptake of increasing concentration of 6-CF in COS-7 cells stably expressing hOAT1 and hOAT3 and subtracting the background values from parental COS-7 cells. The uptake value was fitted to the Michaelis-Menten equation $V = V_{max}S/(K_m + S)$ where V_{max} is the maximum transport rate, K_m is the substrate concentration resulting in half-maximum uptake rate, and S is the concentration of 6-CF, using GraphPad Prism software (GraphPad Software Inc, USA). Z assay factor was calculated according to the equation $Z = 1 - (3SD_{sample} + 3SD_{control}) / (\text{Mean sample} - \text{Mean control})$ (Zhang et al., 1999).

Transporter inhibition assay — Nonspecific transport was determined by subtracting the uptake value from half-maximum inhibitory concentration (IC₅₀) were estimated from the screening inhibition measurements as $V = V_0 / [1 + (I/IC_{50})]$ ((Kido et al., 2011)), where V

and V_0 are the activity with and without inhibitor, respectively, and I is the inhibitor concentration of 20 μM for hOAT3 and 50 μM for hOAT1. This estimated IC_{50} was further confirmed with experimental IC_{50} . The estimated IC_{50} values were compared with plasma concentration (C_{max}) data of each tested chemicals collected from the literature.

Experimental IC_{50} values were measured as the uptake of 6-CF in the presence of increasing concentration of inhibitors (0.5 μM to 500 μM). Data were fit using nonlinear regression to the Equation 1, where V and V_0 are the 6-CF uptake rate in the presence and absence of the inhibitor, respectively. I is the inhibitor concentration, and n is the slope.

$$V = V_0 / [1 + (I / \text{IC}_{50})^n] \quad (\text{Equation 1})$$

IC_{50} was converted to K_i by Equation 2 before conversion to the -log value (pK_i), where C is the substrate concentration and K_m is the Michaelis constant.

$$K_i = \frac{\text{IC}_{50}}{[1 + (\frac{C}{K_m})]} \quad (\text{Equation 2})$$

Molecular descriptor generation — The descriptors, molecular weight, number of rotatable bonds (RB), Log P, the calculated molar refractivity, hydrogen bond donor, and number of hydrogen bond acceptor were calculated using Chemaxon JChem package (ChemAxon, USA).

Pharmacophore construction — The software MOE was used for the detection and interpretation of chemical features of sixteen OAT inhibitors with IC_{50} values determined by the experiment (Experimental IC_{50}). MOE automatically detects pharmacophoric features and generates annotations for each ligand. Then common features among

structural diverse ligands were identified through three steps: (1) Each compound was energy minimized to the putative global low-energy conformation in the following manner using MOE energy minimize Module. Using the standard Tripos molecular force field with a dielectric constant of $\epsilon=4.0$, molecules were first geometry optimized to the nearest local minimum energy conformation until an energy difference of 0.001 kcal/mol between successive iterations was achieved. All rotatable (i.e., single) bonds were then systematically searched in 10° increments and, after setting the torsion angles to the lowest-energy conformer among those scanned, the molecule was geometry optimized a final time. (2) Pharmacophore sites are created based on the selected molecular alignment by the unified scheme in MOE pharmacophore module. (3) Common pharmacophores are found by distance-based inter-site grouping.

4.3 Results

Establishment of fluorescent probe for high-throughput screening (HTS) assay –

The compound 6-CF was previously used as a fluorescent tracer for mouse OAT-mediated transport in *Xenopus* oocytes (4). In the present study, uptake of 6-CF into hOAT1- and hOAT3-expressing COS-7 cells, measured fluorometrically, was linear up to 30 min and gave a K_m of 12.7 μM for hOAT1 and 7.24 μM for hOAT3 (Fig. 1). We then evaluated Z' factor, a parameter to determine the suitability of an assay for HTS¹⁰. An excellent assay is indicated by the condition $1 \geq \text{Z' factor} \geq 0.5$. The Z' factor for hOAT1 and hOAT3 were 0.70 and 0.66, respectively, indicating excellent assay performance for HTS.

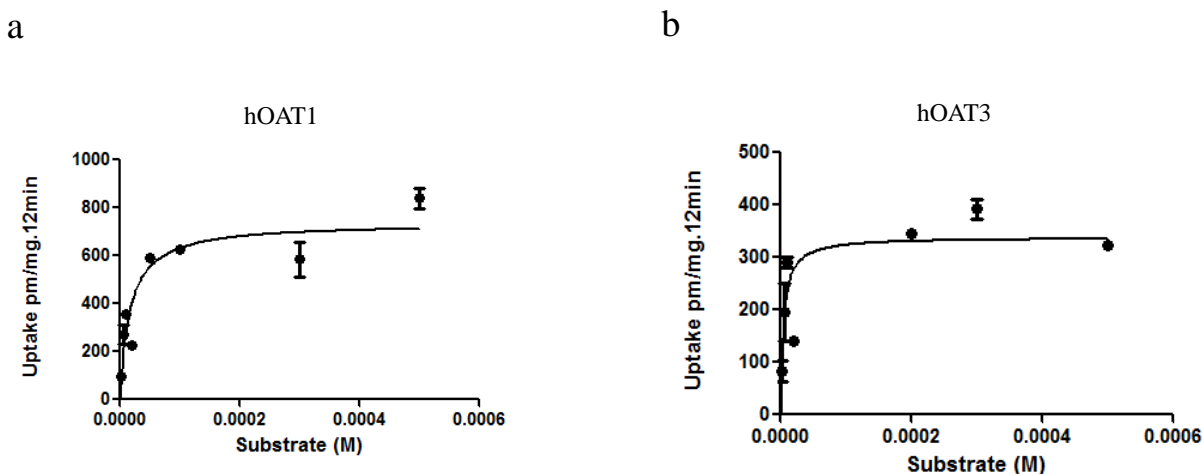


Fig. 1. Concentration dependence of 6-CF uptake in hOAT1- and hOAT3- expressing cells. a. The hOAT1-mediated specific uptake was calculated by subtracting the nonspecific uptake in control cells from that in the cells expressing hOAT1. b. The hOAT3-mediated specific uptake was calculated by subtracting the nonspecific uptake in control cells from that in the cells expressing hOAT3.

Identification of hOAT1 and hOAT3 inhibitors from drug libraries — The NIH Clinical Collection (NCC) and NIH Clinical Collection 2 (NCC2) drug libraries used for HTS consisted respectively of 446 and 281 small molecules (727 total) approved for clinical use or having a history of use in human clinical trials. The clinically tested compounds in the NCC and NCC2 libraries are highly drug-like with known safety profiles. At the indicated concentrations, 92 compounds resulted in 50 % decrease in hOAT1-mediated 6-CF transport, whereas 262 compounds resulted in 50 % decrease in hOAT3-mediated 6-CF transport (Fig. 2). All of the 92 hOAT1 inhibitors were also inhibitors for hOAT3 but with a different potency. Among the 262 inhibitors for hOAT3, 8 compounds were specific for hOAT3 (Table 1), i.e., they lacked appreciable inhibitory activity for hOAT1. For example, stiripentol inhibited hOAT3 with an IC_{50} of $27.6 \pm 1.28 \mu M$, but it barely had any effect on hOAT1 (not shown). These inhibitors for hOAT1 and hOAT3 included classes of anti-inflammatory, antiseptic/anti-infection, antineoplastic, steroid hormones,

cardiovascular, antilipemic, CNS, gastrointestinal, respiratory and reproductive control drugs.

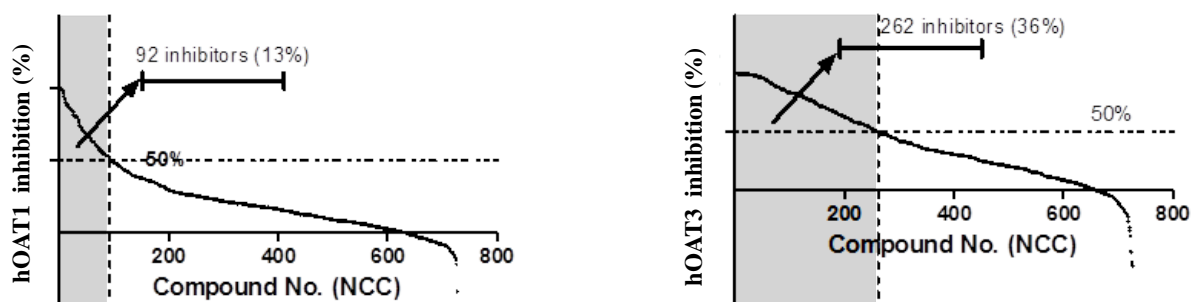


Fig. 2. Inhibitors of hOAT1 and hOAT3 identified in a screen of 700 prescription drugs. a. Overview of the results from the screening of hOAT1 inhibition. The 92 compounds resulting in at least 50% decreased uptake of 6-CF were classified as inhibitors (shaded in light gray). Data are presented as the mean \pm SD (samples in triplicate from one experiment). b. Overview of the results from the screening of hOAT3 inhibition. The 262 compounds resulting in at least 50% decreased uptake of 6-CF were classified as inhibitors (shaded in light gray). Data are presented as the mean \pm SD (samples in triplicate from one experiment).

Table 1. hOAT3-specific Inhibitors

Stiripentol	Cortisol succinate	Demeclocycline
Penciclovir	Ornidazole	Benazepril
Chlorpropamide	Artesunate	

Among those inhibitors retrieved from the initial screening, we selected clinically relevant inhibitors for hOAT1 and hOAT3 based on the criteria that the ratio of their peak plasma concentrations (C_{\max}) to their estimated IC_{50} (Eq. 1) exceeded 0.1 (1) at typical clinical doses and they were commercially available. For hOAT1, 35 of the 92 inhibitors were selected with ten compounds showing high inhibition potency (>95% inhibition of

hOAT1 activity in transporter inhibition assay, Table 2). For hOAT3, 73 of the 262 inhibitors were selected with fourteen showing high inhibition potency (>95% inhibition of hOAT3 activity in transporter inhibition assay, Table 3).

Table 2. Highly potent inhibitors for hOAT1 at peak plasma concentrations

Mefenamic Acid	Meclofenamic Acid	Pioglitazone
Oxaprozin	Nateglinide	Amlexanox
Ketorolac Tromethamine	Diffunisal	Nitazoxanide
Irbesartan	Valsartan	Telmisartan
Balsalazide	Ethacrynic Acid	

Table 3. Highly potent inhibitors for hOAT3 at peak plasma concentrations

Amlexanox	Telmisartan	Mefenamic Acid
Oxaprozin	Parecoxib Na	Meclofenamic Acid
Nitazoxanide	Ketoprofen	
Ketorolac Tromethamine	Diffunisal	

We further increased the stringency of our selection criteria by incorporation of peak unbound plasma concentration of drugs since, for drugs tightly bound to plasma proteins, the free concentration in plasma is a better estimate of the drug level interfering with OAT transport function. Further screening using the peak unbound plasma concentration yielded three inhibitors of hOAT1 (Table 4) and seven inhibitors of hOAT3 (Table 5) with potency >95% inhibition.

Table 4 . Highly potent inhibitors for hOAT1 at peak unbound plasma concentrations

Compounds	IC50 in COS-7 cells (μM)	Cmax (μM)	Cmax Unbound (Cu.p) (μM)	Cu.p/IC50
Oxaprozin	0.891±0.292	501 ¹⁶	5.01*	5.62
Mefenamic Acid	1.085±0.124	83.0*	8.30*	7.60
Ketorolac Tromethamine	0.653±0.130	9.50 ¹⁷	0.100 ¹⁷	0.150

*Data comes from Dailymed.nlm.nih.gov

Table 5 . Highly potent inhibitors for hOAT3 at peak unbound plasma concentrations

Compounds	IC50 in COS-7 cells (μM)	Cmax (μM)	Cmax Unbound (Cu.p) (μM)	Cu.p/IC50
Nateglinide	0.860±0.0953	18.0 ¹⁸	0.230 ¹⁹	0.270
Oxaprozin	0.870±0.0704	501 ¹⁶	5.01*	5.76
Nitazoxanide	0.154±0.0711	31.2 [■]	0.0300 [■]	0.200
Valsartan	0.250±0.143	14.8 ²⁰	0.850 ²¹	3.47
Ethacrynic Acid	0.662±0.261	30.9 ²²	0.600 [▲]	0.910
Diflunisal	0.720±0.290	496 [■]	0.490 [■]	0.680
Mefenamic Acid	1.75±0.258	83.0*	8.30*	4.74

* Data comes from Dailymed.nlm.nih.gov

■ Data comes from Drug.com

▲ Data comes from Drugbank.ca

Comparison of molecular characteristics between inhibitors and non-inhibitors –

Next, we examined the distribution of calculated molecular features among inhibitors and non-inhibitors of hOAT1 or hOAT3 (Fig 3). The molecular descriptors of all the compounds in the library were first generated by the Chemaxon JChem package followed by frequency distribution analysis between inhibitors (from the initial screening, which resulted in >50% decrease in transport activity at indicated concentrations in Fig. 2 legend; 92 compounds for hOAT1 and 262 compounds for hOAT3) and non-inhibitors. For hOAT1, statistically significant differences ($p < 0.05$) were found in number of hydrogen-bond donors, number of rotatable bonds, and topological polar surface area (TPSA) (Fig. 3a). For hOAT3, statistically significant differences ($p < 0.05$) were found in molecular weight, number of hydrogen-bond donors and acceptors, TPSA, Log $P_{7.4}$, and molecular polarizability (Fig. 3b).

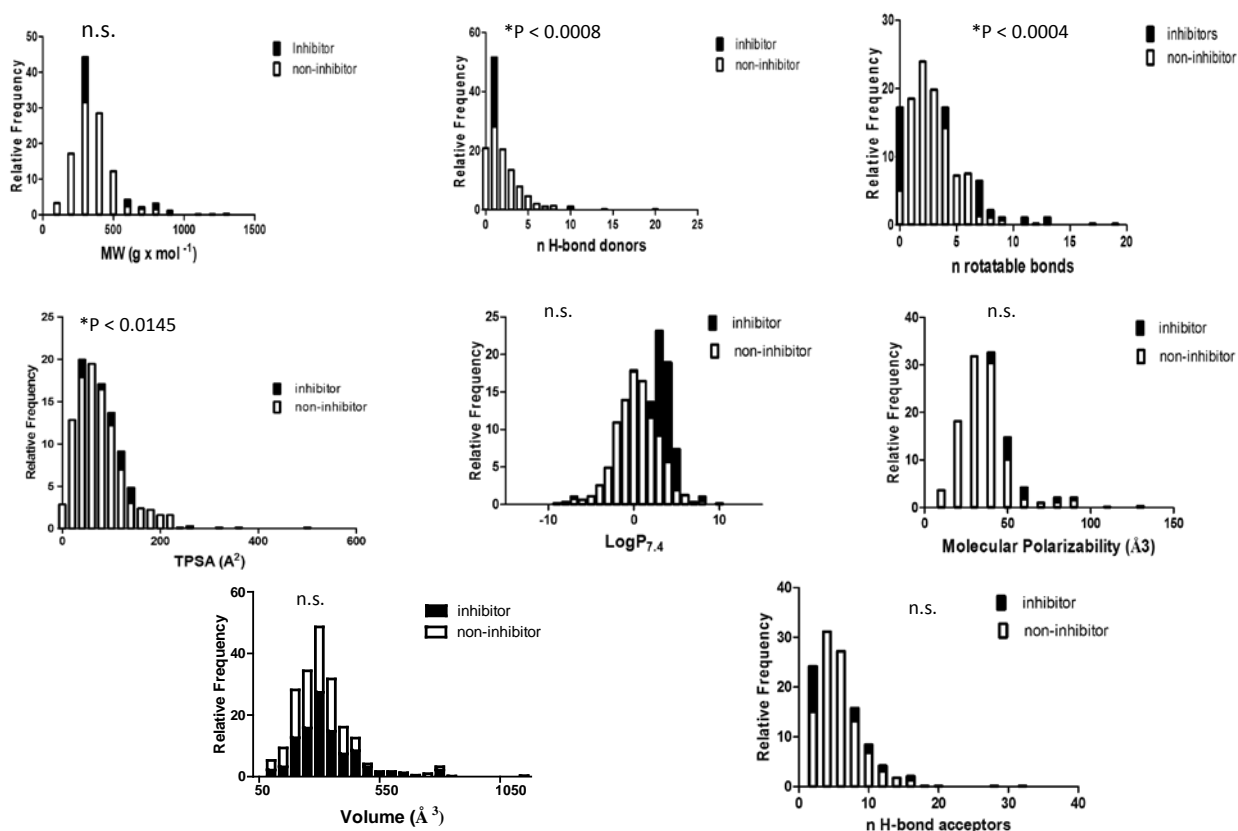


Fig. 3a. Structural features of hOAT1 inhibitors. Distribution of key physicochemical properties of hOAT1 inhibitors. The calculated descriptors (viz., TPSA, molecular weight, volume, number of rotatable bonds, Log $P_{7.4}$, molecular polarizability, number of hydrogen-bond donors and hydrogen-bond acceptors) were calculated using Chemaxon JChem package (ChemAxon, USA). The frequency distribution analysis was conducted between inhibitors and non-inhibitors by Graphpad prism 5.0. * $P < 0.05$ was considered significantly different, and n.s. stood for no significant difference.

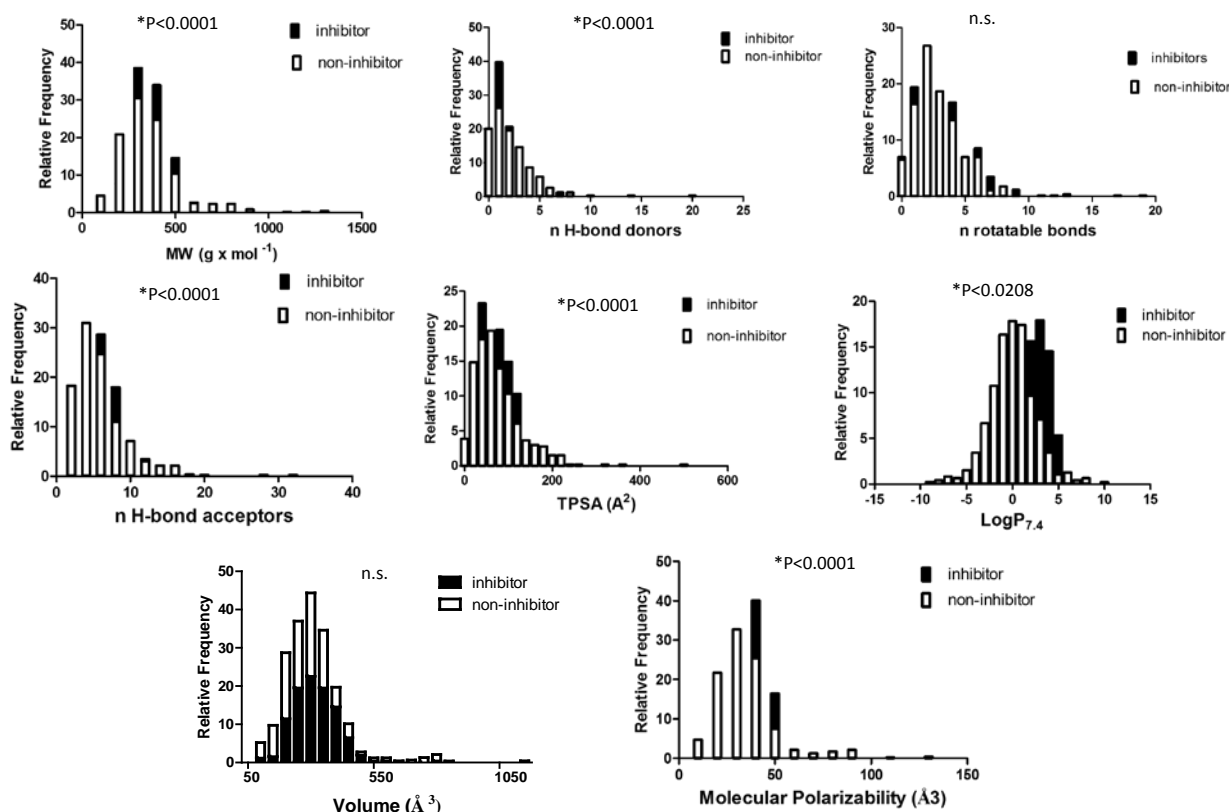


Fig. 3b. Structural features of hOAT3 inhibitors. Distribution of key physicochemical properties of hOAT3 inhibitors. The calculated descriptors (viz., TPSA, molecular weight, volume, number of rotatable bonds, Log $P_{7.4}$, molecular polarizability, number of hydrogen-bond donors and hydrogen-bond acceptors) were calculated using Chemaxon JChem package (ChemAxon, USA). The frequency distribution analysis was conducted between inhibitors and non-inhibitors by Graphpad prism 5.0. * $P < 0.05$ was considered significantly different, and n.s. stood for no significant difference.

Structural alignment and pharmacophore prediction — In order to understand the structure–activity relationship of hOAT1 inhibition, we further performed pharmacophore analysis to identify the important common features of OAT inhibitors. Based on analysis of the sixteen inhibitors with $> 95\%$ inhibition potency (Table 2, Table 3, Fig. 4), we

proposed a simple pharmacophore model to discriminate between OAT inhibitors and non-inhibitors. This two-point model has two structural features (one anionic hydrogen-bond acceptor atom, and an aromatic center) separated by ~ 5.7 Å (Fig. 5). Searching the collection of OAT non-inhibitors using the pharmacophore model produced no hits, thus attesting to the specificity of the model.

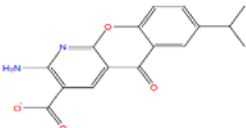
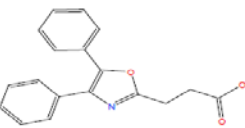
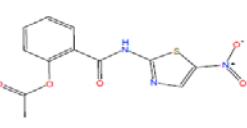
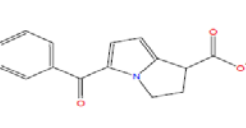
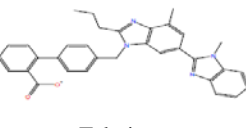
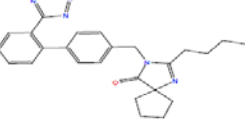
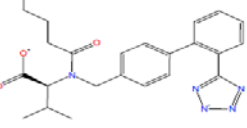
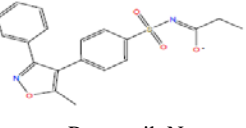
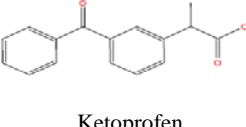
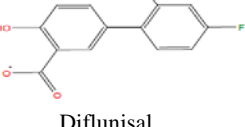
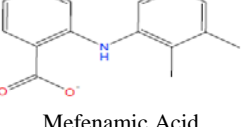
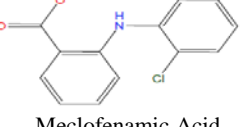
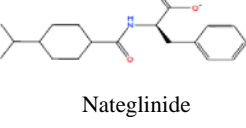
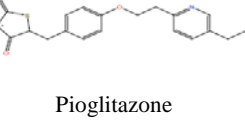
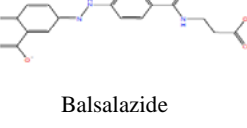
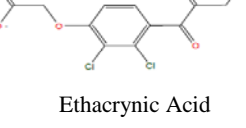
<p>CID: 2161</p>  <p>Amlexanox</p>	<p>CID: 4614</p>  <p>Oxaprozin</p>	<p>CID: 41684</p>  <p>Nitazoxanide</p>	<p>CID: 84003</p>  <p>Ketorolac Tromethamine</p>
<p>CID: 65999</p>  <p>Telmisartan</p>	<p>CID: 3749</p>  <p>Irbesartan</p>	<p>CID: 60846</p>  <p>Valsartan</p>	<p>CID: 9576744</p>  <p>Parecoxib Na</p>
<p>CID: 3825</p>  <p>Ketoprofen</p>	<p>CID: 3059</p>  <p>Diflunisal</p>	<p>CID: 4044</p>  <p>Mefenamic Acid</p>	<p>CID: 4038</p>  <p>Meclofenamic Acid</p>
<p>CID: 5311309</p>  <p>Nateglinide</p>	<p>CID: 60560</p>  <p>Pioglitazone</p>	<p>CID: 6335412</p>  <p>Balsalazide</p>	<p>CID: 3278</p>  <p>Ethacrynic Acid</p>

Fig. 4. Structures of inhibitors used in pharmacophore analysis.



Fig. 5. Pharmacophore model of hOAT1 and hOAT3 inhibitors. Two representative OAT inhibitors were mapped to the proposed pharmacophore model. The anionic and hydrogen-bond acceptor atom is displayed as cyan sphere and labeled F1:Ani &Acc, while the aromatic center is represented as a yellow sphere and labeled F2:Aro. Carbon atoms in the compound (CID: 84003) is colored in magenta and those in the compound (CID: 60560) is shown in gray. The other atoms in the compounds are colored by atom type (nitrogen: blue; oxygen: red; sulfur: yellow).

4.4 Discussion

In the present study, we analyzed the inhibition of hOAT1 and hOAT3 with the NCC and NCC2 collection of 727 clinically relevant compounds by high-throughput screening. Those compounds found to be potent hits (>95% inhibition of transporter activity) for hOAT1 or hOAT3 were subjected to computational analysis to gain insights into the biophysical features and structural requirements for inhibition of these transporters.

We evaluated the inhibition potential of these 727 test compounds with increasing stringencies. When the clinical peak unbound plasma concentrations were used, potency at >95% inhibition was exhibited by 3 compounds for hOAT1 and seven compounds for hOAT3, suggesting that concomitant administration of these drugs with other drugs might pose a high risk of drug-drug interactions. Whether these inhibitors are translocated across the cell membrane through hOAT1 and hOAT3 will be the subject for future investigation.

Our computational analysis showed that the key molecular descriptors for inhibitors of hOAT1 and hOAT3 are quite broad. The number of H-bond donors, number of rotatable bonds, and TPSA were useful for discriminating between hOAT1 inhibitors and non-inhibitors, whereas molecular weight, number of H-bond donors and H-bond acceptors, TPSA, molecular polarizability and Log $P_{7.4}$ were useful for discriminating between hOAT3 inhibitors and non-inhibitors. Similar molecular features have been proposed in published reports for inhibitors of other transporters. For example, positive charge, lipophilicity, and hydrogen bond donors seem to play important roles for organic cation transporter 1 (OCT1) (5), whereas charge, lipophilicity, molecular size, and flexibility were identified for organic cation transporter 2 (OCT2) (6). Certain descriptors are more important for hOAT3 than for hOAT1. For example, molecular weight was statistically important for hOAT3, but not for hOAT1. It has been shown that the substrate binding regions for hOAT1 and hOAT3 are different¹⁵. Substrates with more bulky groups or larger volumes generally prefer to bind OAT3 rather than OAT1, an observation which may suggest why molecular weight (i.e., molecular size) is more important for hOAT3 inhibitors than for hOAT1 inhibitors. Nonetheless it seems that the potency of hOAT1 and hOAT3 inhibitors depends on contributions from all of these descriptors in some way rather than from a single dominant descriptor, since a

statistically significant correlation was not found between any of these descriptors alone and inhibitor potency pKi (data not shown).

Our pharmacophore modeling deduced a two-point model that manifests two structural features (one anionic hydrogen-bond acceptor atom, and an aromatic center) separated by 5.7 Å. This structural characteristic is present among the high potent inhibitors for both hOAT1 and hOAT3, except Nitazoxanide ([CID:41684](#)) due to lack the anionic atom required to fit our model. However, its active metabolite and hydrolysis product Tizoxanide (CID: 394397) does contain a phenolic OH that may be sufficiently acidic to yield an anion and thereby satisfy our pharmacophore model (Fig. 5). The existence of the common pharmacophore features found in both hOAT1 and hOAT3 inhibitors might explain why inhibitors for hOAT1 also inhibit hOAT3-mediated transport and vice versa, although with different inhibitory potencies. Previous studies on pharmacophore models of most potent inhibitor drugs of OCT2 deduced a similar two-point pharmacophore consisting of a cationic site and a hydrophobic aromatic site separated by 5.0 Å (6). Belonging to the same solute carrier family, OCT2 and OATs all share key structural features, such as twelve transmembrane domains. This may suggest the apparent high degree of similarity between their pharmacophore models. The anionic site in OAT inhibitors and the cationic site in OCT2 inhibitors are consistent with their respective substrate preference.

The significance of our studies is two-fold. First, inhibition of hOAT1 or hOAT3 by one of the drugs identified in the present study (Tables 1-5) may result in the accumulation of another drug in the system, leading to toxic effects. Second, such inhibition may increase the retention time of drugs in the blood, thus improving their therapeutic efficacy if a longer half-life is preferable.

In summary, the present study screened inhibitors for hOAT1 and hOAT3 against a collection of clinical relevant compounds including prescription drugs (viz., NCC and NCC2). The most potent inhibitors (>95% inhibition), especially when considered at their peak unbound plasma concentrations, likely pose the greatest risk of clinical drug-drug interactions. The key molecular descriptors and pharmacophore model presented here for hOAT1 and hOAT3 inhibitors may provide valuable information both for structure-based drug design and for virtual screening of chemical databases in order to flag OAT1 and OAT3 inhibitors.

4.5 References:

1. FDA Administration, Guidance For Industry Drug Interaction Studies-Study Design, Data Analysis, Implications for Dosing, and Labeling Recommendations. 2012.
2. Duan, P.; Li, S.; You, G. Angiotensin II inhibits activity of human organic anion transporter 3 through activation of protein kinase Calpha: accelerating endocytosis of the transporter. *European journal of pharmacology* 2010, 627, (1-3), 49-55.
3. Hong, M.; Zhou, F.; You, G. Critical amino acid residues in transmembrane domain 1 of the human organic anion transporter hOAT1. *The Journal of biological chemistry* 2004, 279, (30), 31478-82.
4. Truong, D. M.; Kaler, G.; Khandelwal, A.; Swaan, P. W.; Nigam, S. K. Multi-level analysis of organic anion transporters 1, 3, and 6 reveals major differences in structural determinants of antiviral discrimination. *The Journal of biological chemistry* 2008, 283, (13), 8654-63.
5. Ahlin, G.; Karlsson, J.; Pedersen, J. M.; Gustavsson, L.; Larsson, R.; Matsson, P.; Norinder, U.; Bergstrom, C. A.; Artursson, P. Structural requirements for drug inhibition of the liver specific human organic cation transport protein 1. *Journal of medicinal chemistry* 2008, 51, (19), 5932-42.
6. Zolk, O.; Solbach, T. F.; Konig, J.; Fromm, M. F. Structural determinants of inhibitor interaction with the human organic cation transporter OCT2 (SLC22A2). *Naunyn-Schmiedeberg's archives of pharmacology* 2009, 379, (4), 337-48.

Chapter 5. Role of transmembrane domain 12 (TM12) of hOAT1 on its function

5.1 Introduction

Despite the clinical importance of OATs, much remains to be understood regarding the contribution of OAT structure to their transport activity and regulation. All of the cloned OATs share several common structural features including 12 transmembrane domains flanked by intracellular N and C termini; multiple glycosylation sites localized in the first extracellular loop between transmembrane domains 1 and 2, and multiple potential phosphorylation sites present in the intracellular loop between transmembrane domains 6 and 7, and in the C terminus. Investigation from our laboratory on the structure-function relationship of OATs revealed that glycosylation is necessary for the targeting of these transporters to the plasma membrane (1, 2). We also showed that the first transmembrane domain of hOAT1 plays an important role in both the targeting of the transporter to the cell surface and its substrate recognition (3). Previously, (4) reported the existence of several alternative splice variants of hOAT1 in the kidney. The functional characterization of these variants revealed that two such variants, hOAT1-3 and hOAT1-4, both of which possess a deletion of TM 11 and TM 12 exhibited no transport activity. Their results prompted us to hypothesize that TM 11 and/or TM 12 may play a critical role in hOAT1 function. In the present study, we investigated the importance of TM 12 in hOAT1. We identified several amino acids critically involved in hOAT1 function.

5.2 Materials and methods

Materials - *p*-[³H]Aminohippuric acid (PAH) was from PerkinElmer Life and Analytical Sciences (Waltham, MA). Membrane-impermeable biotinylation reagent NHS-SS-biotin and streptavidin agarose beads were purchased from Pierce Chemical (Rockford, IL). Rec-Protein G Sepharose 4B beads were purchased from Invitrogen (Carlsbad, CA). QuickChange site-directed mutagenesis kits were purchased from Stratagene (La Jolla, CA). COS-7 cells and LLC-PK1 cells were purchased from American Type Culture Collection (Manassas, VA). All other reagents were purchased from Sigma-Aldrich (St. Louis, MO).

Site-Directed Mutagenesis - Mutant transporters were generated by site-directed mutagenesis by use of hOAT1 or hOAT1-*myc* as a template. hOAT1-*myc* contains a 10-amino-acid *c-myc* tag at the C terminus of hOAT1. Previous studies from our laboratory (Tanaka et al., 2004) showed that the *myc*-tagged protein retained the functional properties of the native (unmodified) structure. The mutant sequences were confirmed by the dideoxy chain termination method.

Cell Culture and Transfections - COS-7 cells were grown in Dulbecco's modified Eagle's medium containing 10% fetal bovine serum and antibiotics. LLC-PK1 cells were grown in Medium 199 containing 10% fetal bovine serum. Cells were grown to 90 to 100% confluence and transfected with the appropriate plasmids by use of Lipofectamine 2000 (Invitrogen).

Transport Measurements - For each well, uptake solution was added. The uptake solution consisted of phosphate-buffered saline (PBS)/CM (137 mM NaCl, 2.7 mM KCl, 4.3 mM Na₂HPO₄, 1.4 mM KH₂PO₄, 0.1 mM CaCl₂, and 1 mM MgCl₂, pH 7.3) and [³H]PAH (20uM). At the times indicated in the figure legends, the uptake was stopped by

aspirating the uptake solution off and rapidly washing the cells with ice-cold PBS solution. The cells were then solubilized in 0.2 N NaOH, neutralized in 0.2 N HCl, and aliquoted for liquid scintillation counting. The uptake count was standardized by the amount of protein in each well.

Cell Surface Biotinylation - Cell surface expression levels of hOAT1 and its mutants were examined by use of the membrane-impermeable biotinylation reagent, NHS-SS-biotin (Pierce Chemical). hOAT1 and its mutants were expressed in cells grown in 6-well plates by use of Lipofectamine 2000 as described above. After 48 h, the medium was removed and the cells were washed twice with 3 ml of ice-cold PBS/CM, pH 8.0. The plates were kept on ice and all solutions were ice-cold for the rest of the procedure. Each well of cells was incubated with 1 ml of NHS-SS-biotin (0.5 mg/ml in PBS/CM) in two successive 20-min incubations on ice with very gentle shaking. The reagent was freshly prepared for each incubation. After biotinylation, each well was rinsed briefly with 3 ml of PBS/CM containing 100 mM glycine, then incubated with the same solution for 20 min on ice, to ensure complete quenching of the unreacted NHS-SS-biotin. The cells were then dissolved on ice for 1 h in 400 μ l of lysis buffer (10 mM Tris, 150 mM NaCl, 1 mM EDTA, 0.1% SDS, 1% Triton X-100 with 1:100 protease inhibitor cocktail (Sigma-Aldrich)). The cell lysates were cleared by centrifugation at 16,000g at 4°C. Fifty microliters of streptavidin-agarose beads (Pierce Chemical) were then added to the supernatant to isolate cell membrane protein. hOAT1 and its mutants were detected in the pool of surface proteins by SDS-PAGE and immunoblotting.

Metabolic Labeling and Immunoprecipitation - LLC-PK1 cells expressing hOAT1 and its mutants were washed twice with PBS and incubated for 45 min in methionine-free DMEM at 37°C and 5% CO₂. Radiolabeling of cell proteins was carried out by replacing the medium with fresh methionine-free DMEM supplemented with 100 μ Ci

[³⁵S]methionine and incubated for 30 min at 37°C and 5% CO₂. The chase was started by aspirating the [³⁵S]methionine-containing medium, followed by two PBS washes and incubation in the complete DMEM containing 10% fetal calf serum for different time periods. The labeled cells were then washed twice with PBS and harvested for lysate preparation with use of 400 µl of lysis buffer. The cell lysates were cleared by centrifugation at 16,000g for 30 min at 4°C. The supernatants were then precleaned with 30 µl of Protein G beads to reduce nonspecific binding. The precleaned cell lysates were incubated with 4 µg of anti-*myc* antibody for overnight at 4°C. Thirty microliters of Protein G beads were then added and mixed with end-over-end rotating at 4°C for 3 h. Proteins bound to the Protein G beads were denatured in Laemmli buffer for SDS-PAGE and autoradiography.

Protease Treatment - hOAT1 and its mutants were transfected into LLC-PK1 cells grown in 12-well plates by use of Lipofectamine 2000. Cells were then incubated in DMEM containing proteasome inhibitors MG132 (10 µM), lactacystin (10 µM), or lysosomal inhibitors leupeptin/pepstatinA (50, 100 µg/ml), NH₄Cl (2, 5, 15 mM), and chloroquine (100, 200 µM) individually. Treated cells were collected at specific time points as indicated in the figure legends and lysed. Equal amount of proteins were loaded on 7.5% SDS-PAGE minigels and analyzed by immunoblotting as described earlier.

Electrophoresis and Immunoblotting - Protein samples (100 µg) were resolved on 7.5% SDS-PAGE minigels and electroblotted on to polyvinylidene difluoride membranes. The blots were blocked for 1 h with 5% nonfat dry milk in PBS-0.05% Tween 20, washed, and incubated for 1 h at room temperature with appropriate primary antibodies followed by horseradish peroxidase-conjugated secondary antibodies. The signals were detected by SuperSignal West Dura Extended Duration Substrate kit (Pierce Chemical).

Nonsaturating immunoreactive protein bands were quantified by scanning densitometry with FluorChem 8000 imaging system (Alpha Innotech, San Leandro, CA).

Data Analysis - Data were analyzed for statistical significance by use of one-way ANOVA analysis or Student's *t* test. Differences with *p* values of 0.05 were considered statistically significant.

5.3 Results

Alanine Scanning of Residues in TM12 - To probe the contribution of each residue in TM 12 to hOAT1 function, we systematically replaced each residue with alanine (A) using hOAT1-myc as template. Because of the multiple roles of dileucine motif (LL) plays in other transporters (5-7), the double mutant L503/L504A was also generated. The functional properties of these mutants were then determined by measuring the uptake of [³H] PAH in mutant-transfected cells. Results obtained from this analysis are shown in Fig.1. Although most of the mutants exhibited significant transport activities compared to hOAT1 wild type, mutants Y490A (Y=Tyr=tyrosin) and L503/L504A almost completely lost transport activity. Mutants Y490A and L503/L504A were also generated using untagged hOAT1 as template, and the similar results were obtained (data not shown). Wild type hOAT1 functions as an organic anion exchanger with one anion being transported into the cells in exchange of another anion being effluxed out of the cells. Wild type hOAT1 is also sensitive to the inhibition by probenecid. Our efflux experiment as well as inhibition study revealed that all the active mutants retained the characteristic of hOAT1 wild type as an organic anion exchanger and being sensitive to the inhibition by probenecid (data not shown). Because of the loss in the uptake of PAH by Y490A and L503/L504A, additional studies were focused on these mutants.

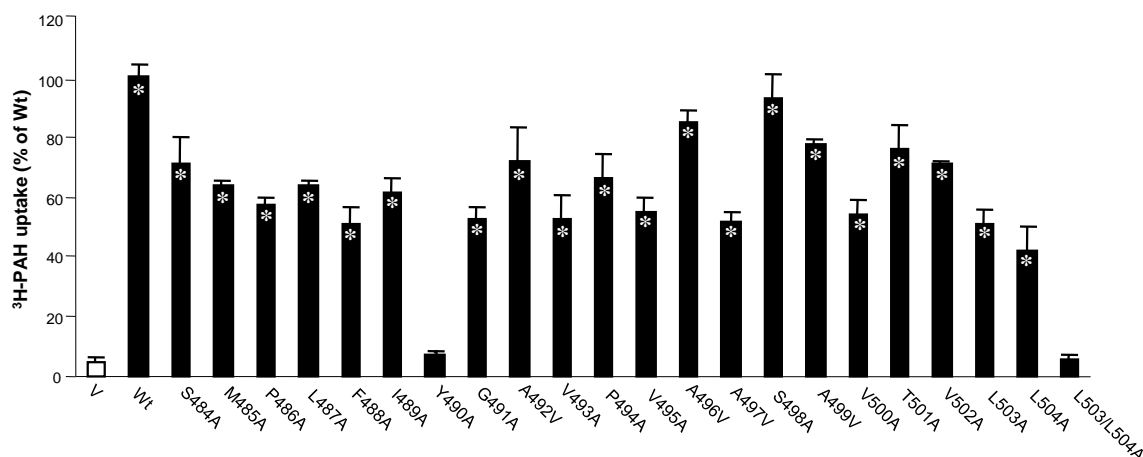


Fig.1. ³H-labeled PAH uptake by hOAT1 wild type (Wt) and its alanine-substituted mutants. The mutants were generated by use of hOAT1-cmyc as template. Transport of PAH (20 μ M, 3 min) in COS-7 cells expressing hOAT1 Wt and its alanine-substituted mutants was measured. Uptake activity was expressed as a percentage of the uptake measured in Wt. The results represent data from three experiments, with triplicate measurements for each mutant. * values significantly different ($p < 0.05$) from that of pcDNA vector (V, mock control). The uptake in LLC-PK1 cells gave similar results (not shown).

The role of Tyr-490 in hOAT1 Function -To further evaluate the role of Tyr-490 in hOAT1 function, we mutagenized Tyr-490 to two other aromatic residues Phe (Phe = F) and Trp (Try=W). As shown in Fig. 2a, substitution of Tyr-490 with Trp (the resulting mutant Y490W) partially recovered the transport activity lost by substitution with alanine, whereas substitution of Tyr-490 with Phe (the resulting mutant Y490F) almost completely recovered the transport activity. Such pattern of uptake was observed in both COS-7 cells and in LLC-PK1 cells. Kinetic analysis of Y490W (Figs. 2b, 2c) showed that the decreased transport activity of this mutant mainly resulted from a decreased V_{max} (V_{max} : 0.037 ± 0.004 pmol/ μ g.3 min with wild type hOAT1, and 0.021 ± 0.005 pmol/ μ g.3 min with Y490W) without significant change in K_m (K_m : 16.7 ± 0.7 μ M for wild type hOAT1 and 15.9 ± 0.6 μ M for Y490W).

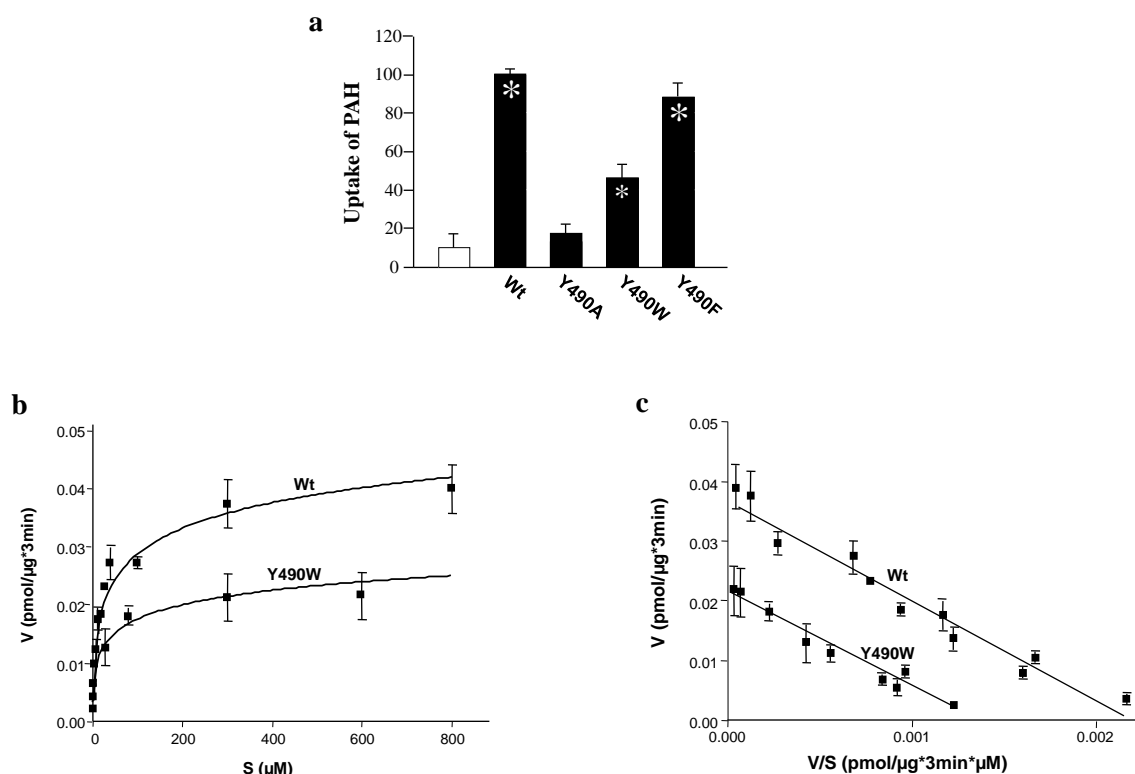


Fig. 2. Effects of mutation at Tyr-490 on hOAT1 function. a, effects of mutation at Tyr-490 on the function of hOAT1. ^3H -Labeled PAH uptake (20 μM , 3 min) was measured in cells expressing hOAT1 wild-type (Wt), pcDNA vector (V, mock control), Y490A, Y490W, and Y490F. The results represent data from three experiments, with triplicate measurements for each mutant. * values significantly different ($p < 0.05$) from that of mock control (V). b, kinetic analysis of PAH transport mediated by hOAT1 Wt and mutant Y490W. Kinetic characteristics were determined at the initial rate of uptake (3-min uptake) with substrate concentration ranging from 2 to 800 μM in cells expressing hOAT1Wt, mutant Y490W, or pcDNA vector (mock control). The data represent uptake into hOAT1 Wt-, hOAT1 mutant Y490W/transfected cells minus uptake into pcDNA vector-transfected cells. Values are mean \pm S.E. ($n = 3$). c, transport kinetic values were calculated by use of the Eadie-Hofstee transformation. V, velocity; S, substrate concentration. Values were mean of three experiments, and the error bars show the range of observations.

As cellular uptake of PAH requires that the transporter be localized to the plasma membrane, we tested whether the reduced or the abolished transport activity was due to abnormal expression of the transporter on the cell surface as well as in the total cell extracts by immunoblot analysis. As shown in the top panel of Fig. 3a, cell surface expression of Y490A dramatically decreased. In total cell lysates (bottom panel of Fig. 3a), the transporter runs as two bands of 60 (shown as arrow head) and 80 (shown as arrow) kDa apparent sizes. We previously showed (2) that the lower band was sensitive

to the treatment of endoglycosidase H (endo H), and therefore corresponds to core-glycosylated immature form of the protein, which resides in the endoplasmic reticulum (ER). The upper band was resistant to the treatment of endo H, and therefore corresponds to the fully processed and glycosylated mature form of the protein, which is expressed at the cell surface. The low level of the immature band as compared to the high level of mature band indicates the high maturation efficiency of the transporter in these cells. The total expression of Y490A (both the mature and the immature form) was also dramatically decreased (bottom panel of Fig. 3a). The expression of the mutants correlated well with their functional activity. Mutant Y490F had similar expression as that of the wild type hOAT1. Y490W had moderate expression, whereas the expression of Y490A was undetectable.

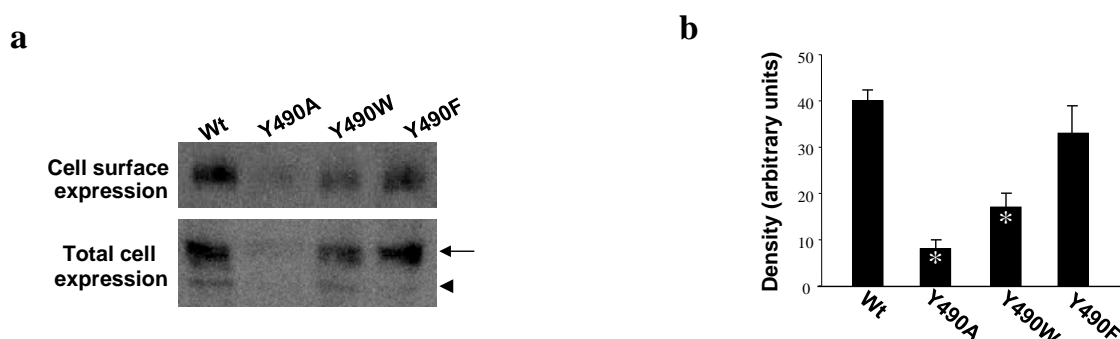


Fig. 3. Effects of mutations at Tyr-490 on cell surface and total cell expression of hOAT1. a. *Top panel:* Western blot analysis of cell surface expression of hOAT1 Wt and its mutants. Cells were biotinylated, and the labeled cell surface proteins were precipitated with streptavidin beads, separated by SDS-PAGE, followed by Western blotting with anti-myc antibody (1:100). *Bottom panel:* Total cell expression of hOAT1 Wt and its mutants. Cells were lysed, and their proteins were separated by SDS-PAGE, followed by Western blotting with anti-myc antibody. Mature form was shown as arrow and immature form was shown as arrowhead. b. Densitometry analysis of cell surface expression of Y490 mutants shown in top panel of a. Asterisks indicate values significantly different ($p < 0.05$) from that of wild type (Wt).

The lack of the expression of the transporter when Tyr-490 was substituted by alanine could result from the decreased protein synthesis or accelerated degradation. To investigate the underlying mechanisms, we used a battery of protease inhibitors. Cells degrade proteins through two major systems, the proteasome and the lysosome. The

proteasome is involved in the degradation of most cytosolic and nuclear proteins as well as some membrane proteins (8-10) and removes misfolded or misaggregated proteins in the endoplasmic reticulum (11). The lysosome degrades membrane proteins and extracellular materials that enter the cell via endocytosis (10). These different pathways of proteolysis can be determined by their sensitivity to different inhibitors. Degradation of polypeptides by the proteasome can be inhibited by MG132 and lactacystin. Lysosomal proteolysis can be inhibited by leupeptin, pepstatin A, ammonium chloride (NH_4Cl) or chloroquine. As shown in Fig. 4, treatment of cells expressing wild type hOAT1 and mutant Y490A with lysosomal inhibitors led to the accumulation of the mature form (80 kDa) for both the wild type and its mutant in the total cell lysates (Fig. 4a). Further studies through cell surface biotinylation and functional analysis showed that the increased mature form in the total cell lysate was accompanied by an increase of Y490A at the cell surface (Fig. 4c), as a consequence, resulting in an increased transport activity (Fig. 4e).

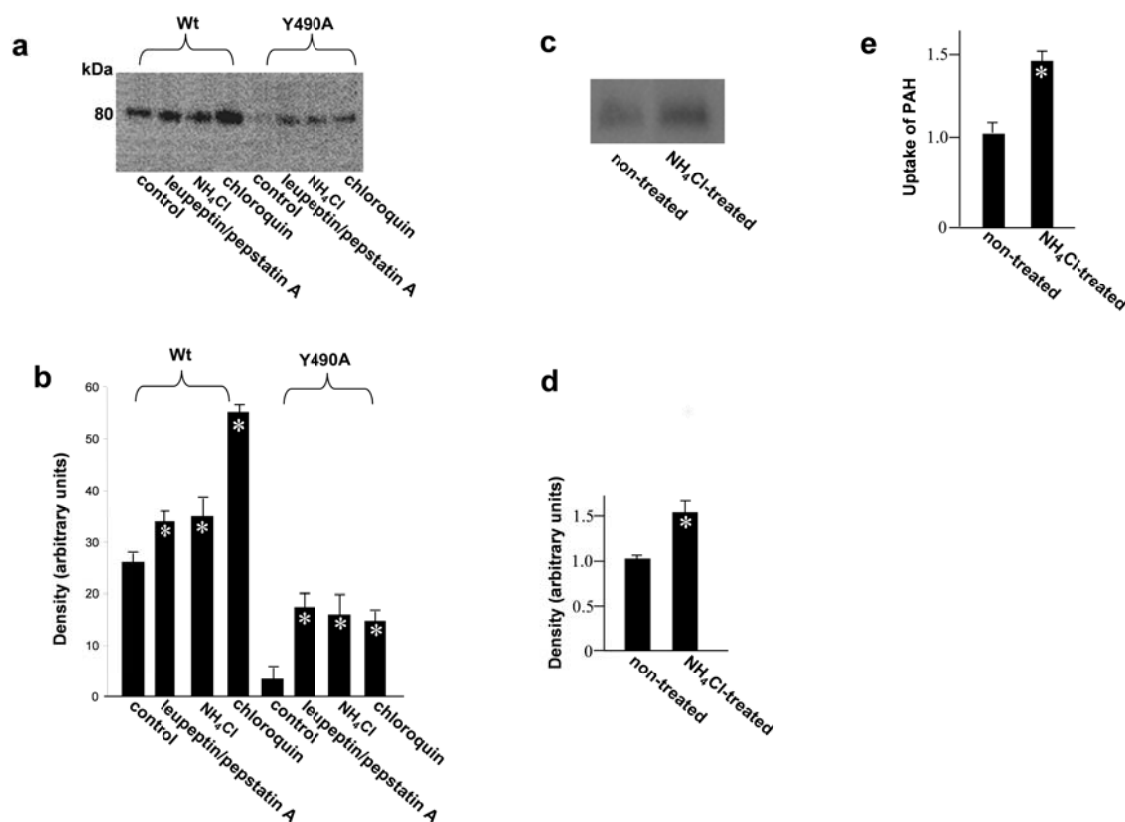


Fig. 4. Effect of lysosomal inhibitors on wild type (Wt) hOAT1 and its mutant Y490A. a. Western blot analysis of total cell expression of hOAT1 Wt and Y490A in cells treated with or without lysosomal inhibitors. Cells were treated for 16 hrs with or without lysosomal inhibitors leupeptin /pepstatin A (50 µg/ml), NH₄Cl (2 mM), chloroquin (100 µM). Treated cells were then lysed, followed by Western blotting using anti-myc antibody (1:100). b. Densitometry analysis of band densities from a. The results represent data from three experiments. c. Cell surface expression of Y490A in cells treated with or without lysosomal inhibitor NH₄Cl. Cells were treated for 16 hrs with or without lysosomal inhibitor NH₄Cl (2 mM), followed by cell surface biotinylation and Western blotting using anti-myc antibody (1:100). d. Densitometry analysis of band densities from c. The results represent data from three experiments. Asterisks indicate values significantly different (p < 0.05) from that of the density measured in Y490A-expressing cells treated without NH₄Cl. e. ³H-labeled PAH uptake in Y490A-expressing cells treated with or without lysosomal inhibitor NH₄Cl. Uptake activity was expressed as a percentage of the uptake measured in Y490A-expressing cells treated without NH₄Cl. The results represent data from three experiments, with triplicate measurements for each mutant. Asterisks indicate values significantly different (p < 0.05) from that of the uptake measured in Y490A-expressing cells treated without NH₄Cl.

Treatment of cells with proteasomal inhibitors MG132 (Fig. 5a) and lactacystin (Fig. 5c) resulted in the accumulation of a nonglycosylated form (47 kDa), a partially glycosylated immature form (60 kDa), a fully glycosylated cell mature form (80 kDa) and some high-molecular weight band for both the wild type and its mutant in the total cell lysates. These OAT1-immunoreactive bands are MG132-, and lactacystin-specific, because

they were not observed in the absence of the inhibitors. The high molecular weight band may result from the aggregation of the immature form and was also observed in other transporters when treated with the proteasomal inhibitors (12). However, cell surface biotinylation study showed that the increased mature form of Y490A in the total cell lysates by MG-132 and lactacystin treatments did not result in any detectable cell surface expression of this mutant (not shown).

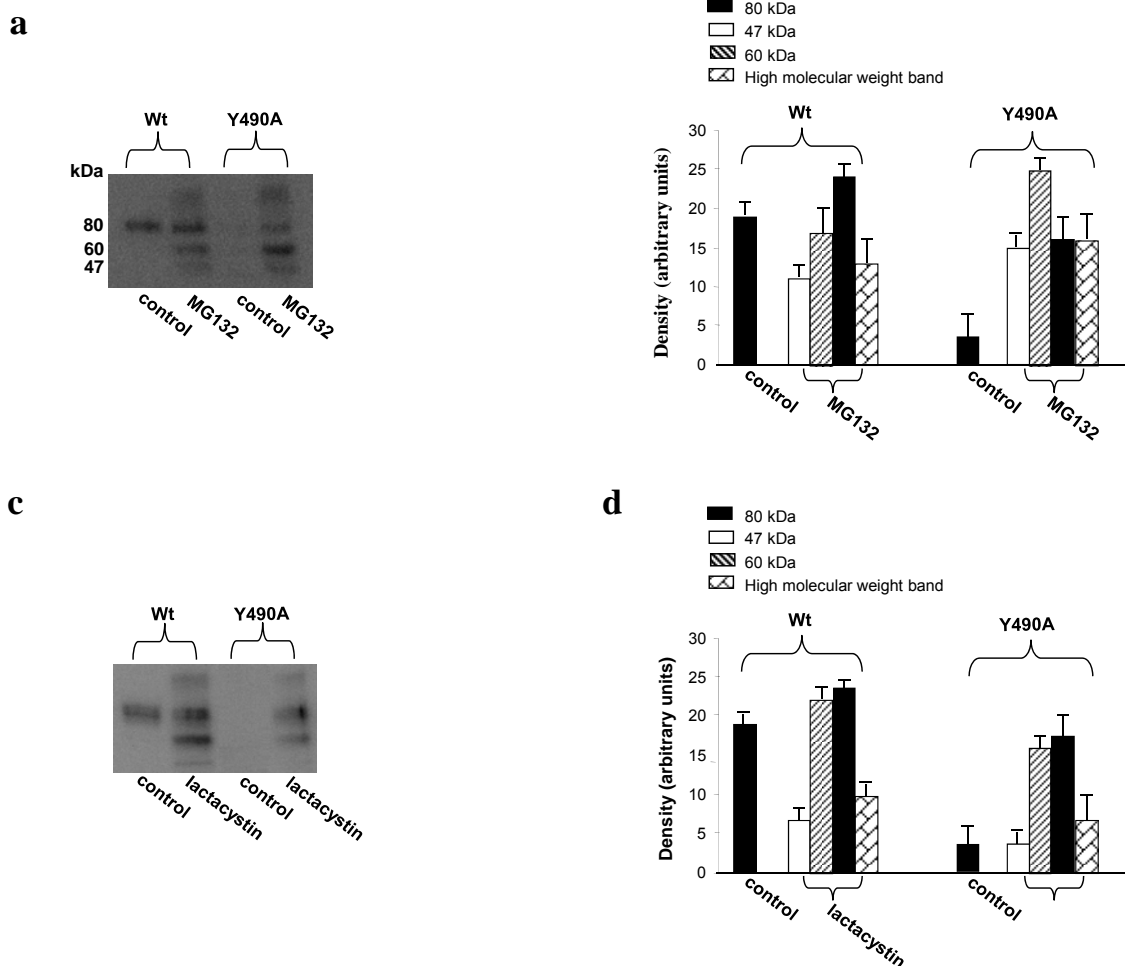


Fig. 5. Effect of proteasomal inhibitors on wild type (Wt) hOAT1 and its mutant Y490A. a, c. Western blot analysis of total cell expression of hOAT1 Wt and Y490A in cells treated with or without proteasomal inhibitors. Cells were treated for 6 hrs with or without proteasomal inhibitors MG132 (10 μ M) (a) or lactacystin (10 μ M) (c). Treated cells were then lysed, followed by Western blotting using anti-myc antibody (1:100). b, d. Densitometry analysis of band densities from a and c as well as other experiments. The results represent data from three experiments.

The effect of Y490A on the maturation efficiency of the transporter was then examined by pulse-chase experiments (Fig. 6). The newly synthesized proteins were pulse-

labeled with ^{35}S methionine and chased for different time periods. After 2 h of chasing, significant amount of immature form (shown as arrow head) of hOAT1 wild type (Wt) and mutant Y490A was converted to mature form (shown as arrow). Therefore, mutant Y490A had similar maturation efficiency as that of the wild type.

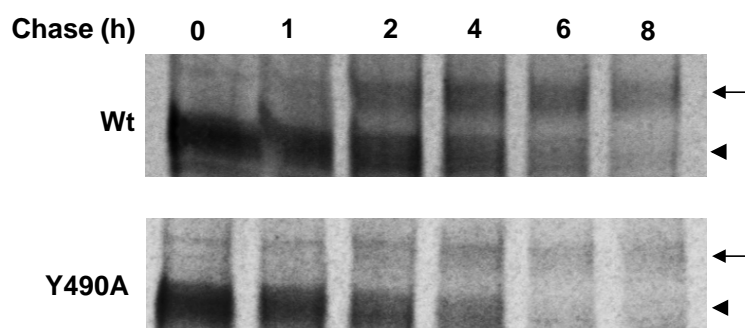


Fig. 6. Pulse-chase analyses of the role of Y490 in the maturation of hOAT1. The chase began after 30 min pulse labeling. Mature form was shown as arrow and immature form was shown as arrowhead.

The role of L503/L504 in hOAT1 Function - Similar to Y490A, substitution of L503/L504 with alanine also resulted in an abolished transport activity due to the loss of the expression of the transporter both at the cell surface (Fig. 7a) and in the total cell lysates (both the mature form and the immature form) (Fig. 7b).

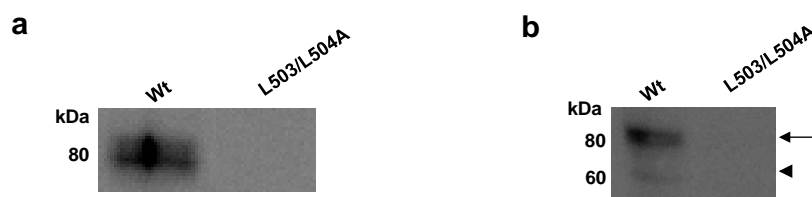


Fig. 7. Cell surface and total cell expression of hOAT1 wild type (Wt) and its mutant L503A/L504A. a. Western blot analysis of cell surface expression of hOAT1 Wt and its mutant L503A/L504A. Cells were biotinylated, and the labeled cell surface proteins were precipitated with streptavidin beads, separated by SDS-PAGE, followed by Western blotting with anti-myc antibody (1:100). b. Total cell expression of hOAT1 wild type (Wt) and its mutant L503A/L504A. Cells were lysed, and their proteins were separated by SDS-PAGE, followed by Western blotting with anti-myc antibody. Mature form was shown as arrow and immature form was shown as arrowhead.

However, in contrast to Y490A, treatment of cells expressing L503/L504A with lysosomal inhibitors did not lead to the accumulation of either the mature form (80 kDa), or the immature form of the transporter in the total cell lysates (Fig. 8).

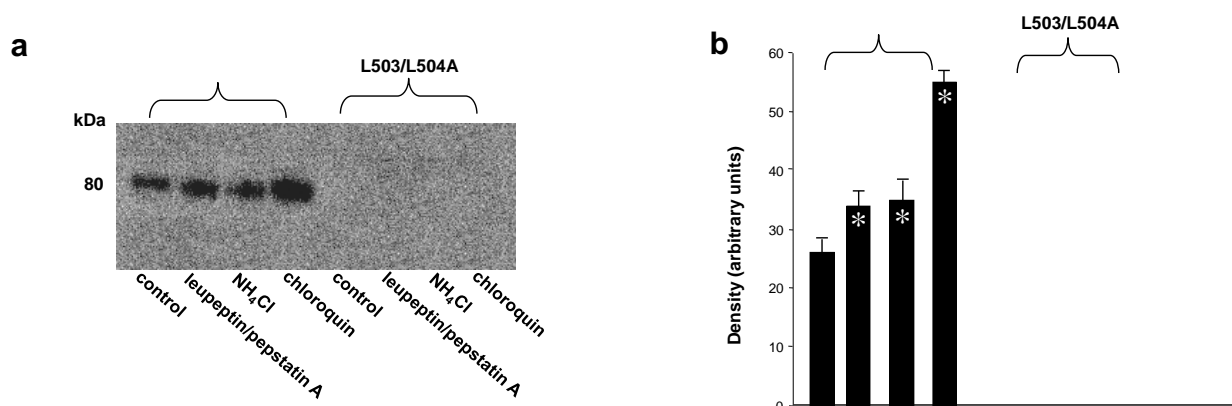


Fig. 8. The effect of lysosomal inhibitors on the expression of hOAT1 wild type (Wt) and its mutant L503/L504A. a. Western blot analyses. Cells were treated for 16 hrs with lysosomal inhibitors leupeptin /pepstatin A (50, 100 μ g/ml), NH₄Cl (2, 5, 15 mM), chloroquin (100, 200 μ M). Treated cells were lysed, followed by Western blotting using anti-myc antibody (1:100). The blot only showed the result with lysosomal inhibitors at the following concentrations: leupeptin /pepstatin A (50 μ g/ml), NH₄Cl (2 mM), and chloroquin (100 μ M). Inhibitors at other concentrations gave similar results (not shown). b. Densitometry analysis of band densities from a. The results represent data from three experiments.

Treatment of the cells with proteasomal inhibitors MG132 or lactacystin only resulted in the accumulation of small amount of partially glycosylated form (60 kDa) of the mutant transporter (Fig. 9) in the total cell lysate.

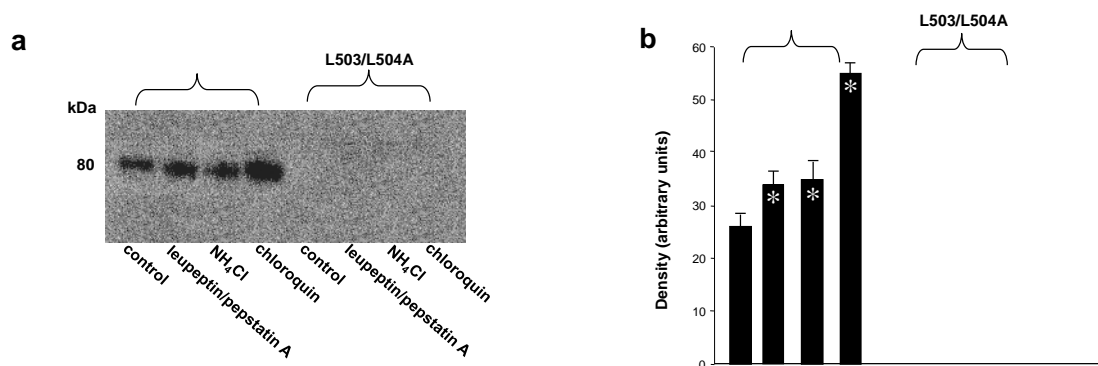


Fig. 9. The effect of proteasomal inhibitors on the expression of hOAT1 wild type (Wt) and its mutant L503/L504A. a, c. Cells were treated for 6 hrs with proteasomal inhibitors MG132 (10 μM) (a) or lactacystin (10 μM) (c). Treated cells were lysed, followed by Western blotting using anti-myc antibody (1:100). b, d. Densitometry analysis of band densities from a and c as well as other experiments. The results represent data from three experiments.

The inability of these protease inhibitors to accumulate the mature form of L503/L504A suggests that accelerated degradation may not be the main mechanism for the lack of mature form of this mutant. To determine whether the lack in the mature form of this mutant reflects decreased maturation efficiency, we again performed pulse-chase experiments (Fig. 10). After 2 h of chasing, significant amount of immature form (shown as arrow head) of hOAT1 wild type (Wt) was converted to mature form (shown as arrow). In contrast, the conversion of the immature form of mutant L503/L504A to mature form never occurred, suggesting that L503/L504 is critical for the maturation of the transporter.

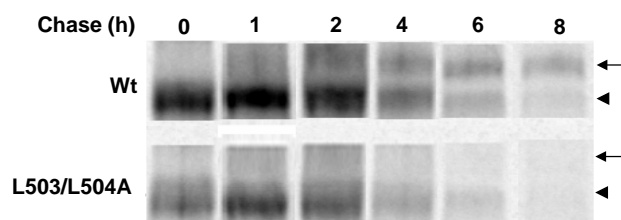


Fig. 10. Analyses of the role of dileucine L503/L504 in the maturation of hOAT1 by pulse-chase labeling. The chase began after 30 min pulse labeling. Mature form was shown as arrow and immature form was shown as arrowhead.

However, the lack of maturation of L503/L504A could be due to the alteration of the specific dileucine, or due to the simultaneous alteration of two amino acids at a specific location. To differentiate between these possibilities, we constructed a different double mutant of Leu-503 with another adjacent residue Val-502. Our results (Fig. 11) showed that the mutant V502/L503A exhibited significant transport activity indicating that mutation at V502/L503 did not prevent the transporter from producing a fully glycosylated cell surface form of the transporter. These results suggest that it is the dileucine rather than the specific location of L503/L504 that has a specific role in promoting the maturation of hOAT1.

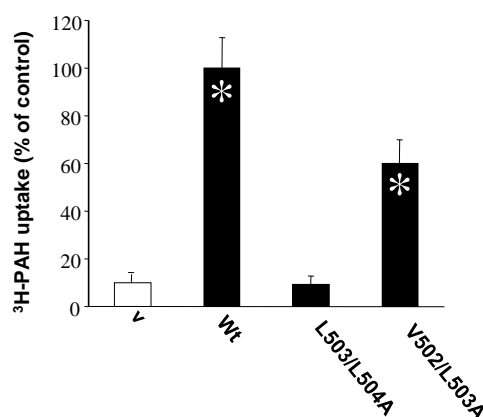


Fig. 11. PAH uptake by hOAT1 wild type (Wt) and its mutants V502/L503A and L503/L504A. Transport of PAH (20 μ M, 3 min) in cells expressing hOAT1 Wt and its mutants was measured. Uptake activity was expressed as a percentage of the uptake measured in Wt. The results represent data from three experiments, with triplicate measurements for each mutant. Asterisks indicate values significantly different ($p < 0.05$) from that of mock control (V).

5.4 Discussion

OAT family and another closely related organic cation transporter OCT family belong to a large group of related proteins, the major facilitator superfamily (MFS). The members of MFS share common structural features, including 12 putative

transmembrane-spanning domains and intracellular carboxyl and amino termini. The elucidation of high-resolution crystal structures of two other MFS members, LacY (13) and GlpT (14) suggests that all MFS members may share a common fold. Based on such assumption, three-dimensional structure models of rat OCT1, rabbit OCT2, and human OAT1 have been developed using the template structure of LacY and GlpT (14-16). In these models, transmembrane domains 1, 2, 4, 5, 7, 8, 10, and 11 form a large hydrophilic cleft for substrate binding, whereas other transmembrane domains such as transmembrane domain 12 (TM 12) were thought to provide support for the transporter. In the current studies, important role of TM 12 has been revealed. This information may improve our understanding in individual difference in drug response related to potential genetic variation.

In the current studies, we employed alanine-scanning mutagenesis to examine the functional importance of each residue within TM12 of hOAT1. Through this approach, we discovered several amino acids. Tyr-490, and a dileucine L503/L504, when substituted with alanine, had the most dramatic functional effects. However, other mutants with reduced transport activity may also be functionally important and need to be further investigated.

Tyr-490 seems to be critical for the stability of the transporter. We showed that substitution of Tyr-490 with alanine led to the dramatic loss of transport activity. To explore the underlying mechanisms for such loss of transport activity, we replaced Tyr-490 with Phe or Trp (Fig. 2). The side chain of Tyr contains an aromatic ring and a -OH group. The side chain of Phe contains only an aromatic ring, whereas the side chain of Trp contains both an aromatic ring and an indole ring. We showed that substitution of Tyr-490 with Trp partially recovered the transport activity lost by substitution of Tyr-490 with alanine, and substitution of Tyr-490 with Phe fully recovered the transport activity, suggesting that the aromatic ring

and the size of the side chain of Tyr-490, but not its –OH group are critically involved in hOAT1 function. Our kinetic analysis showed that the reduced transport activity of Y490W was mainly due to a reduced V_{max} . We further showed that the loss of function by substitution of Tyr-490 with alanine resulted from the loss of total expression of the transporter protein (Fig. 3). By testing the effects of a battery of protease inhibitors on mutant Y490A, we observed that lysosomal inhibitors resulted in the accumulation of the mature form of the mutant transporter (Fig. 4a), and part of the accumulated mature form was able to target to the cell surface (Fig. 4c), which led to an increased transport activity (Fig. 4e). These results suggest that mutation at Tyr-490 may destabilize the transporter at the cell surface, which led to the internalization of the transporter and the subsequent degradation through the lysosomal pathway. Proteasomal inhibitors resulted in the accumulation of both the immature form and the mature form of the mutant transporter (Fig. 5). However, our biotinylation study showed that the mature form accumulated by protease inhibitors was not delivered to the cell surface. It is possible that the immature form accumulated by proteasomal inhibitors escaped from the ER quality control and was further processed to mature form with a defective conformation, which was unable to insert to the cell surface. It is also possible that the protease inhibitors affect the expression/function of hOAT1-interacting proteins that prevent mature hOAT1 from inserting into the plasma membrane.

Our conclusion that Tyr-490 is critical for the stability of the transporter was further reinforced by our pulse-chase studies (Fig. 6). We showed that hOAT1 mutant Y490A matured as efficiently as that of hOAT1 wild type. Therefore, Tyr-490 does not seem to play a role in the maturation efficiency of the transporter.

In contrast to Tyr-490, mutation of which caused an accelerated degradation of the transporter, mutation at L503/L504 seems to mainly prevent the maturation of the transporter (Fig. 10), although certain role of L503/L504 in stabilizing the transporter may also be possible due to the fact that the treatment of L503/L504A-expressing cells with proteasome inhibitors slightly increased the expression of a band centered around 60 kDa (Fig. 9). The specific role of L503/L504 in the maturation of hOAT1 was further reinforced by our demonstration that when Leu-503 was simultaneously mutated with another adjacent residue Val-502 instead of Leu-504, the double mutant V502A/L503A exhibited significant transport activity (Fig. 11), indicating that this mutant is capable to produce a fully glycosylated cell surface form of the transporter. Therefore, it is the alteration of a specific dileucine rather than the simultaneous alteration of two amino acids at a specific location of the TM 12 that impairs the maturation. Dileucine mutation may impose a folding defect on hOAT1, which is recognized by the ER quality control machinery as non-native and therefore marked for degradation by proteasome. As a result, escape from the ER for maturation is severely compromised.

In summary, our current studies are the first to highlight the central role of the TM12 of hOAT1: Tyr-490 is essential in maintaining the stability of the transporter, and dileucine L303/L304 is critically involved both in correct folding of the transporter, which is required for the maturation of the transporter, and in maintaining the stability of the transporter. We have previously demonstrated that hOAT1 function could be disrupted by impaired cell surface targeting or impaired substrate recognition (2, 3). The current studies demonstrated that hOAT1 dysfunction could be determined within TM 12 by the accelerated degradation and defective maturation of the transporter.

5.5 References

1. Tanaka K, Xu W, Zhou F, and You G (2004) Role of glycosylation in the organic anion transporter OAT1. *J Biol Chem* 279:14961–14966.
2. Zhou F, Xu W, Hong M, Pan Z, Sinko PJ, Ma J, and You G (2005) The role of N-linked glycosylation in protein folding, membrane targeting, and substrate binding of human organic anion transporter hOAT4. *Mol Pharmacol* 67:868–876.
3. Hong M, Zhou F, and You G (2004) Critical amino acid residues in transmembrane domain 1 of the human organic anion transporter hOAT1. *J Biol Chem* 279:31478–31482.
4. Bahn A, Ebbinghaus C, Ebbinghaus D, Ponimaskin EG, Fuzesi L, Burckhardt G, and Hagos Y (2004) Expression studies and functional characterization of renal human organic anion transporter 1 isoforms. *Drug Metab Dispos* 32:424–430.
5. Bello V, Goding JW, Greengrass V, Sali A, Dubljevic V, Lenoir C, Trugnan G, and Maurice M (2001) Characterization of a di-leucine-based signal in the cytoplasmic tail of the nucleotide-pyrophosphatase NPP1 that mediates basolateral targeting but not endocytosis. *Mol Biol Cell* 12:3004–3015.
6. Pen˜a-Mu˜n˜oz nzenmayer G, Catalaˆn M, Cornejo I, Figueroa CD, Melvin JE, Niemeyer MI, Cid LP, and Sepuˆlveda FV (2005) Basolateral localization of native CIC-2 chloride channels in absorptive intestinal epithelial cells and basolateral sorting encoded by a CBS-2 domain di-leucine motif. *J Cell Sci* 118:4243–4252.
7. Eckhardt ER, Cai L, Shetty S, Zhao Z, Szanto A, Webb NR, and Van der Westhuyzen DR (2006) High density lipoprotein endocytosis by scavenger receptor SR-BII is clathrin-dependent and requires a carboxyl-terminal dileucine motif. *J Biol Chem* 281:4348–4353.
8. Jensen TJ, Loo MA, Pind S, Williams DB, Goldberg AL, and Riordan JR (1995) Multiple proteolytic systems, including the proteasome, contribute to CFTR processing. *Cell* 83:129–135.
9. Sepp-Lorenzino L, Ma Z, Lebwohl DE, Vinitsky A, and Rosen N (1995) Herbimycin A induces the 20 S proteasome- and ubiquitin-dependent degradation of receptor tyrosine kinases. *J Biol Chem* 270:16580–16587.
10. Ward CL, Omura S, and Kopito RR (1995) Degradation of CFTR by the ubiquitin-proteasome pathway. *Cell* 83:121–127.
11. Kopito RR (1997) ER quality control: the cytoplasmic connection. *Cell* 88:427–430.
12. Bauman PA and Blakely RD (2002) Determinants within the C-terminus of the human norepinephrine transporter dictate transporter trafficking, stability, and activity. *Arch Biochem Biophys* 404:80–91.

13. Abramson J, Smirnova I, Kasho V, Verner G, Kaback HR, and Iwata S (2003) Structure and mechanism of the lactose permease of *Escherichia coli*. *Science* **301**:610–615.
14. Huang Y, Lemieux MJ, Song J, Auer M, and Wang DN (2003) Structure and mechanism of the glycerol-3-phosphate transporter from *Escherichia coli*. *Science* **301**:616–620.
15. Popp C, Gorboulev V, Müller TD, Gorbunov D, Shatskaya N, and Koepsell H (2005) Amino acids critical for substrate affinity of rat organic cation transporter 1 line the substrate binding region in a model derived from the tertiary structure of lactose permease. *Mol Pharmacol* **67**:1600–1611.
16. Zhang X, Shirahatti NV, Mahadevan D, and Wright SH (2005) A conserved glutamate residue in transmembrane helix 10 influences substrate specificity of rabbit OCT2 (SLC22A2). *J Biol Chem* **280**:34813–34822.
17. Perry JL, Dembla-Rajpal N, Hall LA, and Pritchard JB (2006) A three-dimensional model of human organic anion transporter 1: aromatic amino acids required for substrate transport. *J Biol Chem* **281**:38071–38079.

Chapter 6. Regulation of OATs by oligomerization

6.1 Introduction

Oligomerization plays critical role in various aspects of transporter function. Multiple subunits in an oligomer may form a single translocation pathway, allowing substrates to be transported. Oligomerization may also facilitate transporter to target to the cell surface and increase transporter stability. We have previously demonstrated that hOAT1 forms homo-oligomers in cultured cells and in rat kidney (1). However, the functional consequence of such oligomerization has never been elucidated. In the current study, we employed a novel approach by examining the effects of short hydrophobic peptides corresponding to transmembrane domains (TMDs) 1-12 of hOAT1 on the oligomerization and function of the transporter.

6.2 Materials and methods

Materials - [^3H]*p*-Aminohippuric acid (PAH) was from PerkinElmer Life Sciences. Membrane-impermeable biotinylation reagent NHS-SS-biotin, cross-linking reagent BS3, and streptavidin-agarose beads were purchased from Pierce. Protein A-agarose beads were purchased from Invitrogen, USA. All other reagents were purchased from Sigma, USA.

Construction of Expression Vectors for Short TMs - pSecTag 2B vector (Invitrogen, USA) is a mammalian expression vector, which contains a cytomegalovirus promoter for high level constitutive expression and a T7 priming site followed by a murine Ig k leader sequence, a multiple cloning site, and two tag sequences (myc and polyhistidine). The

minigenes encoding the short TMD sequence peptides of hOAT1 were constructed by ligation of synthetic oligonucleotides by using the *EcoRV* and *HindIII* restriction sites. The final sequence comprised the signal peptide and an adjacent extracellular sequence joined to a sequence incorporating the entire putative TMD and C-terminal intracellular tag sequences (Myc and polyHis) (Figure 1). Plasmids were checked by sequencing using the dideoxy chain termination method.

Cell Culture - Parental COS-7 cells were grown in DMEM supplemented with 10% fetal bovine serum, penicillin/ streptomycin (100 U/ml), and glucose (100 mg/ml) in a 5% CO₂ atmosphere at 37°C. COS-7 cells stably expressing hOAT1-myc (Hong et al., 2005) were maintained in the same medium containing 0.2 mg/ml geneticin (G418; Invitrogen, Carlsbad, CA). The myc epitope was tagged to the carboxyl terminus of hOAT1 to facilitate the immuno-detection of hOAT1.

Transfection of Plasmids - Cells were transfected with Lipofectamine 2000 (Invitrogen, USA) as suggested by manufacturer. Briefly, $\sim 1 \times 10^6$ of COS-7 cells were plated in 6-well one day before transfection with 4 μ g of individual TM plasmid. 24 hr after transfection, cells were ready for following experiments.

Transport Measurement - Cells were plated in 48-well plates. For each well, uptake solution was added. The uptake solution consisted of phosphate-buffered saline/Ca²⁺/Mg²⁺ (137 mM NaCl, 2.7 mM KCl, 4.3 mM Na₂HPO₄, 1.4 mM KH₂PO₄, 1 mM CaCl₂, and 1 mM MgCl₂, pH 7.4) and [³H] PAH. At the times indicated, uptake was stopped by aspirating off the uptake solution and rapidly washing the well with ice-cold PBS. The cells were then solubilized in 0.2 N NaOH, neutralized in 0.2 N HCl, and

aliquotted for liquid scintillation counting. The uptake count was standardized by the amount of protein in each well. Values are means \pm SE ($n = 3$).

Cell Surface Biotinylation - Cell surface expression levels of hOAT1 were examined using the membrane-impermeant biotinylation reagent Sulfo-NHS-SS-biotin. The cells were seeded onto six-well plates at 8×10^5 cells per well. After 24 h, the medium was removed and the cells were washed twice with 3 ml of ice-cold PBS, pH 8.0. The plates were kept on ice, and all solutions were kept ice-cold for the rest of the procedure. Each well of cells was incubated with 1 ml of Sulfo-NHS-SS-biotin (0.5 mg/ml in PBS) in two successive 20-min incubations on ice with very gentle shaking. The reagent was freshly prepared for incubation. After biotinylation, each well was briefly rinsed with 3 ml of PBS containing 100 mM glycine and then incubated with the same solution for 20 min on ice to ensure complete quenching of the unreacted sulfo-NHS-SS-biotin. The cells were then dissolved on ice for 1 h in 400 μ l of lysis buffer (10 mM Tris, 150 mM NaCl, 1 mM EDTA, 0.1% SDS, 1% Triton X-100, 1/100 protease inhibitor mixture, pH 7.4). The unlysed cells were removed by centrifugation at 13,000 rpm at 4°C. Streptavidin-agarose beads were then added to the supernatant to isolate cell membrane protein. hOAT1 was detected in the pool of surface proteins by electrophoresis and immunoblotting using an anti-myc antibody (1:500) (Mount Siani Medical Center, USA).

Purification of Crude Membrane Proteins - COS-7 cells were homogenized in isolation buffer (250 mM sucrose, 10 mM triethanolamine with 1/100 protease inhibitor mixture) and centrifuged at $1,000 \times g$ for 10 min at 4 °C. The supernatant was then centrifuged at $17,000 \times g$ for 20 min at 4 °C. The pellet was resuspended in appropriate volume of isolation buffer. Protein concentrations were determined using the Bio-Rad protein assay kit. The protein solutions were stored at -80 °C before further use.

Chemical Cross-linking - Membrane proteins were diluted to 1 mg/ml with cross-linking buffer (NaCl 150 mM, HEPES 100 mM, dithiothreitol 5 mM, EDTA 5 mM with 1/100 protease inhibitor mixture) and then incubated with 1–5 mM cross-linking reagent BS3 with end-over-end mixing for 30 min at room temperature. The cross-linking reaction was then stopped by incubation with 100 mM Tris/HCl, pH 7.5, for 15 min at room temperature. Appropriate volume (~ 50 μ l) of Laemmli buffer was added to denature the protein at 50 °C for 30 min, followed by electrophoresis and immunoblotting.

Co-immunoprecipitation - hOAT1-Flag was transfected into COS-7 cells stably expressing hOAT1-myc. The cells were lysed in immunoprecipitation buffer (10 mM Tris/HCl, pH 7.5, 10 mM NaCl, 0.5~1% Triton X-100, 2 mM EDTA, 10% glycerol, and 1/100 protease inhibitor mixture). Cell lysates were precleaned with protein A-agarose beads to reduce nonspecific binding. The precleaned cell lysates were incubated with anti-Flag antibody (1:100) for 1.5 h at room temperature. Protein A-agarose beads were then added and mixed with end-over-end rotating at 4 °C overnight. Proteins bound to the protein A-agarose beads were eluted with Laemmli buffer containing β -mercaptoethanol and analyzed by immunoblotting with horseradish peroxidase-conjugated anti-myc antibody (1:500, Sigma, USA).

Electrophoresis and Immunoblotting - Protein samples (100 μ g) were resolved on 7.5% SDS-PAGE minigels and electroblotted onto polyvinylidene difluoride membranes. The blots were blocked for 1 h with 5% nonfat dry milk in PBS-0.05% Tween 20, washed, and incubated overnight at 4°C with primary antibody. The membranes were washed and then incubated with appropriate secondary antibody conjugated to horseradish

peroxidase (1:5,000), and signals were detected using a SuperSignal West Dura extended duration substrate kit (Pierce Chemical, USA).

Data Analysis - Statistical analysis was conducted using Student's paired *t* test for comparing two treatments. A one-way ANOVA followed by a Dunnett's post hoc test was used for comparing among more than two treatments. A *P* value <0.05 was considered significant.

6.3 Results

Expression of short hydrophobic peptides - To test the potentially inhibitory effects of short hydrophobic peptides on oligomerization and function of hOAT1, we took advantage of the characteristics of the pSecTag 2B expression plasmid. In this plasmid, we constructed minigenes comprising a sequence signal at the N terminus, which should direct the protein to the cell surface, a short extracellular fragment, the sequences corresponding to TMDs 1-12 of hOAT1, a basic short stop-sequence to anchor the peptide in the proper orientation, and two C terminal intracellular tags (myc and polyHis).

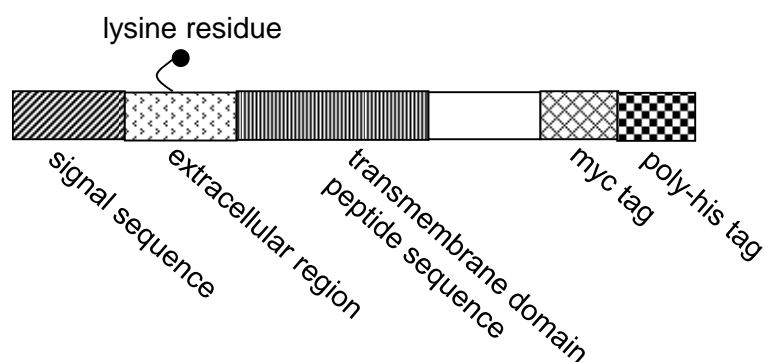


Fig. 1. Schematic diagram of minigenes used to encode the TMD sequences. Each box represents a section of the constructions made within the Invitrogen pSecTag 2B plasmid.

The plasmids containing these minigenes were transfected into COS-7 cells separately. Transfected cells were lysed, followed by immunoblotting with anti-myc antibody. As shown in Fig. 2a, these short hydrophobic peptides were efficiently expressed in COS-7 cells.

Surface expression of short hydrophobic peptides - To determine whether these short hydrophobic peptides can be inserted into plasma membrane, we took advantage of a single lysine residue in the short extracellular fragment of the minigene, which can be labeled by cell-impermeable biotinylation reagent NHS-SS-biotin and therefore allows the determination of surface expression of these peptides. The plasmids containing these minigenes were transfected into COS-7 cells separately. Transfected cells were biotinylated with NHS-SS-biotin, followed by immunoblotting with anti-myc antibody. As shown in Fig. 2b, these peptides were indeed expressed at the cell membrane.

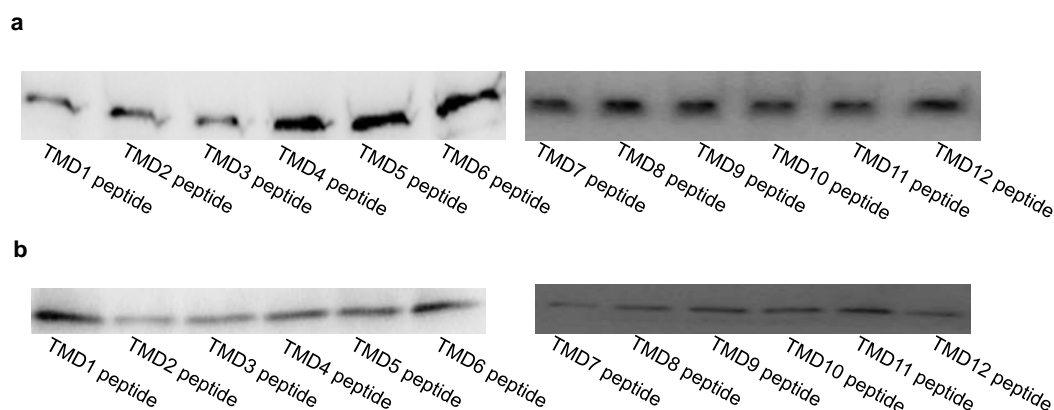


Fig. 2. Expression of short peptides. *a. Total expression of short peptides.* 4 μ g of plasmids encoding short peptides corresponding to TMDs 1-12 of hOAT1 were transfected into COS-7 cells as described in the section "Materials and Methods". 24 hrs after transfection, cells were lysed followed by immunoblotting with anti-myc antibody (1:500). *b. Cell surface expression of short peptides.* 4 μ g of plasmids encoding peptides corresponding to TMDs 1-12 of hOAT1 were transfected into COS-7 cells. 24 hrs after transfection, surface expression of these peptides was analyzed by cell surface biotinylation approach as described in the section "Materials and Methods".

Effects of short hydrophobic peptides on hOAT1 oligomerization - We previously demonstrated (1) that chemical cross-linking of intact membrane proteins from hOAT1-expressing cells converted quantitatively hOAT1 monomer to putative dimer and trimer, indicating that hOAT1 is present in the membrane as multimeric complexes. To determine the effects of these short hydrophobic peptides on hOAT1 oligomerization, cross-linking experiments were performed with membrane proteins isolated from hOAT1-myc-expressing cells transfected with or without these peptides. As shown in Fig. 3, the degree of hOAT1 oligomerization (ratios of oligomer/monomer, oligomer = the sum of dimer + trimer) is similar between control cells and cells transfected with peptides corresponding to TMDs 1-5, and 7-12 of hOAT1, whereas the degree of hOAT1 oligomerization was significantly decreased in cells transfected with peptide corresponding to TMD 6 (TMD6-peptide) of hOAT1, suggesting that TMD6-peptide is a potent inhibitor for hOAT1 oligomerization. Because of the significant role of TMD6 peptide in hOAT1 oligomerization, additional studies were focused on this peptide.

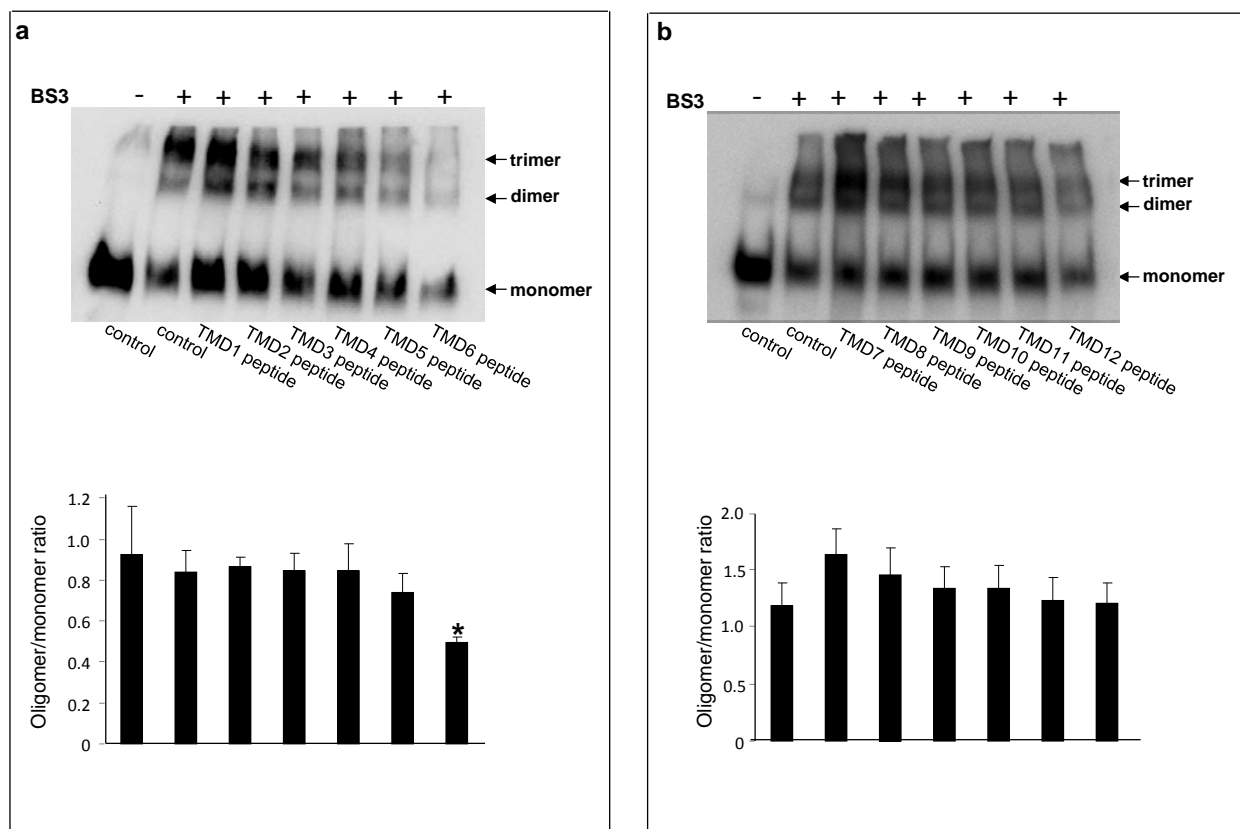


Fig. 3. Cross-linking analyses of the effect of short peptides on oligomerization of hOAT1. a. 4 μ g of plasmids encoding peptides corresponding to TMDs 1-12 of hOAT1 were transfected into COS-7 cells. Twenty-four hours after transfection, membrane proteins were collected and then cross-linked with a cross-linker BS3. After 30min of the reaction, the crosslink was stopped by addition of 1 M of Tris-HCl (pH 7.5). The cross-linked proteins were then subjected to immunoblotting with anti-myc antibody. The apparent molecular masses of hOAT1 oligomers were estimated based on the linear regression of the molecular mass markers used. b. Densitometry analysis of results from result shown in a as well as two other experiments. Asterisks indicate values significantly different ($p < 0.05$) from that of control.

The effect of TMD6 peptide on hOAT1 oligomerization was further analyzed through co-immunoprecipitation experiments. Flag-tagged hOAT1 was cotransfected with TMD6 peptide into hOAT1-myc-expressing cells. Flag-tagged hOAT1 was immunoprecipitated with anti-Flag antibody followed by immunoblotting with anti-FLAG antibody (to detect FLAG-tagged hOAT1) or anti-Myc antibody (to detect Myc-tagged hOAT1). As shown in Fig. 4, although the amount of Flag-tagged hOAT1

immunoprecipitated was similar in the presence and absence of TMD6 peptide (Fig. 4a), an indication of similar immunoprecipitation efficiency in both situations, the amount of myc-tagged hOAT1, which co-immunoprecipitated with Flag-tagged hOAT1, was much smaller in the presence of TMD6 peptide than in the absence of the peptide (Fig. 4b), suggesting that the association between Flag-tagged hOAT1 and myc-tagged hOAT1 was weakened in the presence of TMD6 peptide.

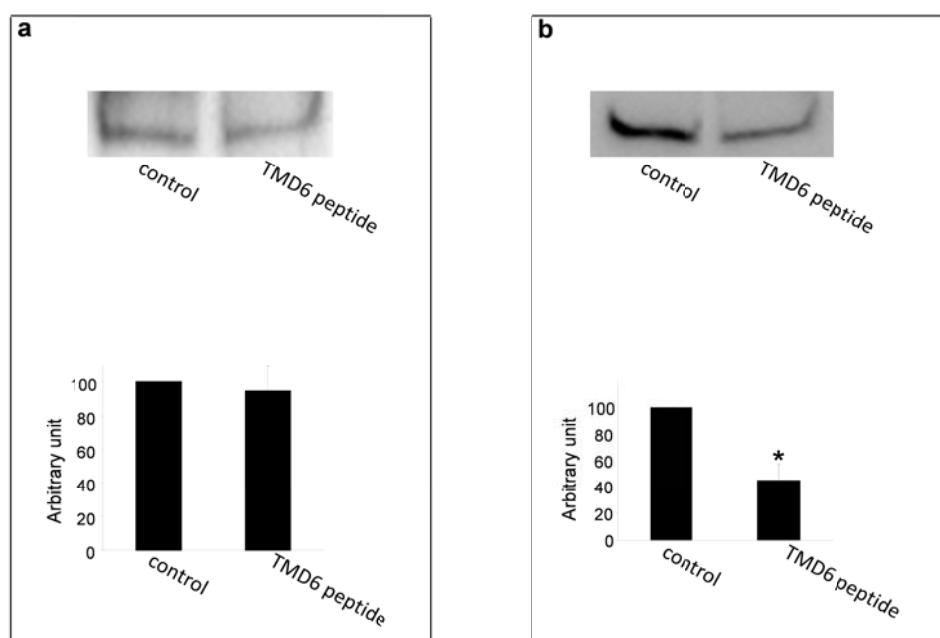


Fig. 4. Effect of TMD6 peptide on the association of hOAT1-FLAG with hOAT1-myc. Flag-tagged hOAT1 and TMD6 peptide were co-transfected into COS-7 cells stably expressing hOAT1-myc. Twenty-four hours after transfection, cells were lysed and subjected to immunoprecipitation with anti-Flag antibody, followed by immunoblotting with anti-FLAG (a) or anti-myc (b) antibodies.

Effects of TMD6 peptide on hOAT1 function - Our data above showed that TMD6 peptide disrupted hOAT1 oligomerization. To determine the functional consequence of hOAT1 oligomerization, hOAT1-mediated uptake of ^3H -PAH, a prototypical OAT1 substrate, was measured in cells transfected with or without TMD6 peptide. As shown in Fig. 5, hOAT1 transport activity was much reduced in the presence of TMD6 peptide as compared with that of the control. An Eadie-Hofstee plot analysis showed that the

reduced transport activity resulted from a decrease in the maximum transport velocity V_{\max} (0.012 ± 0.001 pmol $\cdot\mu\text{g}^{-1}\cdot\text{min}^{-1}$ in control cells and 0.008 ± 0.001 pmol $\cdot\mu\text{g}^{-1}\cdot\text{min}^{-1}$ in TMD6 peptide-transfected cells) without significant change in the affinity (K_m) for the substrate (5.71 ± 0.21 μM in control cells, and 5.44 ± 0.26 μM in TMD6 peptide-transfected cells).

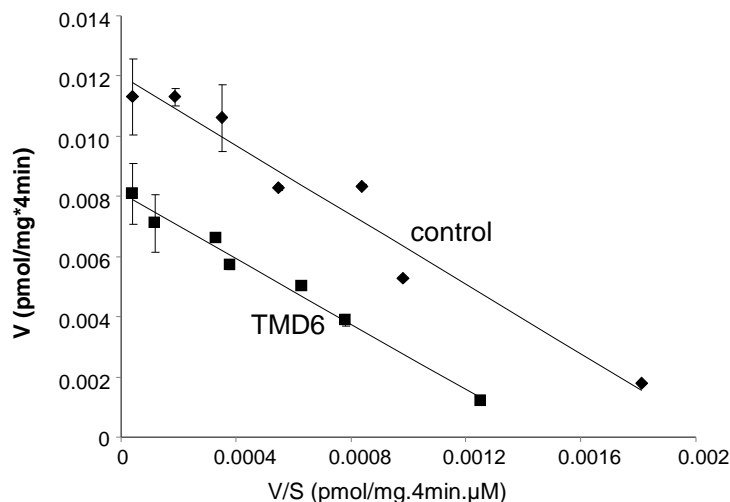


Fig. 5. Effect of TMD6 peptide on hOAT1-mediated transport. 0.8 μg of TMD6 peptide was transfected into COS-7 cells stably expressing hOAT1-myc. Twenty-four hours after transfection, initial uptake (4 min) of ^3H -PAH was measured at 8–800 μM PAH. The data represent uptake into hOAT1-expressing cells minus uptake into mock cells (parental COS-7 cells). Values are means \pm SE ($n = 3$). V, velocity; S, substrate concentration.

Effects of TMD6 peptide on hOAT1 expression - A decreased V_{\max} could be affected by either a decreased number of the transporter at the cell surface or a decreased transporter turnover number. Experiments that differentiate between these possibilities were conducted by measuring transporter expression both at the cell surface and in the total cell lysate through cell surface biotinylation approach. Our result showed that transfection of TMD6 peptide into the cells resulted in a decreased expression of hOAT1 at the cell surface (Fig. 6a) without affecting the total cell expression of the transporter (Fig. 6b).

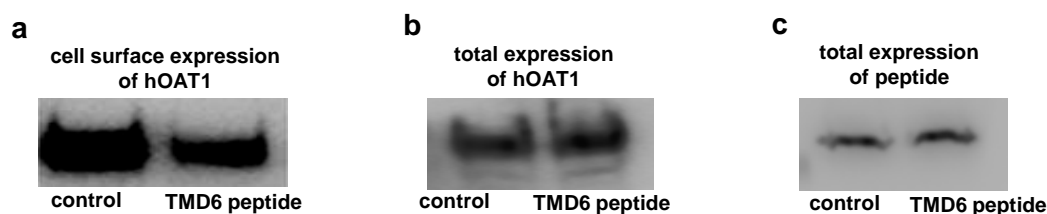


Fig. 6. Effect of TMD6 peptide on the expression of hOAT1. 4 μ g of plasmid encoding TMD6 peptide was transfected into COS-7 cells stably expressing hOAT1-myc as described above. Twenty-four hours after transfection, the surface expression of hOAT1 (a), the total expression of hOAT1 (b), and the total expression of peptides (c) were determined by immunoblotting.

6.4 discussion

We previously demonstrated that hOAT1 forms oligomer both in cultured cells and in rat kidney (1). However, the functional consequence of such oligomerization and the structural segments of hOAT1 involved in such oligomerization have never been elucidated. In the current study, we investigated the effects of short hydrophobic peptides on the oligomerization and function of hOAT1. The short hydrophobic peptides corresponding to TMDs of several receptors have been used to demonstrate the role of interaction between transmembrane domains in receptor oligomerization and function. It has been shown that introduction of plasmid-encoded short peptide with homologous sequence corresponding to TMD of the receptor can act as competitor and interfere with receptor oligomerization and function (2, 3). Such effects are highly selective because one homologous transmembrane domain sequence is only inhibitory for its “parental and cognate” receptor but not for unrelated receptor. We employed such an approach in our current study.

Our cell surface biotinylation experiments showed (Fig. 2) that all of the 12 exogenous peptides were efficiently inserted into the plasma membrane of the cells. We

previously demonstrated (1) that chemical cross-linking of intact membrane proteins from hOAT1-expressing cells converted quantitatively hOAT1 monomer to putative dimer and trimer, indicating that hOAT1 is present in the membrane as multimeric complexes. To determine the effects of these short hydrophobic peptides on hOAT1 oligomerization, cross-linking experiments were performed with membrane proteins isolated from hOAT1-expressing cells transfected with or without these peptides. Among all the peptides examined, only the peptide corresponding to TMD 6 (TMD6 peptide) of hOAT1 significantly reduced the amount of oligomer formed (Fig. 3), suggesting that TM6-peptide is a potent inhibitor for hOAT1 oligomerization. It is important to note that the lower ratios of oligomer/monomer in sample containing TMD6 peptide do not seem to result from a reduced cross-linking efficiency due to a lower amount of hOAT1 in the sample. For example, the amount of hOAT1 containing TMD1 peptide is higher than that containing TMD5 peptide (Fig. 3a). Yet, both situations had similar cross-linking efficiencies as that of the control.

The observation that TMD6 peptide was a potent inhibitor for hOAT1 oligomerization was further reinforced through co-immunoprecipitation study (Fig. 4). The association between Flag-tagged hOAT1 and myc-tagged hOAT1 was much weaker in the presence of TMD6 peptide as compared to control. Therefore, TMD6 peptide can serve as a potent inhibitor for hOAT1 oligomerization. The moderate inhibition of hOAT1 oligomerization by TMD6 peptide may result from the possibility that TMDs may not be the only driving force for hOAT1 oligomerization. Addressing this interesting question will be the focus of our future study.

Our result also indicated that TMD 6 of hOAT1 may contribute to the oligomerization of the transporter. If this is indeed the case, it seems that a non-classical

oligomerization motif is involved because the classical oligomerization motives such as GXXXG (4, 5), and alpha-helical coiled coil, a heptad repeat pattern of primarily apolar residues (6), are not present in this TMD. A similar situation was encountered in the study of an ATP-binding cassette transporter ABCG2 (7) . In their study, the removal of GXXXG motif in TMD 1 by site-directed mutagenesis did not show any effect on the oligomerization of ABCG2, which suggests that GXXXG motif in TMD 1 does not play an essential role in ABCG2 oligomerization.

Transfection of TMD6 peptide induced a ~50% inhibition of uptake of PAH mediated by hOAT1. Our kinetic analysis showed that the reduced transport activity was contributed by a reduced maximum transport velocity (V_{\max}) without affecting the binding affinity (K_m) for the substrates (Fig. 5). V_{\max} can be affected by either the number of the transporter at the cell surface or the transporter turnover number. To differentiate between these possibilities, we determined the effect of this peptide on hOAT1 expression both at the cell surface and in the total cell lysates. Our results showed that transfection of TMD6 peptide resulted in a reduced cell surface expression of hOAT1 without affecting its total cell expression (Fig. 6).

Oligomerization plays critical role in various aspects of transporter function. Several subunits in the oligomer may be required to form a single translocation pathway for the substrate to move across membrane (8). Oligomerization is also believed to play a role in membrane trafficking of the transporters. After synthesis in the endoplasmic reticulum (ER), proteins undergo a strict process of quality control. Newly synthesized transporters may contain retention signal and are thereby retained in the ER. Oligomerization may shield/hide such retention signal and therefore is essential for the

egress of the transporters from ER for subsequent targeting to the plasma membrane (9-11). Our future studies will explore the sites at which hOAT1 forms oligomers.

In conclusion, our study provides the first demonstration that i) short hydrophobic peptide approach not only can be used for the study of the oligomerization of single TMD-containing receptors but also can be employed for the study of the oligomerization of multiple TMD-containing transporters such as hOAT1, ii), peptide corresponding to TMD 6 of hOAT1 can serve as a potent inhibitor for hOAT1 oligomerization, and iii) oligomerization of hOAT1 is critical for the expression of the transporter at the cell surface.

6.5 References

1. Hong M, Xu M, Yoshida T, Wolff D, Zhou FF, Inouye M, and You G. Human organic anion transporter hOAT1 forms homooligomers. (2005). *J. Biol. Chem.* 280: 32285 – 32290.
2. Bennasroune A, Fickova M, Gardin A, Dirrig-Grosch S, Aunis D, Cremel G and Hubert P (2004) Transmembrane peptides as inhibitors of ErbB receptor signaling. *Mol Biol Cell* 15(7):3464-3474.
3. Bennasroune A, Gardin A, Auzan C, Clauser E, Dirrig-Grosch S, Meira M, Appert-Collin A, Aunis D, Cremel G and Hubert P (2005) Inhibition by transmembrane peptides of chimeric insulin receptors. *Cell Mol Life Sci* 62(18):2124-2131.
4. Eilers M, Patel AB, Liu W and Smith SO (2002) Comparison of helix interactions in membrane and soluble alpha-bundle proteins. *Biophys J* 82(5):2720-2736.
5. Russ WP and Engelman DM (2000) The GxxxG motif: a framework for transmembrane helix-helix association. *J Mol Biol* 296(3):911-919.
6. Burkhard P, Stetefeld J, Strelkov SV. (2001) Coiled coils: a highly versatile protein folding motif. *Trends Cell Biol.* 2001 Feb;11(2):82-8.
7. Polgar O, Robey RW, Morisaki K, Dean M, Michejda C, Sauna ZE, Ambudkar SV, Tarasova N and Bates SE (2004) Mutational analysis of ABCG2: role of the GXXXG motif. *Biochemistry* 43(29):9448-9456.
8. Monte JC, Nagle MA, Eraly SA and Nigam SK (2004) Identification of a novel murine organic anion transporter family member, OAT6, expressed in olfactory mucosa. *Biochem Biophys Res Commun* 323(2):429-436.
9. Enomoto A, Kimura H, Chairoungdua A, Shigeta Y, Jutabha P, Cha SH, Hosoyamada M, Takeda M, Sekine T, Igarashi T, Matsuo H, Kikuchi Y, Oda T, Ichida K, Hosoya T, Shimokata K, Niwa T, Kanai Y and Endou H (2002) Molecular identification of a renal urate anion exchanger that regulates blood urate levels. *Nature* 417(6887):447-452.
10. Veenhoff LM, Heuberger EHML, and Po B (2002) *TRENDS in Biochem. Sci* 27:242-249
11. Shin HJ, Anzai N, Enomoto A, He X, Kim do K, Endou H and Kanai Y (2007) Novel liver-specific organic anion transporter OAT7 that operates the exchange of sulfate conjugates for short chain fatty acid butyrate. *Hepatology* 45(4):1046-1055.

7. Curriculum Vitae

Shanshan Li

Education

Rutgers University at New Brunswick, School of Pharmacy, **Ph.D** in **Pharmaceutics**, Oct, 2013.

Iowa State University, Ames, IA. **M.S.** in **Nutritional Science**, conferred 05/2007.

Tsinghua University, Beijing, China. **B.S.** in **Chemistry**, conferred 07/2003.

Publications:

1. Li, S., Zhang, Q., Wu, J., You, G. Three ubiquitination sites of organic anion transporter-1 synergistically mediate protein kinase C-depend endocytosis of the transporter. Submitted to *Mol. Pharmacol.*
2. Zhang, Q., **Li, S.**, You., G. Lysine 48-linked polyubiquitination of organic anion transporter-1 is essential for its protein kinase C-regulated endocytosis. *Mol. Pharmacol.* **2013**, 83 (1), 217-24
3. Duan, P., **Li, S.**, You., G. Regulation of human organic anion transporter 4 by parathyroid hormone-related protein and protein kinase A. *Int J Biochem Mol Biol.* **2012**, 3 (3), 322-7
4. Duan, P., **Li, S.**, Ai, N., Hu. L., Welsh, WJ., You., G. Potent inhibitors of human organic anion transporters 1 and 3 from clinical drug libraries: Discovery and molecular characterization. *Mol. Pharmacol.* **2012**, 9 (11), 3340-6
5. Duan, P., **Li, S.**, You., G. Transmembrane peptide as inhibitor of oligomerization and function of human organic anion transporter 1. *Mol. Pharmacol.* **2011**, 79 (3), 569-74
6. **Li, S.**, Duan, P., You., G. Regulation of human organic anion transporter 3 by Peptide hormone bradykinin. *J. Pharmacol. Exp. Ther.* **2010**, 333 (3), 970-5
7. **Li, S.**, Hong, M., Zhou, F., Thoma, PE., You., G. Putative transmembrane domain 12 of the human organic anion transporter hOAT1 determines transporter stability and maturation efficiency. *J. Pharmacol. Exp. Ther.* **2010**, 332 (2), 650-8

8. Duan, P., **Li, S.**, You., G. Angiotensin II inhibits activity of human organic anion transporter 3 through activation of protein kinase C: accelerating hOAT3 endocytosis. *Eur. J. Pharmacol.* **2010**, 627 (1-3), 49-55
9. **Li, S.**, Duan, P., You., G. Regulation of human organic anion transporter 1 by AngII: involvement of protein kinase C alpha. *Am. J. Physiol. Endocrinol. Metab.* **2009**, 296 (2), E378-83
10. **Li, S.**, Nugroho, A., Rocheford, T., White, W. Vitamin A equivalence of β -carotene in β -carotene-biofortified maize porridge consumed by women. *Am. J. Clin. Nutr.* **2010**, 92(5), 1105-12
11. Taber. H., Perkins-Veazie, P, **Li, S.**, White, W., Rodermel, S., Xu., Y. Enhancement of tomato fruit lycopene by potassium is cultivar dependent. *Hort. Sci.* **2008**, 43, 159-165
12. Aluru, M., Xu, Y., Guo, R., Wang, Z., **Li, S.**, White, W., Wang, K., Rodermel, S. Generation of transgenic maize with enhanced provitamin A content. *J. Exp. Botany* **2008**, 59, 3551-62
13. **Li, S.**, Tayie, F.A.K., Young, M.F., White, W. Retention of provitamin A carotenoids in high β -carotene maize during traditional African household. *J. Agric. Food Chem.* **2007**, 55, 10744-10750